Fakultät Wissenschaftszentrum Weihenstephan für Ernährung, Landnutzung und Umwelt

Lehrstuhl für Ernährungsmedizin

Adipocytes and their metabolic function on hepatocytes

Simone Matthä

Vollständiger Abdruck der von der Fakultät Wissenschaftszentrum Weihenstephan für Ernährung, Landnutzung und Umwelt der Technischen Universität München zur Erlangung des akademischen Grades eines

Doktors der Naturwissenschaften

genehmigten Dissertation.

Vorsitzende: Univ.-Prof. Dr. H. Daniel

Prüfer der Dissertation:

1. Univ.-Prof. Dr. J. J. Hauner
2. Univ.-Prof. Dr. M. Klingenspor

Die Dissertation wurde am 22.07.2013 bei der Technischen Universität München eingereicht und durch die Fakultät Wissenschaftszentrum Weihenstephan für Ernährung, Landnutzung und Umwelt am 18.01.2014 angenommen.

Gewidmet

Meiner Familie

Acknowledgements

Special thanks go to my supervisor Prof. Dr. J. J. Hauner for contribution to this work by valuable discussions and ideas, his constant support and motivation.
I also want to thank my second supervisor PD Dr. Thomas Skurk for helpful discussions and a lot of good advice during the practical part of the thesis. He taught me to look at things from many different points of views.
Many thanks go to Prof. Dr. Martin Klingenspor for a lot of advice.
I thank Prof. Dr. Hannelore Daniel for taking the chair in the dissertation procedure.
Special thanks go to my collaboration partners Prof. Dr. Bernhard Küster, Fiona Pachl and Dr. Martin Irmler for excellent support.
I would like to thank Dr. Helmut Laumen for his great support and helpful discussions.
I am deeply thankful to all my colleagues. Many thanks to Manuela Hubersberger, Elisabeth Hofmair, Stephanie May, Eva-Maria Sedlmeier and Christoph Dahlhoff for their great help, explanations, patience, and the good working atmosphere. Special thanks go to Dr. Ramona Pais for valuable discussions and providing animal tissues. Furthermore, special thanks go to Dr. Christina Holzapfel for her great support especially during the writing phase and for reading the thesis.
Many thanks to Patricia Krinninger, Melina Claußnitzer, Heekyoung Lee, Dr. Tobias Ludwig, Julia Stoll, Susanne Krug, Stefanie Brunner, Daniela Much, Sebastian Dreyer, Kerstin Ehlers, Tina Brand, Carola Herrmann, Anna Bhandari, Aline Lukacs and Stefanie Worsch for personal support and the good working atmosphere.
I thank Sylvia Heinrich for assistance with administrative work and for her sympathetic ear.

I thank the European Commission (HEPADIP), the EKF-foundation and the TUM Diversity for funding.

Finally, I would particularly like to thank my family for their personal advice and support.

Table of Contents

Zusammenfassung

Übergewicht und Adipositas sind durch eine Zunahme des Fettgewebes sowie durch eine vermehrte Produktion pro-inflammatorischer Faktoren, den sogenannten Adipokinen, charakterisiert. Da Übergewicht häufig mit Fettlebererkrankungen verbunden ist, wird vermutet, dass Adipokine an der Entstehung der nichtalkoholischen Fettlebererkrankung (NAFLD) beteiligt sind. Die genauen Mechanismen sind bislang nicht vollständig aufgeklärt.

Eine Vergrößerung des Fettgewebes erfolgt über Hypertrophie und / oder Hyperplasie, wobei die Hypertrophie eine vermehrte Produktion pro-inflammatorischer Adipokine bewirkt. Die Ziele der vorliegenden Arbeit waren (1) kleine und große humane Fettzellen der gleichen Person hinsichtlich ihrer Insulinsensitivität, ihres Transkriptoms und Proteoms zu vergleichen, (2) den Einfluss von fettzellkonditionierten Medium sowie einzelner pro-inflammatorischer Adipokine (TNFα, IL6, Ang II, PAI-1, SDF-1α, MCP-1, RANTES) auf die hepatische Glukoseproduktion zu prüfen und (3) die Wirkung von RANTES als neu etabliertes Adipokin auf den hepatischen Glukose- und Fettstoffwechsel näher zu untersuchen.

Die Ergebnisse dieser Arbeit zeigen, dass die Fettzellgröße *per se* das Insulinsignal, die Stressantwort und die Zusammensetzung der extrazellulären Matrix (EZM) im Fettgewebe beeinflusst. Die insulinsupprimierte hepatische Glukoseproduktion verschlechterte sich mit wachsender Fettzellgröße und durch den Einfluss pro-inflammatorischer Adipokine. RANTES wurde dabei als neues Adipokin erkannt, welches sowohl den hepatischen Lipid- als auch Glukosestoffwechsel beeinflusst. Es induziert den Erk 1/2-Signalweg sowie die Produktion von *IL6* in der Leber. Eine vermehrte Expression von *IL6* und eine zeitgleiche Reduktion von *C/EBPα* und *SREBP-1c* mRNA weisen auf ein erhöhtes Fibroserisiko durch die Behandlung mit RANTES hin.

Zusammenfassend liefert die Fettzellgröße einen besseren Hinweis auf Übergewichts-assoziierte Erkrankungen als das Körpergewicht selbst. Von großen Fettzellen sezernierte pro-inflammatorische Adipokine können mit der Leber kommunizieren. Somit kann bei Übergewicht das veränderte Sekretionsmuster des Fettgewebes den Lebermetabolismus beeinflussen und dabei zu Erkrankungen der Leber führen. Große Fettzellen und ihre Adipokine stellen daher potenzielle Angriffspunkte für die Therapie von NAFLD dar.

Summary

Overweight and obesity are characterised by an expanded adipose tissue (AT) mass as well as an increased production of pro-inflammatory factors, so called adipokines. Since obesity is frequently associated with fatty liver disease, it is suggested that these adipokines are potentially involved in the development of non-alcoholic fatty liver disease (NAFLD). The exact mechanisms leading to NAFLD are currently not completely known.

AT growth occurs through hypertrophy and / or hyperplasia, whereby hypertrophy leads to higher secretion of pro-inflammatory adipokines. The aims of the present study were (1) to compare small and large human adipocytes from the same subject according to insulin sensitivity, transcriptome and proteome (2) to test the effect of adipocyte-conditioned medium (CM) and single pro-inflammatory adipokines (TNFα, IL6, Ang II, PAI-1, SDF-1α, MCP-1, RANTES) on hepatic glucose production, and (3) to investigate the impact of RANTES as a newly identified adipokine on hepatic glucose and lipid metabolism.

The present results demonstrate that fat cell size *per se* influences insulin signaling and stress responses as well as extracellular matrix (ECM) composition in AT. The insulin-suppressed hepatic glucose production was impaired by expanding adipocyte cell size and through the influence of pro-inflammatory adipokines. RANTES was thereby recognised as a new adipokine, which affects both hepatic lipid and glucose metabolism. Its impact was combined with the induction of Erk 1/2 pathway and the following production of *IL6* in the liver. Enhanced expression of *IL6,* in addition to decreased *C/EBPα,* as well as *SREBP-1c* mRNA indicates an increased risk for the progression of fibrosis due to RANTES treatment.

In conclusion, adipocyte cell size rather than body weight *per se* is a good predictor for obesity related dysfunctions. Large fat cells released pro-inflammatory adipokines may cross-talk with the liver. Thus, in obesity, an altered secretion pattern from AT can substantially contribute to changes in hepatic metabolism followed by liver impairments. Thus, hypertrophic fat cells and their adipokines serve as potential targets in NAFLD therapy.

Abbreviations

A	
ACACA /ACC	Acetyl-CoA carboxylase alpha
ACE	Angiotensin-converting enzyme
Acox1	Acyl-CoA oxidase 1, palmitoyl
ADD1	Adipocyte determination and differentiation factor 1
Akt/PKB	Protein Kinase B
AMPK	AMP-activated protein kinase
Ang	Angiotensinogen
Ang II	Angiotensin II
ANOVA	Analysis of variance
APS	SH2B adaptor protein 2
AT (W, B, Y)	Adipose tissue (white, brown, yellow)
ATBF	AT blood flow
ATF 6	Activating transcription factor 6
ATGL	Adipose triglyceride lipase
ATP	Adenosine triphosphate
B	
BMI	Body-Mass-Index
bp	Base pair
BSA	Bovine serum albumin
C	
°C	Degree Celsius
C/EBP	CCAAT-enhancer-binding protein
C3G	guanine nucleotide exchange protein
Ca^{2+}	Calcium
$CaCl_2$	Calcium chloride
cAMP	Cyclic adenosine monophosphate
CAP	Cbl associated protein
Cbl	Casitas B-lineage Lymphoma
cDNA	Complementary DNA
CM	Conditioned medium
CO_2	Carbon dioxide
CPT-1	Carnitine palmitoyltransferase I
cRNA	Complementary RNA
CVD	Cardiovascular disease
D	
DAPI	4',6-diamidino-2-phenylindole
db-cAMP	N6,2′-O-Dibutyryladenosine 3′,5′-cyclic monophosphate
db-CD	Db-cAMP/dexamethasone
DF	Dilution factor
DHAP	Dihydroxyacetonphosphate
DM	Differentiation medium
DMEM	Dulbecco's modified Eagle's medium
DMSO	Dimethylsulfoxide
DNA	Deoxyribonucleic acid
ds	Double stranded
DTT	Dithiothreitol
E	
ECL	Enhanced chemiluminescence
ECM	Extracellular matrix
EDTA	Ethylenediaminetetraacetic acid
EGF	Epidermal growth factor
eIF-2a	Eukaryotic Initiation Factor 2
ELISA	Enzyme-Linked Immunosorbent Assay
EOR	Endoplasmic overload response
ER	Endoplasmic reticulum
Erk 1/2	Extracellular-signal-regulated kinase 1/2
ESI	Electrospray ionization
F	
f	Female
F1	Fraction 1 (small fat cells)
F4	Fraction 4 (large fat cells)
FAs / FFAs	Fatty acids / free fatty acids
FAS	Fatty acid synthase
FATP	Fatty acid transport protein
FBPase	Fructose bisphosphatase
FCS	Fetal calf serum
FDR	False discovery rate
FGF	Fibroblast growth factor
FOXO	Forkhead box protein O
G	
g/d	Gram per day
G6P	Glucose-6-phosphate
G6Pase	Glucose 6-phosphatase
Gab-1	GRB2-associated binding protein 1
GAPDH	Glyceraldehyde 3-phosphate dehydrogenase
GDP	Guanosine diphosphate
GLUT	Glucose transporter
GPDH	Glycerol-3-phosphate dehydrogenase
Grb2	Growth factor receptor-bound protein-2
GS	Glycogen synthase
GTP	Guanosine triphosphate
H	
HCD	Higher-energy collisional dissociation
HCl	Hydrogen chloride
HDL	High-density lipoprotein
HEPADIP	Hepatic and Adipose Tissue and Functions in the Metabolic Syndrome
HEPES	4-(2-hydroxyethyl)-1-piperazineethanesulfonic acid
HGNG	Hepatic gluconeogenesis
HIV	Human immunodeficiency virus
HPLC	High-performance liquid chromatography
HRP	Horseradish peroxidase
HSC	Hepatic stellate cell
HSL	Hormone-sensitive lipase

I	
IAA	Indole-3-acetic acid
IBMX	3-isobutyl-1-methylxanthine
IFNγ	Interferon gamma
IL6, IL8	Interleukin 6, Interleukin 8
IM	Induction medium
IR	Insulin receptor
IRE1α	Inositol requiring enzyme 1 alpha
IRS	Insulin receptor substrate
J	
JNK	c-Jun N-terminal kinases
JUN /c-Jun	Jun proto-oncogene
K	
KCl	Potassium chloride
kDa	Kilodalton
kg/m^2	Kilogram per square meter
KOH	Potassium hydroxide
KRP	Krebs-Ringer-phosphate buffer
L	
LC	Liquid chromatography
LDH	Lactate dehydrogenase
LDL	Low-density lipoprotein
LPL	Lipoprotein lipase
LPS	Lipopolysaccharides
M	
m	Male
µm	Micrometre
m/z	Mass-to-charge ratio
MAPK	Mitogen-activated protein (MAP) kinases
MCP-1 (CCL2)	Monocyte chemotactic protein-1
MEK	MAP/Erk Kinase
MetS	Metabolic syndrome
$MgSO_4$	Magnesium sulfate
MIF	Macrophage migration inhibitory factor
min	Minute
mRNA	Messenger RNA
MS	Mass spectrometry
MS/MS	Tandem mass spectrometry
MSC	Mesenchymal stem cell
MTS	3-(4,5-dimethylthiazol-2-yl)-5-(3-2H-carboxymethoxyphenyl)-2-(4-sulfophenyl)-tetrazolium
N	
n.s.	Statistically not significant
NaCl	Sodium chloride
NAD	Nicotinamide adenine dinucleotide
NADH	Nicotinamid-Adenin-Dinucleotid-Hydrogen
NAFLD	Non-alcoholic fatty liver disease
NaH_2PO_4	Monosodium phosphate
NaOH	Sodium hydroxide
NASH	Non-alcoholic steatohepatitis
NCBI	National Center for Biotechnology Information
NEFAs	Nonesterified fatty acids
NfkB	Nuclear factor kappa-light-chain-enhancer of activated B cells
nm	Nanometre
NOD	Non-obese diabetic
NTP	Nucleoside triphosphate
O	
ob	Obese
P	
%	Percent
P	Proteome
Page	Polyacrylamide gel electrophoresis
PAI-1	Plasminogen activator inhibitor-1
PBS	Phosphate buffered saline
PCR	Polymerase chain reaction
Pen/Strep	Penicillin Streptomycin
PEPCK	Phosphoenolpyruvate carboxykinase
PERK	PKR-like ER kinase
π	Pi
PGC-1α	Peroxisome proliferator-activated receptor gamma coactivator 1-alpha
PI3-K	Phosphatidylinositol 3-kinases
PIP3	Phosphatidylinositol (3,4,5)-triphosphate
PKA	Protein kinase A
pl	Picolitre
PM	Proliferation medium
PMSF	Phenylmethanesulfonylfluoride
pO_2	Partial pressure of Oxygen
PPAR	Peroxisome proliferator-activated receptor
PVDF	Polyvinylidene fluoride
Q	
qRT-PCR	Quantitative real time polymerase chain reaction
R	
r	Radius
Raf	Rat Firbosarcoma
RANTES (CCL5)	Regulated on activation normal T cell expressed and secreted
RAS	Renin-angiotensin system
rh / m / r	Recombinant human / mouse / rat
RIN	RNA integrity number
RIPA-buffer	Radioimmunoprecipitation assay buffer
RNA	Ribonucleic acid
ROS	Reactive Oxygen Species
rpm	Revolutions per minute

RT	Room temperature
S	
SCAP	SREBP cleavage activating protein
SCD	Stearoyl-CoA desaturase
SDF-1α (CXCL12)	Stromal cell-derived factor-1 alpha
SDS	Sodium dodecyl sulfate
SE	Standard error
sec	Second
siRNA	Small interfering RNA
SIRT1	Sirtuin 1
SNP	Single-nucleotide polymorphism
SOCS-3	Suppressor of cytokine signaling 3
SOS	Son of sevenless
SREBP	Sterol Regulatory Element-Binding Protein
ss	Single-stranded
T	
T	Transcriptome
T3	Triiodothyronine
TAE-buffer	Tris acetate EDTA buffer
TBST	Tris-buffered saline-Tween 20
TEMED	Tetramethylethylendiamin
TF	Total fat cell fraction
TG / TGs	Triglyceride / Triglycerides
TLR	Toll-like receptor
TNFα	Tumor necrosis factor-alpha
tPA / uPA	Tissue plasminogen activator / urokinase plasminogen activator
TRAM-buffer	Triethanolamin buffer
U-Z	
UPR	Unfolded protein response
V	Volume
VEGF	Vascular endothelial growth factor
VLDL	Very-Low-Density-Lipoproteins
WHO	World health organization
Wnt	Wingless-Int
x g	Relative Centrifugal Force
XBP-1	X-box binding protein 1
y	Year
z score	Standard score

1 Introduction

1.1 Adipose tissue

AT mass of healthy normal weight men and women comprises of between 10 to 20 % and 15 to 25 % of total body weight, respectively [1]. Three different forms of fat tissue exist: white adipose tissue (WAT), brown adipose tissue (BAT) and bone marrow fat (yellow adipose tissue (YAT)). WAT is, however, the major form of AT [2]. Depending on its localisation a distinction is made between the subcutaneous fat (below the skin) and the visceral fat (in the mesentery, omentum and around abdominal viscera) [3]. The distribution of WAT strongly depends on age and sex. In particular, visceral AT increases with age and women tend to have more subcutaneous AT compared to men with higher amounts of visceral fat mass [4].
WAT has multiple functions in the body. It protects against mechanical and thermal influences, is an important endocrine and secretory organ and serves as an energy reservoir [1]. In periods of high food intake, fat cells store triglycerides (TGs) synthesised from glucose and fatty acids (FAs) (lipogenesis), which are taken up by adipocytes. TGs, in turn, can be mobilised during fasting periods (lipolysis) to supply energy [5]. Lipids, mainly in the form of TGs (90 - 99 %), represent about 85 % of the WAT weight. WAT further includes macrophages, vascular endothelial cells, fibroblasts as well as preadipocytes (adipocyte precursor cells) and mature adipocytes for incorporation of fat droplets. Compared to brown fat cells white adipocytes are unilocular and have only few mitochondria [5].

1.1.1 Adipose tissue growth and adipogenesis

AT growth occurs either because of an increased number of fat cells (hyperplasia) or an increased fat cell volume (hypertrophy) (chapter 1.2.1) [6]. While hyperplasia mainly takes place during pregnancy, infancy and adolescence until the age of 20, hypertrophy occurs at any time of life [7, 8]. The annual turnover rate of fat cells is

about 10 % and happens through the generation of adipocytes from mesenchymal stem cells as well as preadipocytes and adipocyte death [8].

Adipogenesis of white adipocytes begins with the transformation of embryonic stem cells into multipotent mesenchymal stem cells (MSCs), which further develop into committed white preadipocytes [9]. The presence of different adipogenic stimuli (insulin, cyclic adenosine monophosphate (cAMP), glucocorticoids (for example dexamethasone)) contribute to changes in the gene expression profile, which, in turn, result in the differentiation of preadipocytes into mature white fat cells [9, 10]. Adipocyte differentiation occurs thereby through stimulating the activity of transcription factors like CCAAT/enhancer binding protein β and δ (C/EBPβ and δ) resulting in the expression of peroxisome proliferator-activated receptor γ (PPARγ) and *C/EBPα*. C/EBPα and PPARγ regulate each other in order to preserve the differentiation process. In addition, the transcriptional activity of PPAR γ, known as master regulator of adipogenesis, is also controlled by the activity of adipocyte determination and differentiation factor 1 / sterol regulatory element-binding protein-1c (ADD1 / SREBP-1c) [11]. Finally, the transcriptional regulation of adipocyte differentiation leads to an adipocyte specific phenotype including secretion of adipokines (for example leptin) and insulin sensitivity through enhanced production of glucose transporter 4 (GLUT4) and insulin receptor (IR)) [12, 11].

1.1.2 Insulin signaling in adipose tissue

Insulin is a pancreatic hormone which reduces blood glucose concentration by stimulating glucose uptake into muscle, AT and other insulin-sensitive peripheral organs. However, the insulin-stimulated glucose absorption occurs mainly by the skeletal muscle and, to a lesser degree, by the liver and AT [13].

The function of insulin is mediated by binding to its receptor and the subsequent activation of various intracellular signaling pathways. The IR is a transmembrane receptor consisting of 4 subunits (two α- (135 kDa) and two β- (95 kDa) subunits) [14]. The α-subunits reach the extracellular space, whereas the β-subunits pass through the cellular membrane into the cytosol [14, 15]. The subunits are connected by disulfide bonds [16]. Insulin binding to the α-subunits results in an altered conformation and further autophosphorylation of tyrosine residues on the β-subunits

[15]. After transphosphorylation, the activated IR phosphorylates several proximal proteins, including insulin receptor substrate (IRS) proteins, GRB2-associated binding protein 1 (Gab-1), Shc protein isoforms, SH2B adaptor protein 2 (APS) and the proto-oncogene Casitas B-lineage lymphoma (Cbl) [17]. This leads to the activation of three different pathways: the phosphatidylinositol 3-kinase (PI3K)–AKT/protein kinase B (PKB) pathway, the Cbl/ Cbl associated protein (CAP) pathway and the Ras–mitogen-activated protein kinase (MAPK) pathway (Figure 1). While both the PI3K and the Cbl/CAP pathway in parallel seem to regulate the GLUT4 translocation process in response to insulin, the MAPK pathway plays a role in cell growth and differentiation [15, 18]. In the following, all three pathways are described in detail.

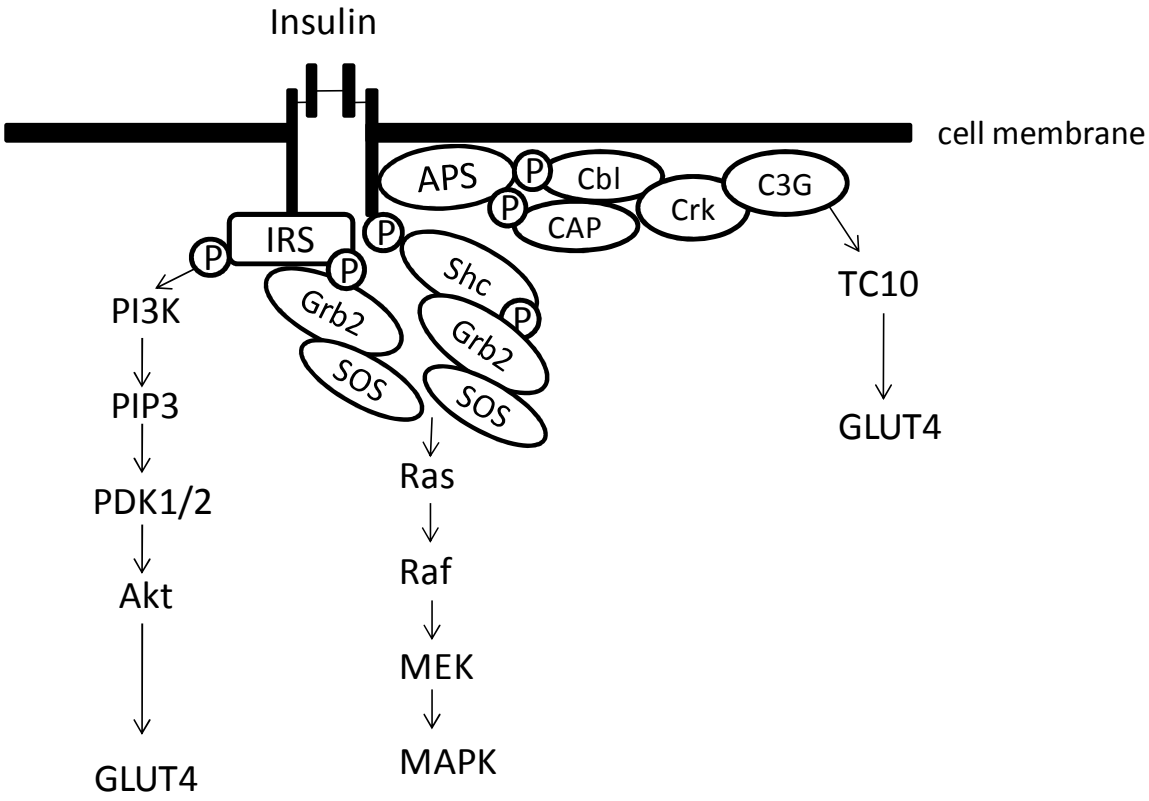

Figure 1: Insulin signaling pathways (adapted from [19]).

PI3K-pathway

Tyrosine phosphorylation of IRS proteins results in the binding of the PI3K complex. Activation of PI3K and the following generation of Phosphatidylinositol (3,4,5)-triphosphate (PIP3) cause the activation of PI-dependent kinases. Finally, PI-dependent kinases phosphorylate and activate the protein kinase Akt/PKB. Phosphorylated Akt/PKB controls protein and glycogen synthesis, glucose metabolism via GLUT4 translocation to the plasma membrane and cell survival [18] (Figure1).

Cbl/CAP pathway

The Cbl/CAP pathway involves the insulin-stimulated phosphorylation of APS and c-Cbl. Phosphorylated c-Cbl interacts with CAP, followed by binding to the lipid raft protein flotillin. Thus, the adaptor protein Crk translocates to lipid rafts and binds to the guanine nucleotide exchange protein C3G. C3G activates the small guanosine triphosphate (GTP)-binding protein TC10. Activated TC10 is required for insulin-stimulated GLUT4 translocation to the plasma membrane [18] (Figure 1).

MAPK pathway

The MAPK signaling cascade starts with the phosphorylation of IRS proteins / or Shc followed by association with the growth factor receptor bound protein-2 (Grb2). Grb2, in turn, binds and activates the guanine nucleotide exchange factor son of sevenless (SOS). This results in the conversion of guanosine diphosphate (GDP)-Ras to GTP-Ras. Subsequently, GTP-Ras activates the protein kinases Raf, MEK and MAPK leading to transcriptional regulation of cell growth and differentiation [18, 20] (Figure 1).

1.2 Obesity and adipose tissue

Obesity is defined as a body mass index (BMI) of ≥ 30 kg/m^2 [21]. In both industrialised and developing countries, the number of obese subjects has continuously increased during the last decades. In particular, more and more children

and adolescence are obese. According to the world health organization (WHO), approximately 43 million children with an age under five years are overweight [21].
As described before, AT growth occurs by hyperplasia and / or hypertrophy, where adipocytes are able to increase from a fat cell size of 25 µm up to 200 µm [5]. Some studies have already shown that obesity-linked disorders are more pronounced in hypertrophic obesity, once mean fat cell size seems to exceed a critical size [22, 23].

1.2.1 Hypertrophic adipocytes

Impaired insulin signaling

Body weight reduction is combined with a decrease in adipocyte cell size as well as improvement of insulin sensitivity [8, 24]. Small adipocytes thereby reveal a higher association with insulin sensitivity compared to the large ones [22, 25]. As mentioned above, in adipocytes, insulin acts via three pathways and two of them are involved in the GLUT4 translocation to the plasma membrane. An impaired insulin-stimulated GLUT4 translocation, which was found in hypertrophic adipocytes [26], can lead to a reduced glucose uptake in fat cells followed by an enhanced blood glucose level as well as increased hepatic glucose entrance and de novo lipogenesis [27]. Furthermore, insulin functions as an inhibitor of lipolysis in AT. Large fat cells show higher lipolytic activity compared to non-hypertrophic adipocytes [28] (see below).

Hypoxia

In AT a decreased partial pressure of oxygen (pO_2) is linked to a higher percentage of body fat and hypertrophic adipocytes are prone to hypoxic cell stress [29]. The reasons for hypoxia in AT are increased adipocyte cell size and low AT blood flow (ATBF) because of enhanced vasoconstriction or decreased fat tissue vascularisation per weight [30]. Enlarged fat cells could thereby exceed the limit of oxygen diffusion distance of 100 µm [31, 32], which leads to impaired oxygen availability. Hypoxic AT is assumed to be a reason for obesity-associated disturbances [33]. Consequences of hypoxia are, for example, insulin resistance and following induction of lipolysis in adipocytes [34, 35]. Furthermore, hypoxia is

associated with impaired adipogenesis [36] and increased production of pro-inflammatory cytokines [37, 38]. The enhanced gene expression of leptin by hypoxia provided the basis for hypoxia-induced inflammatory response of AT in obese individuals [39, 40].

Dysregulated adipocyte secretion

During weight gain, adipocyte growth leads to enhanced secretion of pro-inflammatory adipokines from the AT [41], which is suggested to cause a chronic low-grade inflammation and subsequent obesity-related dysfunctions. To date, more than 100 factors have been identified to be produced and released by AT. These products belong to different families of molecules and may exert a variety of actions.

Tumor necrosis factor-α (TNFα)

The first notion of the close link between obesity, insulin resistance and cytokine release was based on a positive correlation between *TNFα* gene expression, fat mass and hyperinsulinemia [42, 43]. TNFα, a cytokine primarily produced from macrophages, causes inflammation and insulin resistance through activation of the nuclear factor kappa-light-chain-enhancer of activated B cells (NF_KB)- or the c-Jun N-terminal kinase (JNK) pathway [44–46]. TNFα deteriorates insulin action by the stimulation of serine-phosphorylation of IRS-1 [47], by reduction of the amount of IR, IRS-1 and GLUT4 [48] as well as through the inhibition of the activity of lipoprotein lipase (LPL) [49]. TNFα knock-out mice are protected from insulin resistance despite being obese [50]. Hypertrophic fat cells were shown to have a higher secretion of TNFα compared to non-hypertrophic adipocytes [41, 51].

Leptin

Leptin is a peptide hormone (16 kDa) that is primarily produced in WAT. The main function of the satiety factor leptin is to regulate energy homeostasis [52]. Obese subjects have high plasma leptin levels despite impaired feeling of satiety due to a leptin resistance in the brain [53].Circulating levels of leptin and its expression from AT increase according to the amount of body fat mass and fat cell size [54, 55, 41]. High levels of leptin are associated with AT hypoxia [40]. In addition, leptin controls the production of pro-inflammatory cytokines [56].

Interleukin 6 (IL6)

IL6 is a cytokine which is produced at higher levels in visceral AT compared to subcutaneous fat [57, 58]. Elevated circulating levels of IL6 correlate with obesity [59]. The role of IL6 on metabolic is currently the subject of controversially discussion. IL6 is a pro-inflammatory cytokine [60], but it can also be active as an anti-inflammatory cytokine [61, 62]. Acute treatments with IL6 exhibited improved insulin sensitivity [63], whereas chronically increased IL6 levels led to impaired insulin sensitivity [64, 65]. IL6 negatively affects insulin signaling in adipocytes by the induction of the suppressor of cytokine signaling 3 (SOCS-3) mRNA expression [66] as well as the reduction of both IRS-1 and GLUT4 expression [67]. Furthermore, IL6 increases lipolytic activity in adipocytes [68] and is linked to the amount of circulating C-reactive protein [69]. IL6 therefore plays a central role in the development of cardiovascular disease (CVD) in obese subjects.

Angiotensinogen (Ang) / Angiotensin II (Ang //)

Human AT produces all components of the renin-angiotensin system (RAS) including Ang and Ang II [70, 71]. The main function of the RAS is to regulate fluid homeostasis and blood pressure [72]. Mice, which over-express Ang are hypertensive [73]. Obese subjects exhibit higher expression of Ang in AT compared to lean subjects [74]. Moreover, Ang II, which is synthesised from Ang directly induces the secretion of pro-inflammatory adipokines from AT and is thus involved in the chronic low-grade inflammation state commonly observed in obesity. For example, Ang II induces the production of plasminogen-activator-inhibitor-1 (PAI-1) [75], IL6, interleukin 8 (IL8) [76], leptin [77], monocyte chemotactic protein-1 (MCP-1) and resistin from AT [78].

Plasminogen-activator-inhibitor-1 (PAI-1)

The serine protease inhibitor PAI-1 is an adipokine secreted at higher levels from visceral compared to subcutaneous fat cells [79]. PAI-1 has anti-fibrinolytic properties. It inhibits the activation of plasminogen by inhibiting both the tissue plasminogen activator (tPA) and the urokinase plasminogen activator (uPA) [80]. Elevated levels of PAI-1 correlate with insulin resistance and CVD [81–83]. PAI-1-deficient mice are protected against obesity and insulin resistance induced by a high fat diet [84].

Chemokines

Chemokines are chemoattractive cytokines, which play a role in the infiltration of immune cells into inflamed tissue [85]. In obesity, the number of immune cells is increased because of the production of chemokines from fat tissue.[86] Enhanced penetration, especially of macrophages, induces inflammation in the tissue contributing to insulin resistance and following obesity-related diseases [87–89]. Nearly 50 chemokines are known and are grouped into the 4 distinct families CC, CXC, XC and CX3C. From these, the CC and the CXC chemokines constitute the largest families [85].

One example for the CXC family is CXCL12 (stromal cell-derived factor-1; SDF-1). According to gene splicing, two isoforms of SDF-1 exist: SDF-1α and SDF-1β. In AT, SDF-1 is produced by endothelial cells as well as adipocytes [90]. Different roles of SDF-1 and its receptor CXCR4 were observed in diabetes. In mice, SDF-1 improves pancreatic ß-cells survival and so protects against diabetes [91]. In contrast, SDF-1 is implicated in the progression of diabetes in non-obese diabetic animals (NOD) [92]. In embryonic development deficiency of SDF-1 or its receptor CXCR4 leads to lethality [93, 94].

CCL2 (monocyte chemoattractant protein-1; MCP-1) and CCL5 (Regulated upon Activation, Normal T-cell Expressed, and Secreted; RANTES) are members of the CC family.

In AT, MCP-1 is secreted by non-adipocyte and adipocyte cells [95]. Visceral AT expresses higher levels of MCP-1 compared to subcutaneous fat tissue [96]. Moreover, obese humans and animals show enhanced production of MCP-1 in AT [86, 97]. Mice lacking MCP-1 are resistant to atherosclerosis induced by visceral fat [98]. Furthermore, in differentiated 3T3-L1 cells, a murine adipocyte cell line, MCP-1 reduces insulin-induced glucose uptake as well as the expression of genes involved in adipogenesis and might therefore be linked to obesity and insulin resistant-associated diseases [97].

RANTES is expressed by T lymphocytes [99] and has a chemoattractive action towards other T cells and monocytes [100]. Both TNFα and hypoxia increase the production of RANTES in human adipocytes [101, 102]. In obesity and type 2 diabetes the transcriptional activity of RANTES in AT is enhanced with predominantly higher levels in visceral compared to subcutaneous fat tissue [86, 59, 103, 104]. Furthermore, RANTES induces a pro-inflammatory environment in the tissue [105]

and is implicated in CVD due to its involvement in the progression and composition of atherosclerotic plaques [106]. The expression of CCL5 and its receptor CCR5 is linked to the development of breast cancer [107] as well as hepatic fibrosis [108]. In contrast, RANTES protects against the human immunodeficiency-virus (HIV-1) replication [109]. RANTES blocks the viral co-receptor CCR5 on the surface of responsive cells and inhibits thereby the infection of these cells with HIV-1 [110, 111].

Hyperlipolytic adipocytes

AT is a lipid storing organ whereby up to 99 % of the lipids are TGs [5]. In case of exercise or in the fasting state, energy is provided by the activation of lipolysis in adipocytes. TGs are thus hydrolysed into FFAs and glycerol. Lipolysis is regulated via hormone-sensitive lipase (HSL), adipose triglyceride lipase (ATGL) and LPL. HSL is responsible for catecholamine- and natriuretic peptide-stimulated lipolysis, ATGL is implicated in basal-stimulated lipolysis [112] and LPL hydrolyses circulating TGs from chylomicrons and very low density lipoproteins (VLDLs) into monoacylglycerol and FFAs [113].

Different hormones and effectors can influence lipolytic activity. For example, catecholamines induce the acute adaption of lipolysis [114], whereas TNFα and glucocorticoids promote a chronic lipolytic response [115–117]. Insulin is a lipolysis inhibiting hormone. In the fed state, it suppresses adipocyte lipolysis through inhibiting HSL activity, whereas LPL activity is enhanced in AT [118]. In parallel, in muscle cells, insulin reduces LPL activity to guide FAs towards adipocytes instead of muscle cells [119, 120]. In obesity, the insulin-stimulated effect on LPL and HSL activity in adipocytes is impaired [118]. Fat cells from subcutaneous AT have an increased lipolytic action compared to those of visceral fat tissue [121]. But, adipocytes adjusted for cell size exhibit similar lipolytic capacity in both abdominal subcutaneous and omental fat cells since hypertrophic adipocytes have higher lipolytic activity compared to non-hypertrophic fat cells [121, 28].

1.3 NAFLD

NAFLD is a form of chronic liver disease. It is defined as having a fat content of more than 5 to 10 % of liver wet weight despite only moderate (less than 20 g/d for women and 30 g/d for men) alcohol consumption. NAFLD ranges from simple fatty liver (steatosis), non-alcoholic steatohepatitis (NASH) and fibrosis up to cirrhosis [122].

1.3.1 Pathogenesis of NAFLD / NASH

NAFLD is closely associated with components of the metabolic syndrome (MetS) such as obesity, type 2 diabetes and hyperlipidemia [123–125].

Currently, apart from invasive liver biopsy there are no reliable non-invasive diagnostic methods for the diagnosis of NAFLD [126]. Because of these diagnostic difficulties, the true prevalence of NAFLD is unknown. However, NAFLD is present in about 20 % of the general population [127]. The frequency of NASH increases from 3 % in non-obese subjects up to 40 % in individuals with a BMI over 40 kg/m^2 [128]. Furthermore, there are age and gender differences in the frequency of fatty liver. In younger populations, the prevalence of NAFLD is higher in men than in women, but from the age of 60 years this association inverses, probably due to the hormonal changes during menopause and following altered fat distribution as well as adipokine production [129–132]. Additionally, the development of NAFLD is influenced by genetic factors. Two single nucleotide polymorphisms (SNPs) in the apolipoprotein C3 gene (C-482T and T-455C) are linked to NAFLD as well as insulin resistance [133].

NASH represents a part within the wide spectrum of NAFLD. In 1998, the “two-hit” hypothesis was generated to explain the development of NASH [134, 135].
The increased fat accumulation in the liver (steatosis) represents the “first hit”. Under normal circumstances, insulin inhibits lipolysis in AT, but due to insulin resistance HSL activity is increased leading to enhanced FFA release from fat tissue into the circulatory system. These FFAs enter the hepatocytes (passive or via fatty acid

transport proteins (FATPs)) [136]. It is estimated that in patients with NAFLD 75 % of intra-hepatic lipids are from the periphery (60 % are AT-released FAs, 15 % are FAs from diet) and 25 % come from enhanced hepatic *de novo* lipogenesis [137, 138]. Usually, FFAs in the liver are either oxidised for adenosine triphosphate (ATP) synthesis or released as VLDL. During the development of NASH both are impaired, leading to hepatic steatosis [139, 140].

The “second hit” in the development of NASH represents the progression from fatty liver to steatohepatitis as a result of elevated hepatic FAs (lipotoxicity) and higher secretion of pro-inflammatory adipokines.

High levels of hepatic FAs are associated with extrinsically and intrinsically induced hepatic apoptosis [141]. While the extrinsic pathway includes the activation of death receptors, the intrinsic pathway is induced by 1) endoplasmic reticulum (ER) stress (chapter 1.3.2), 2) cathepsins in the cytosol as well as 3) mitochondrial dysfunctions in terms of structural (megamitochondria with crystalline inclusions) and functional abnormalities (cytochrome c release, accumulation of lipid peroxides, formation of reactive oxygen species (ROS)) [141].

Pro-inflammatory adipokines were observed to induce inflammation and fibrosis in the liver. Moreover, adipokines in the early event of liver injury can induce the synthesis of other cytokines in the liver. For instance, TNFα stimulates the secretion of the pro-inflammatory chemokine RANTES [101], which was found to be highly expressed in fibrotic livers [142].

1.3.2 NASH and inflammation

Inflammation during the development of NASH may occur due to several processes including dietary factors, ER stress, endotoxins as well as adipokines [143]. In the following, these factors are described in detail.

Dietary factors involved in the development of NASH include *trans*-FAs as well as sucrose, especially fructose. *Trans*-FAs are unsaturated FAs with trans-isomer configuration and occur as a product of bacterial metabolism or food technology [144]. Consumption of *trans*-FAs enhances the risk of CVD and liver damage by the induction of inflammation, endothelial dysfunction as well as dyslipidemia [145, 146].

Sucrose is a disaccharide composed of glucose and fructose. Consumption of fructose especially is associated with the progression of NAFLD. High intake of fructose induces intestinal bacterial overgrowth, gut permeability and endotoxin translocation into the portal vein, which may lead to ER stress, insulin resistance and enhanced hepatic TG content [147].

ER stress is caused by functional defects of the ER resulting in the activation of an unfolded protein response (UPR), the endoplasmic overload response (EOR) and / or the SREBP-pathway [148].
UPR is triggered when un- or misfolded proteins are accumulated in the ER lumen. It is mediated by three pathways, the activating transcription factor 6 alpha (ATF6 α) -, Inositol requiring enzyme 1 alpha (IRE1α)- as well as the PKR-like ER kinase (PERK)-pathway, and leads to reduced protein synthesis alongside increased expression of proteins that assist protein folding (chaperones) [141]. In patients with NASH, UPR is activated by enhanced phosphorylation of eukaryotic initiation factor 2 (eIF-2α) within the PERK pathway and the induction of JNK as well as reduction of spliced X-box binding protein 1(XBP-1) mRNA as targets of the IRE1 pathway [149].
EOR occurs when the ER is congested with proteins and contributes to the activation of the transcription factor NF-$_{\kappa}$B [150]. NF-$_{\kappa}$B in turn may induce the expression of inflammatory mediators such as TNFα and could thereby result in the progression of NASH [151].
The transcription factor SREBP is generated as inactive precursor and is fixed in the ER membrane together with *SREBP* cleavage activating protein (SCAP), a sensor for cholesterol, and Insig, which inhibits the translocation of SREBP into the nucleus. Both low levels of cholesterol and ER stress-reduced protein synthesis weaken the binding of SREBP to the ER membrane leading to its activation and binding to the Deoxyribonucleic acid (DNA) [148, 152]. Activated SREBP, in turn, could causes steatosis and insulin resistance because of its involvement in lipogenesis [153].

Endotoxins are lipopolysaccharides (LPS) in the outer membrane of gram-negative bacteria. In patients with NAFLD, plasma concentrations of endotoxins are increased (endotoxinemia) due to an enhanced intestinal permeability [154, 155]. In the liver, LPS induce NF-$_{\kappa}$B via the toll-like receptor 4 (TLR 4) and therefore lead to liver impairments [156].

Adipokines involved in NAFLD are, for example, adiponectin and TNFα. Adiponectin has anti-inflammatory properties and affects the liver through the activation of the sirtuin 1 (SIRT1)-AMP-activated protein kinase (AMPK) pathway [157]. In NAFLD, both the circulating level of adiponectin and expression of SIRT1 are reduced [158, 159], which may result in diminished FA oxidation, enhanced lipogenesis, apoptosis and increased levels of pro-inflammatory cytokines like TNFα [160]. TNFα causes insulin resistance and impairs insulin-suppressed hepatic glucose production [161]. Gluconeogenesis is defined as synthesis of glucose from non-carbohydrate sources like lactate or pyruvate. Glucose production mainly occurs in the liver where the key enzymes of gluconeogenesis pyruvate carboxylase, phosphoenolpyruvate carboxykinase (PEPCK), fructose-1,6-bisphosphatase (FBPase) and glucose-6-phosphatase (G6Pase) are expressed. Insulin inhibits hepatic glucose production, whereas glucagon stimulates it [162]. In type 2 diabetes, hepatic gluconeogenesis is enhanced, resulting in hyperglycemia predominantly in the fasting state [163]. Hyperglycemia in turn increases the progression of NAFLD via generation of TGs, oxidative stress as well as pro-inflammatory mediators [164].

2 Aim of thesis

In obesity, hypertrophic fat cells are linked to impaired insulin sensitivity of AT resulting in hyperlipolytic activity and altered adipocyte secretion pattern. Hyperlipolytic activity of AT leads to an increased release of FFAs into the circulation, which in turn can further be taken up by the liver. Next to FFAs, there is also strong evidence that secretory products of fat cells are involved in the development of NAFLD. Several pro-inflammatory adipokines were shown to be increased in subjects with NAFLD.

The aim of this thesis was therefore to gain a better insight into the biological differences between hypertrophic and non-hypertrophic adipocytes as well as to unravel the influence of increased adipocyte secreted products on hepatocytes. The analysis aimed therefore to investigate the differences between isolated small and large adipocytes within the same subject according to insulin sensitivity, their transcriptome and proteome. Furthermore, the influence of adipocytes on liver metabolism was analysed by the treatment of the rat hepatoma cell line Fao with either adipocyte-CM or defined recombinant adipokines (TNFα, IL6, Ang II, PAI-1, SDF-1α, MCP-1 and RANTES) (Figure 2). The impact of RANTES as novel adipokine was investigated in more detail according to its *in vivo* and *in vitro* effects on hepatic metabolism.

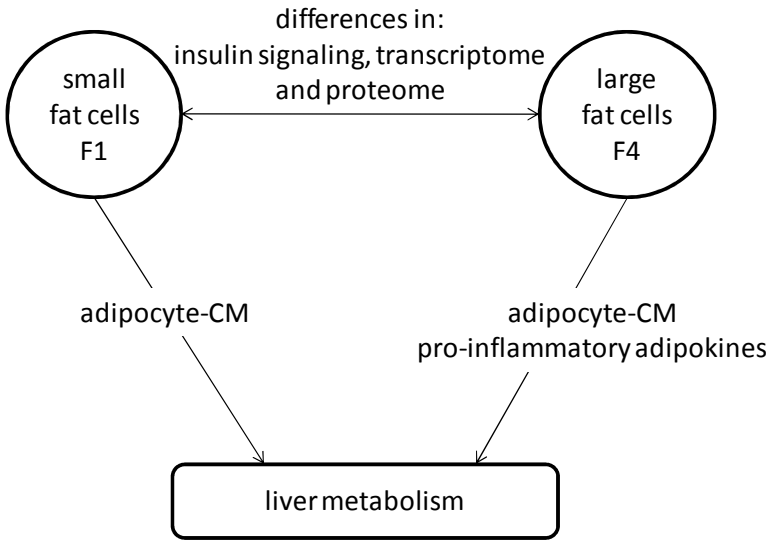

Figure 2: Schematic workflow description

3 Materials

3.1 Recombinant proteins

Lyophilised proteins were reconstituted in phosphate buffered saline (PBS) plus 0.01 % bovine serum albumin (BSA), then aliquoted and stored at - 80 °C.

- rat TNFα purchased by ImmunoTools (Friesoythe, Germany)
- rat IL6 purchased by ImmunoTools (Friesoythe, Germany)
- human Ang II purchased by Sigma-Aldrich (Steinheim, Germany)
- stable rat PAI-1 purchased by Molecular Innovations (Novi, Michigan, USA)
- rat SDF-1α purchased by PeproTech (Hamburg, Germany)
- rat MCP-1 purchased by ImmunoTools (Friesoythe, Germany)
- rat RANTES purchased by ImmunoTools (Friesoythe, Germany)
- murine RANTES purchased by PeproTech (Hamburg, Germany)
- human RANTES purchased by ImmunoTools (Friesoythe, Germany)
- human met-RANTES purchased by R&D (Wiesbaden-Nordenstadt, Germany)

3.2 Antibodies

Primary	**Catalog number; manufacturer; dilution factor (DF)**
- IRS-1	#2382; Cell signaling (Frankfurt am Main, Germany); 1:1,000
- p-IRS-1	#44-816G; Invitrogen (Karlsruhe, Germany); 1:1,000
- Akt	#9272; Cell signaling (Frankfurt am Main, Germany); 1:1,000
- p-Akt	#9271; Cell signaling (Frankfurt am Main, Germany); 1:1,000
- Erk1/2	#9102; Cell signaling (Frankfurt am Main, Germany); 1:1,000
- p-Erk1/2	#9101; Cell signaling (Frankfurt am Main, Germany); 1:1,000
- c-Cbl	#2747; Cell signaling (Frankfurt am Main, Germany); 1:1,000
- p-c-Cbl	#3555; Cell signaling (Frankfurt am Main, Germany); 1:1,000
- CCR1	#7934; Santa cruz (Heidelberg, Germany); 1:250
- CCR5	#17833; Santa cruz (Heidelberg, Germany); 1:250
- GAPDH	#AM4300; Ambion (Darmstadt, Germany); 1:4,000

Secondary	Catalog number; manufacturer; DF
Anti-mouse	#926-68020; LI-COR Biosciences GmbH (Bad Homburg); 1:20,000
Anti-rabbit	#926-32211; LI-COR Biosciences GmbH (Bad Homburg); 1:20,000
Anti-mouse	#7076; Cell signaling (Frankfurt am Main, Germany); 1:1,000
Anti-rabbit	#7074; Cell signaling (Frankfurt am Main, Germany); 1:1,000

3.3 Primers

Gene name	Primer	Sequence (5' → 3')
rat PEPCK	Sense	CATTGCCTGGATGAAGTTTGATG
rat PEPCK	Reverse	GAGCAACTCCAAAAAAACCGTTT
rat G6Pase	Sense	ACAGCGCCCGTATTGGTGGG
rat G6Pase	Reverse	ATGGCATGGCCCGAGGGACT
rat GAPDH	Sense	CCAAGGAGTAAGAAACCC
rat GAPDH	Reverse	GGTGCAGCGAACTTTATT
mouse IL6	Sense	GTACTCCAGAAGACCAGAGG
mouse IL6	Reverse	TGCTGGTGACAACCACGGCC
mouse TNFα	Sense	CCACGTCGTAGCAAACCACCAA
mouse TNFα	Reverse	GAAGAGAACCTGGGAGTAGACAAGG
mouse C/EBPα	Sense	TTTGCACCTCCACCTACATCCC
mouse C/EBPα	Reverse	CCCGTGTCCTCCTATCCC
mouse SREBP-1c	Sense	ATGGATTGCACATTTGAAGACATG
mouse SREBP-1c	Reverse	AGAGGAGGCCAGAGAAGCAG
mouse Acox 1	Sense	GAGATGGATAATGGCTACCTGAAG
mouse Acox 1	Reverse	AAACCATGGTCCCATATGTCAGC
mouse CPT-1α	Sense	GTCCCAGCTGTCAAAGATACCG
mouse CPT-1α	Reverse	ATGGCGTAGTAGTTGCTGTTAACC
mouse PPARα	Sense	CCAGTACTTAGGAAGCTGTCCG
mouse PPARα	Reverse	TATTCGACACTCGATGTTCAGGG
mouse PPARγ	Sense	AGAGTCTGCTGATCTGCGAGC
mouse PPARγ	Reverse	CGGATCGAAACTGGCACC
mouse GAPDH	Sense	CCTGGAGAAACCTGCCAAGTATG
mouse GAPDH	Reverse	GAGTGGGAGTTGCTGTTGAAGTC
mouse ACACA	QT01554441 (Qiagen, Hilden, Germany)	

3.4 Buffer recipes

3.4.1 Cell culture

Krebs-Ringer-phosphate buffer (KRP) pH 7.4
- 126.8 mM NaCl
- 12.3 mM NaH_2PO_4
- 5.1 mM KCl
- 1.3 mM $MgSO_4$
- 1.4 mM $CaCl_2$

Culture medium for adipocytes
- 1:1 vol/vol Dulbecco's modified Eagle's medium (DMEM) no glucose / Ham F12
- 0.22 mM Biotin
- 3.3 mM Sodium-pyruvate
- 1 % Penicillin / Streptomycin (Pen/Strep) (10,000 U/ml)

Proliferation medium (PM) for preadipocytes
- 1:1 vol/vol DMEM/F12
- 33.0 µM Biotin
- 17.0 µM D-panthotenate
- 1.0 % Pen/Strep (10,000 U/ml)
- 2.5 % Fetal calf serum (FCS)-F
- 132.0 nM Insulin
- 10.0 ng/ml Epidermal growth factor (EGF)
- 1.0 ng/ml Fibroblast growth factor (FGF)

Differentiation medium (DM) for preadipocytes
- 1:1 vol/vol DMEM/F12
- 33 µM Biotin
- 17 µM D-panthotenate
- 1 % Pen/Strep (10,000 U/ml)
- 66 nM Insulin
- 1 nM T3
- 0.1 µM Hydrocortison
- 10 µg/ml Transferrin

Induction medium (IM) for preadipocytes
- DM for preadipocytes
- 1 µM Rosiglitazone
- 25 nM Dexamethasone
- 250 µM 3-isobutyl-1-methylxanthine (IBMX)

Frozen medium for preadipocytes
- PM for preadipocytes
- 10 % Dimethyl sulfoxide (DMSO)

PM for Fao cells
- DMEM (25 mM glucose)
- 10 % FCS-Gold
- 1 % Pen/Strep (10,000 U/ml)

3.4.2 Kinetic assays

Glycerol-3-phosphate dehydrogenase (GPDH) activity:

GPDH-buffer
- 50 mM Tris-HCl pH 7.4
- 1 mM Ethylenediaminetetraacetic acid (EDTA)
- 1 mM Mercaptoethanol

Triethanolamin (TRAM)-buffer pH 7.5
- 1 M Triethanolamin-HCl
- 25 mM EDTA

Master-Mix per sample
- 50 µl TRAM-Buffer
- 10 µl of 5 mM Mercaptoethanol
- 5 µl NADH

Nicotinamid-Adenin-Dinucleotid-Hydrogen (NADH)
- 12 mM NADH in TRAM-Buffer

Sample-mix
- undifferentiated cells: 80 µl Sample + 350 µl auqa bidest + 65 µl Master-Mix
- differentiated cells: 40 µl Sample + 390 µl auqa bidest + 65 µl Master-Mix

Lactate dehydrogenase (LDH) activity:

Tris/NaCl
- 81.22 mM Tris
- 200 mM NaCl

NADH
- 0.24 mM NADH in Tris/NaCl

Sodium pyruvate
- 9.72 mM Sodium pyruvate in Tris/NaCl

Hepatic glucose production:

Glucose production buffer pH 7.4:
- glucose-free DMEM
- 20 mM Sodium lactate
- 2 mM Sodium pyruvate
- 15 mM 4-(2-hydroxyethyl)-1-piperazineethanesulfonic acid (HEPES)

3.4.3 Gene expression studies

50 x Tris acetate EDTA (TAE) buffer pH 8

- 242 g Tris
- 57.1 ml of 100 % Acetic acid
- 100 ml of 5 M EDTA pH 8
- ad aqua bidest to 1 l

3.4.4 Proteomic studies

Radioimmunoprecipitation assay (RIPA)-lysis buffer

- 50.0 mM Tris-HCL pH 8.0
- 150.0 mM NaCl
- 0.2 % Sodium dodecyl sulfate (SDS)
- 1 % NP-40
- 0.25 % Sodium deoxycholat
- 1 mM EDTA
- 1 tablet / 10 ml buffer PhosSTOP
- 1 tablet / 10 ml buffer Complete Mini
- 1 mM Phenylmethanesulfonylfluoride (PMSF) (immediately before use)

Buffer A for mass spectrometry (MS):

- 0.1 % Acetic acid in aqua bidest

Buffer B for MS:

- 0.1 % Acetic acid in acetonitrile

Pre-column for MS:

- RepoSil-pur C18-AQ (Dr. Maisch HPLC GmbH, Ammerbuch-Entringen, Germany)
- 20 mm x 50 µm, self packed

Analytic column for MS:

- RepoSil-pur C18-AQ (Dr. Maisch HPLC GmbH, Ammerbuch-Entringen, Germany)
- 400 mm x 50 µm, self packed

Preparation of 1 running gel for SDS-polyacrylamide gel electrophoresis (PAGE)

	7.5 % gel	10 % gel	12.5 % gel
- 30 % Acrylamid / Bis-acylamid	1.5 ml	2.0 ml	2.5 ml
- 1.5 M Tris-HCl pH 8,8	1.5 ml	1.5 ml	1.5 ml
- 10 % SDS	60 µl	60 µl	60 µl
- aqua bidest	3.0 ml	2.5 ml	2.0 ml
- Tetramethylethylendiamin (TEMED)	2 µl	2 µl	2 µl
- 10 % Ammonium persulfate	62 µl	62 µl	62 µl

5 % stacking gel

- 0.33 ml of 30 % Acrylamid / Bis-acylamid
- 0.5 ml of 0.5 M Tris-HCl pH 6,8
- 20 µl of 10 % SDS
- 1.17 ml aqua bidest
- 2 µl TEMED
- 15 µl of 10 % Ammonium persulfate

Sample loading buffer (5x)

- 300 mM Tris-HCL pH 6.8
- 5 % SDS
- 40 % Glycerin
- 0.05 M Dithiothreitol (DTT)
- 2.5 mM EDTA
- 0.01 % Bromophenol blue

Tris-buffered saline-Tween 20 (TBST)

- 2.42 g Tris
- 8 g NaCl
- 1 % Tween 20
- ad aqua bidest to 1 l

SDS-Page running buffer

- 14.4 g Glycin
- 3 g Tris
- 1 g SDS
- ad aqua bidest to 1 l

Transfer buffer semi-dry-blot

- 3.03 g Tris
- 14.4 g Glycin
- 200 ml Methanol
- ad aqua bidest to 1 l

Transfer buffer wet-blot

- 2.4 g Tris ph 8.3
- 11.25 g Glycin
- 200 ml Methanol
- 2 ml of 10 % SDS
- ad aqua bidest to 1 l

Blocking solution semi dry blot (fat cells and Fao cells): 3 % BSA in TBST

Blocking solution semi dry blot (mouse liver): 5 % Skim milk in TBST

Blocking solution wet blot: 2 % Enhanced chemiluminescence (ECL) in TBST

3.4.5 Staining solutions

4',6-diamidino-2-phenylindole (DAPI):

- DAPI: 1 µg DAPI in Methanol
- Blocking solution: 10 % Goat serum in PBS

Oil Red O:

- 0.3 % Oil Red O in 60.0 % Isopropanol

Coomassie staining:

Dyeing solution:
- 2.5 g Coomassie Blue G-250
- 45 % Methanol
- 10 % Acetic acid
- 45 % aqua bidest

Decolorizing solution:
- 10 % Acetic acid
- 30 % Methanol
- 60 % aqua bidest

4 Methods

4.1 Adipocyte culture

4.1.1 Isolation and fractionation of primary human adipocytes

AT samples were obtained from subjects undergoing elective abdominal surgery. All subjects were healthy and did not suffer from acute infections or metabolic diseases. The procedure was approved by the ethical committee of the Technische Universität München, Germany.

After surgery, AT samples were immediately transported to the laboratory in DMEM/F12 containing 1 % Pen/Strep. Connective tissue and visible blood vessels were removed and digested in KRP containing 100 U/ml collagenase and 4 % BSA fraction V for 60 min at 37 °C in a shaking water bath (80 rpm). Afterwards, adipocytes were filtrated twice through a nylon mesh with a pore size of 2,000 µm and 250 µm (VWR, Darmstadt, Germany), respectively, followed by two washing steps with PBS. Immediately after isolation fat cells were separated according to their cell size as described by Skurk et al. [41]. 10 µl of isolated adipocytes were pipetted onto a slide and the diameter of 100 fat cells from each fraction (total fat cell fraction (TF), small fat cell fraction (F1), large fat cell fraction (F4)) was determined by light microscopy (Leica Microsystems GmbH, Wetzlar, Germany). Fat cell volume (V) was calculate from the radius (r) using the equation $V = 4/3\pi r^3$.

4.1.2 Culturing of primary human adipocytes

Isolated fat cells were cultured in T75 culture flasks (BD, Heidelberg, Germany). Cells were cultured at a dilution of 1 : 6 (10 ml of fat cells + 50 ml of medium). To reduce cell stress, the first medium was changed after 30 min followed by culturing for the next two days at 37 °C in an incubator with a humidified atmosphere of 5 % carbon dioxide (CO_2). Medium was changed every day to allow adipocytes to recover from preparation.

4.1.3 Preparation of human adipocyte-CM

Adipocyte-CM was generated by culturing primary human adipocytes for 16 hours. Following, medium from each fat cell fraction was collected and cleared from cell debris by centrifugation (10 min, 1,000 x g, 4 °C) and filtration (0.20 µm pore size; Sartorius, Göttingen, Germany). For further experiments, sterile CM was diluted 1 : 2 in DMEM (5.6 mM glucose) supplemented with 1 % BSA.

4.2 Preadipocyte culture

4.2.1 Isolation and differentiation of primary human preadipocytes

Primary human preadipocytes were prepared as described previously [165]. Isolated preadipocytes were cultured in T75 flasks (BD, Heidelberg, Germany) in PM. The medium was changed every second day until cells reached confluence. Cells were collected by treatment with Trypsin/EDTA solution at 37 °C for 5 min followed by an addition of FCS-medium to interrupt trypsin activity. After determination of the cell number, aliquots of 500,000 cells/ml were frozen and stored in liquid nitrogen until further work. For differentiation studies, cells were thawed by addition of PM followed by seeding them in 6 well culture plates (BD, Heidelberg, Germany) (250,000 cells per 6 well plate). Cells were cultured at 37 °C in an incubator with a humidified atmosphere of 5 % CO_2. PM was changed on the next day and following every second day. After they reached confluence preadipocytes were induced with IM. After 3 days medium was changed to DM, which was refreshed every third day.

4.2.2 GPDH activity

The activity of the enzyme GPDH increases during adipocyte differentiation [166]. GPDH was therefore used as an indicator for adipogenesis. The enzyme GPDH together with the coenzyme $NADH+H^+/NAD^+$ catalyses the reversible reaction between dihydroxyacetone phosphate (DHAP) and glycerol-3-phosphate [162]. The maximal absorption of $NADH+H^+$ is at 260 nm and 340 nm whereas NAD^+ has its

maximal absorption at 260 nm [167]. The reduction of $NADH+H^+$ and therefore of the absorption at 340 nm reflects the amount of converted dihydroxyacetone phosphate. The activity of GPDH can be calculated by a decrease in absorbance at 340 nm.
For the assay, cells were washed twice in cold PBS before they were harvested in GPDH-Buffer. Cell solution was stored in - 80 °C until measurement. For determination of GPDH activity, GPDH samples were sonicated for 7 sec at 29 % power on ice (BANDELIN electronic, Berlin, Germany) and centrifuged (10,000 x g, 10 min, 4 °C). Then, the sample-mix was prepared in a cuvette and put into a DU 800 UV/Vis spectrophotometer (Beckman Coulter, Krefeld, Germany). 5 µl of 20 mM DHAP were added and the measurement was immediately started at 340 nm. GPDH activity was normalised by protein content, which was determined by the RCDC-Assay Kit (Bio Rad, Munich, Germany).

4.3 Hepatocyte culture

The rat hepatoma cell line Fao was kindly obtained from the University Medical Center Hamburg-Eppendorf (UKE, Hamburg, Germany). Fao cells were maintained in PM at 37 °C in an incubator with a humidified atmosphere of 5 % CO_2 in air. Cells were grown in T75 flasks (BD, Heidelberg, Germany) and PM was changed two times a week. Confluent cells were split by washing twice with PBS following treatment with Trypsin/EDTA solution for 5 min at 37 °C. Trypsin/EDTA reaction was stopped by adding PM. One part of the resulting cell suspension was diluted 1 : 10 with PM to get a maintenance culture. For the experiments, Fao cells were grown in 6-, 12-, 48- or 96-well cell culture plates (BD, Heidelberg, Germany). After they reached 80 % of confluence, cells were incubated for 24 hours in DMEM (5.6 mM glucose) supplemented with 10 % FCS and 1 % Pen/Strep.

4.4 Murine liver tissue

All procedures applied were performed by Dr. Ramona Pais and were conducted according to the German guidelines for animal care and approved by the state ethics committee under the reference number 55.2-1-54-2532-67-11. Thus, 16-17 week old

C57BL/6 mice were maintained at 22 ± 2 °C on a 12 : 12 hour light/dark cycle with *ad libitum* access to tap water and standard rodent chow (SSniff GmbH, S5745-E702). Animals were divided into two groups. The RANTES-treated group received a daily intraperitoneal (ip) injection of recombinant murine RANTES (10 µg in 200 µl PBS) for 4 consecutive days, while the control group received the same volume of PBS alone. At day 4 mice were detracted of food for 6 hours (from 7.30 - 13.30) with only *ad libitum* access to water. For an oral glucose tolerance test, each group was additional divided into two groups. 6 g/kg glucose or water were given orally immediately after the injection of RANTES/PBS. After 10 min, mice were anaesthetized with isoflurane and blood samples were obtained from the retro-orbital sinus following which they were culled by cervical dislocation. The liver was immediately isolated and snap frozen in liquid nitrogen until further analysis [168].

4.5 Adipocyte proteome

Liquid chromatography–tandem mass spectrometry (LC-MS/MS) technique is an analytic tool, which combines the separation of the sample through liquid chromatography (LC) with their following characterization by multiple steps of MS. The basic function of MS is to generate and detect ions. Components of MS are an ion source, a mass analyser as well as a detector. Samples are put into the sample introduction system followed by producing gaseous ions in the ion source. In the analyser ions are separated according to their mass-to-charge ratio (m/z), which can be detected and recorded as relative abundance of each ionic species [169].

To investigate differences in the protein composition between F1 and F4 an unlabeled LC-MS/MS analysis was performed. Therefore, isolated and fractionated fat cells were homogenized by grinding in liquid nitrogen. RIPA-buffer was added and the suspensions were treated with ultrasound (7 sec; 29 % power on ice (BANDELIN electronic, Berlin, Germany)) to optimise cell disruption. Samples were incubated on ice for 30 min and then centrifuged at 10,000 x g (10 min, 4 °C) and following at 40,000 x g (60 min, 4 °C). The resulting supernatants were used for proteomic studies. Protein concentration of each sample was determined using the BCA Protein Assay Kit (Thermo Fisher Scientific, Bonn, Germany).

All following steps were done in the lab of Prof. Küster by Fiona Pachl (Technische Universität München, Freising-Weihenstephan, Germany). Samples were lyophilised and dissolved in NuPage LDS Sample buffer supplemented with 50 mM DTT to a final concentration of 5 µg/µl. Afterwards, samples were reduced for 30 min at 70 °C and then alkylated by adding 4 µl of 200 mM iodacetamide (IAA) for 30 min in the dark. 100 µg of each sample were separated by NuPage 4 - 12 % Bis Tris Gel and each sample line was then cut into 12 slices for further digestion by trypsin. Quantitative high-performance liquid chromatography- electrospray ionization-tandem mass spectrometry (HPLC-ESI-MS/MS) was performed using a nanoLC-ultra HPLC (Eksigent, Darmstadt, Germany) coupled with an Orbitrap Elite Hybrid MS mass analyzer (Thermo Fischer Scientific, Schwerte, Germany). Peptide samples were applied to a pre-column in buffer A before transferring to the analytic column. Segmentation was done in a 2 hr-gradient of 2 - 35 % buffer B with a flow rate of 300 nl/min. At the end the eluate was injected into the mass analyzer using electrospray. MS full scan was done in the orbitrap analyzer in a mass range of 300 - 1300 m/z. Peptides were further fractionated by higher energy collisional dissociation (HCD) with normalised collision energy for HCD activation of 30. For protein identification data files from mass analysis were processed with Mascot Distiller 2.3.2 (Matrix Science, London, UK) and further transferred to Mascot 2.2.04. The resulting data file was analysed by proteome software Scaffold 3.1.2 (Proteome Software, Portland, OR, USA) where proteins were identified via database IPI.human version 3.6.8. Protein quantification was performed using Progenesis Software 4.0 (Nonlinear Dynamics, Newcastle upon Tyne, UK) and the statistical evaluation was done with paired t-test. For further investigations and in order to compare the results from proteomic and transcriptomic study accession number were converted into Gene IDs using DAVID (Database for Annotation, Visualisation and Integrated Discovery) [170, 171], NCBI (National Center for Biotechnology Information, Rockville Pike, Bethesda MD, USA (http://www.ncbi.nlm.nih.gov/gene)) as well as UniProt [172]. After removal of duplicate homologous proteins the proteome was analysed by Genomatix Software Suite (Genomatix Software GmbH, Munic, Germany (http://www.genomatix.de)) and PathVisio 2.0.11 [173] with pathways from wikipathways_Homo_sapiens_Curation-AnalysisCollection_gpml (2010-11-04) gene database Hs_derby_20110601.bridge [174].

4.6 Adipocyte transcriptome

DNA microarrays were used for the measurement of gene expression in mature human adipocytes. GeneChips® from Affymetrix were the first commercial arrays for gene expression analysis [175]. Affymetrix GeneChips are quartz chips with oligonucleotides of 25 nucleotides in length (*probes*), which are complementary to a gene specific sequence in the sample. Each probe (*perfect match*) belongs to a negative control (*mismatch*, point mutation in the 13th position). Both are summarised as one *probe pair*. Each gene is represented by 11 to 20 *probe pairs* the so called *probe set* [176]. Isolated sample ribonucleic acid (RNA) is first transcribed into double stranded complementary DNA (cDNA) and further into biotin-labeled complementary RNA (cRNA). The cRNA is next fragmented and added to the chip resulting in hybridization to complementary sequences on the array. For analysis, Streptavidin-Phycoerythrin is used to stain the incorporated biotin-labeled nucleoside triphosphates (NTPs), which can be further detected by a confocal laser scanner. The position and intensity of a probe set explains the expression rate of a single gene [177].

To examine differences between the gene expression pattern of small and large fat cells adipocytes were lysed in Trizol (1 ml Trizol per 1 ml adipocytes) and stored at - 80 °C until further RNA extraction. The Trizol-cell mixture was homogenised with a needle prior to the incubation with 400 µl chloroform for 5 min and following centrifugation at 12,000 x g at 4°C for 15 min. The aqueous layer was collected and supplemented with cold 96 % ethanol. RNA isolation was further done according to the RNeasy Mini Kit protocol (Qiagen, Hilden, Germany). The RNA concentration was quantified spectrophotometrically (Tecan, Männedorf, Switzerland). For RNA quality the RNA Integrity Number (RIN) was measured using the Agilent 2100 Bioanalyzer protocol (Agilent Technologies, Waldbronn, Germany). The RIN value (range from 10 (intact) to 1 (totally degraded)) of our samples was always > 8. All following steps were done by Dr. Martin Irmler (Helmholtz Zentrum, München, Germany). Total RNA (> 100 ng) was amplified using the Ambion WT Expression Kit and the WT Terminal Labeling Kit (Affymetrix, Santa Clara, CA, USA). Amplified cDNA was hybridized on Affymetrix Human Gene 1.0 ST DNA microarrays (Affymetrix, Santa Clara, CA, USA). Arrays were stained (Fluidics script FS450_0007) and scanned according to the Affymetrix expression protocol and

subsequently analysed by the Affymetrix Expression Console software. Statistical analyses were performed employing the statistical programming environment R (R Development Core Team [178]) implemented in CARMAweb [179]. Genewise testing for differential expression was done using the paired limma t-test in combination with the Benjamini-Hochberg multiple testing correction (False discovery rate (FDR) < 10%). After removal of duplicate homologous genes the transcriptome was analysed by the use of the Genomatix Software Suite (Genomatix Software GmbH, München, Germany (http://www.genomatix.de/)) and PathVisio 2.0.11 [173] with pathways from wikipathways_Homo_sapiens _Curation-AnalysisCollection_gpml (2010-11-04) gene database Hs_derby_20110601.bridge [174].

4.7 Adipokine secretion

The sandwich enzyme-linked immunosorbent assay (ELISA) is a method to quantify proteins by the use of antibodies. The capture antibody, a monoclonal antibody specific for the protein (antigen) of interest, is pre-coated to a microplate surface. Standards and samples bind to this antibody, whereas unbound antigens are washed away. Next, an enzyme-labelled detection antibody specific for the antigen, is added. Through the use of a substrate, which is converted by the enzyme, a colour signal is generated. The protein amount is detectable as intensity of the colour [180].
The secretion pattern of primary human preadipocytes during differentiation with and without RANTES was measured using ELISAs for human leptin and adiponectin (R&D, Wiesbaden-Nordenstadt, Germany) as well as IL6 (eBioscience, Frankfurt, Germany). Samples were diluted prior to the measurement and according to the manufacturers recommendations.

Adiponectin	- undifferentiated adipocyte day 0	diluted 1 : 1
	- undifferentiated adipocyte day 3	diluted 1 : 25
	- differentiated adipocytes day 9	diluted 1 : 500
	- differentiated adipocytes day 18	diluted 1 : 100
IL6	- undifferentiated adipocyte day 0	diluted 1 : 50
	- undifferentiated adipocyte day 3	diluted 1 : 2
	- differentiated adipocytes day 9 and 18	diluted 1 : 1

Leptin	- adipocyte differentiation day 0 - 18	diluted 1 : 1

4.8 Hepatic glucose production

Glucose release from Fao cells was determined with an enzymatic assay kit. Glucose was oxidised by glucose oxidase into gluconic acid and hydrogen peroxide. In the presence of hydrogen peroxide the enzyme peroxidase converted o-dianisidine into a coulored product, which was spectrophotometrically detectable.

For effects of adipocyte-CM on hepatic glucose output, Fao cells were washed two times with PBS and treated with adipocyte-CM. After 20 hours Fao cells were washed three times with PBS and incubated in glucose production buffer without or with insulin or db-cAMP/dexamethasone (db-CD) for 6 hours. For effects of adipokines on hepatic glucose release, Fao cells were washed two times with PBS and incubated in DMEM (5.6 mM glucose) with 0.5 % BSA and supplemented without or with adipokines. After 24 hours cells were washed three times with PBS and incubated in glucose production buffer without or with adipokines, insulin or db-CD for 6 hours.

Glucose production buffer was collected and glucose output from Fao cells was measured using the colorimetric Glucose (GO) Assay Kit (Sigma-Aldrich, Steinheim, Germany). Fao cells were washed twice with ice cold PBS and lysed in 0.2 M sodium hydroxide (NaOH). Protein concentration was determined using DC-BioRad protein assay kit (Bio-Rad Laboratories GmbH, Munich, Germany). Glucose production was normalised to protein content and is presented as percent changes of untreated controls.

4.9 Gene expression

The quantitative real time polymerase chain reaction (qRT-PCR) is considered to be a sensitive technique for the detection of gene expression levels. Quantification accomplished for example by measurement of increasing fluorescence signal from SYBR Green which binds to the double stranded DNA (dsDNA). Each PCR cycle

consist of denaturation of dsDNA to single-stranded DNA (ssDNA) followed by primer annealing and the extension step. The products of the previous cycle are used as matrices for the next cycle. The PCR process comprises up to 40 amplification cycles [181].

For RNA isolation of Fao cells, cells were washed two times with PBS and incubated in DMEM (5.6 mM glucose) with 0.5 % BSA. After 24 hours cells were washed three times with PBS and incubated in DMEM (5.6 mM glucose) without or with adipokines, insulin or db-CD for 6 hours. Next, cells were washed twice with ice cold PBS and total RNA was extracted and purified according to the manufacturers protocol (Macherey-Nagel GmbH & co. KG, Düren, Germany). For RNA isolation of mouse liver, frozen tissue was transferred to a 2 ml vial and 1 ml Trizol was added. The Trizol-tissue mixture was ground and homogenised with a needle. Sample was next incubated with 400 µl chloroform for 5 min and centrifuged at 12,000 x g at 4°C for 15 min. The aqueous layer was taken out in a fresh reaction tube and supplemented with cold 96 % ethanol. RNA isolation was further done according to the RNeasy Mini Kit protocol (Qiagen, Hilden, Germany).

Concentration and purity of isolated RNA was measured spectrophotometrically (Tecan, Männedorf, Switzerland). cDNA synthesis of 1 µg of total RNA was performed using the high-capacity cDNA Reverse Transcription Kit (Applied Biosystems, Darmstadt, Germany). The reaction mix was further put into a thermal cycler (Biometra, Göttingen, Germany) with the following program: 10 min at 25 °C; 120 min at 37 °C; 5 sec at 85 °C and ∞ at 4 °C. cDNA was diluted 1 : 5 (rPEPCK, rG6Pase) or 1 : 2 (mTNFα, mIL6, mACACA, mAcox1, mCPT-1α, mPPARα, mPPARγ, mSPREBP-1c, mC/EBPα) in PCR-water prior to qRT-PCR in the realplex2.0 Cycler system (Eppendorf, Hamburg, Germany). qRT-PCR program started with an initial denaturation step of 15 min at 95 °C followed by 15 sec at 95 °C, 30 sec at 60 °C and 30 sec at 72 °C for a total of 40 cycles. Subsequently, a melting curve analysis was performed (95 °C for 15 sec, 60 °C for 15 sec, gradual heating up to 95 °C within 20 min, 95 °C for 15 sec). Gene expression levels were calculated as described previously [182]. Target gene expression was normalised to glyceraldehyde 3-phosphate dehydrogenase (GAPDH), which was used as an endogenous control and amplified in parallel in the same run as the target gene. qRT-PCR products were visualised by agarose gel electrophoresis. A 2 % agarose gel was made in TAE-buffer with ethidium bromide. Samples were mixed with DNA

loading dye and 12 µl of those mixes were separated by electrophoresis. For reference a DNA ladder was used.

4.10 Intrahepatic triglyceride assay

Intrahepatic TGs were determined with an enzymatic assay kit. Isolated TGs were fragmented into glycerol and FAs under the catalytic influence of lipases. Glycerol was further converted to glycerolphosphate by glycerol kinase and to dihydroxyacetone phosphate and hydrogen peroxide by glycerolphosphate oxidase. Subsequently, hydrogen peroxide together with 4-aminoantipyrine and 4-chlorophenol were transformed by the enzyme peroxidase to form the coloured compound quinoneimine, which is spectrophotometrically detectable.
Frozen mice livers were pulverised and admitted in 0.9 % sodium chloride (NaCl). Afterwards, total TGs were extracted from homogenate by hydrolysation using ethanolic 0.5 M potassium hydroxide (KOH) at 71 °C for 30 min. Then, 0.15 M magnesium sulfate ($MgSO_4$) was added. The solution was mixed and centrifuged for 10 min at 13,000 x g. TGs were quantified using the triglycerides liquicolor^{mono} kit (Human GmbH, Wiesbaden, Germany). Spectrophotometric measurement at 500 nm was done using DU 800 UV/Vis spectrophotometer (Beckman Coulter GmbH, Krefeld, Germany). The amount of intrahepatic TGs was normalised to the protein content of the pulverised liver, which was assessed by the BCA protein assay (Thermo Fisher Scientific, Waltham, MA).

4.11 Western blot analysis

The western blot technique was developed in 1979 and is used to detect and quantify specific proteins in a sample probe [183]. The traditional western blot includes the separation of denatured proteins by SDS-PAGE according to their sizes. By the use of electroblotting the negatively charged and separated proteins are transferred from the gel onto a membrane. A primary antibody against the protein of interest is used to detect its antigen on the membrane. The following secondary horseradish peroxidase (HRP)-conjugated antibody binds to the membrane bound primary antibody.

Hydrogen peroxide and the chemiluminescent substrate luminol are added to the blot. Consequently, HRP converts luminol to an exit state product that emits light. The emitted light can be detected by a photographic film [167].
Liver samples were lysed in RIPA-Buffer and fat cells in Bio Rad lysis buffer supplemented with PMSF. Samples were kept on ice for 1 hour prior to centrifugation at 10,000 x g (10 min, 4 °C). Protein lysate was carefully taken off with a needle and put into a fresh reaction tube. Protein concentration was measured using the BCA Protein Assay Kit (Thermo Fisher Scientific, Bonn, Germany). Remaining sample was mixed with loading buffer and kept at 96 °C for 5 min. Each sample was separated by SDS-PAGE and transferred to either nitrocellulose membrane (Whatman GmbH, Dassel, Germany) (fat cell samples) or polyvinylidene fluoride (PVDF) membrane (Zefa-Laborservice, Harthausen, Germany) (mouse liver samples). Transfer was carried out by semi-dry blotting (Biometra, Göttingen, Germany) for p-Akt/PKB, Akt/PKB, p-Erk1/2, Erk1/2, CCR1, CCR5 and GAPDH or by a wet-blot (BioRad, Munich, Germany) for p-IRS-1, IRS-1, p-c-Cbl, c-Cbl and GAPDH. Membranes were blocked in blocking solution and incubated with primary antibodies overnight. Next, the secondary antibody was added to the membrane for 1 hour following protein detection with Odyssey infrared imaging system (LI-COR Biosciences GmbH, Bad Homburg, Germany) or ECL Advanced solution. GAPDH or Coomassie staining with following decolourizing were used for loading control. Protein quantification was done using Odyssey Software version 3.0 and ImageJ (National Institute of Health, USA, http://rsb.info.nih.gov/ij), respectively.

4.12 Cell staining

4.12.1 Oil Red O staining

Oil Red O is a diazo lipophilic dye used to visualise lipid droplets [184].
For staining of lipid droplet formation during adipogenesis cells were washed two times with cold PBS. Next, they were fixed by 3.7 % formaldehyde for 1 hour prior to the staining with Oil Red O for an additional hour. Afterwards, adipocytes were washed two times again with ice cold PBS and stored in fresh PBS at 4 °C. For staining of lipid droplets in treated Fao cells, cells were incubated for 48 hours in

DMEM (5.6 mM glucose) with 0.5 % BSA and supplemented with RANTES or palmitate (0.3 mM in 99 % methanol). Next, hepatocytes were washed two times with cold PBS and fixed by 3.7 % formaldehyde for 1 hour before staining with Oil Red O for 1 hour. Afterwards, cells were washed two times with ice cold PBS and stored in fresh PBS at 4 °C. Fat accumulation was visualised using Leica DM IL light microscopy (Leica Microsystems GmbH, Wetzlar, Germany). The amount of Oil Red O was further quantified in the hepatoma cell line Fao by extracting the dye with 100 % isopropanol for 15 min. Oil Red O intensity was quantified spectrophotometrically (Tecan, Männedorf, Switzerland) at 492 nm.

4.12.2 DAPI-staining

DAPI is a fluorescent dye which passes through cell membranes and binds to adenine-thymine rich regions in the DNA [185]. DAPI staining was therefore used for labeling cell nuclei.
Adipocytes were fixed with ice cold methanol for 5 min at 4 °C. Methanol was subsequently removed and cells were washed two times with PBS before adding the blocking solution for 30 min at room temperature (RT). After three washing steps with PBS cells were incubated in the dark with DAPI at RT for 5 min. Adipocytes were washed and stored in PBS until fluorescence microscopy with the Leica DMI4000 B (Leica Microsystems GmbH, Wetzlar, Germany). The amount of DAPI stained nuclei was analysed using ImageJ (National Institute of Health, USA, http://rsb.info.nih.gov/ij).

4.13 Cell viability

4.13.1 LDH activity in adipocytes

Fat cell viability was assessed by the measurement of LDH activity. LDH is an enzyme in the cell cytoplasm, which catalyses together with the coenzyme $NADH+H^+$ the reversible conversion of pyruvate to L-lactate [162]. LDH could be used as a cell stress marker since it is released into the culture medium upon cell lysis. The activity

of LDH can be determined by a decrease of $NADH+H^+$ and therefore of the absorption at 340 nm.
12.5 µl fat cell infranatant and 625 µl NADH were mixed in a cuvette. Afterwards, the reaction was started by adding 125 µl of sodium pyruvate. The linear decrease in absobance at 339 nm was measured spectrophotometrically (Beckman Coulter GmbH, Krefeld, Germany) for 10 min.

4.13.2 MTS-Assay on hepatocytes

Fao cell viability was assessed by 3-(4,5-dimethylthiazol-2-yl)-5-(3-carboxymethoxyphenyl)-2-(4-sulfophenyl)-2H-tetrazolium (MTS) assay. Living cells produce NADPH and NADH by dehydrogenase enzymes and are therefore able to convert MTS into a colored formazan product [186]. The amount of produced formazan correlate positively with the number of metabolically active cells and can be further quantified spectrophotometrically at 490 nm.
Fao cells were treated with adipokines as described in chapter 4.8. At the end of the incubation period, medium was changed to fresh DMEM (5.6 mM glucose). The CellTiter 96† AQueous One Solution Cell Proliferation Assay® (Promega, Mannheim, Germany) was used to detect cell viability. The reduction of MTS tetrazolium to formazan was quantified after 1.5 hours at 490 nm by spectrophotometric analysis (TECAN, Männedorf, Switzerland).

4.14 Statistical analysis

Data are expressed as mean ± standard error (SE) of the experiments measured in duplicates. Statistical analyses were performed by one-sample t-test, one way analysis of variance (ANOVA), two way ANOVA or Student's t-test. The null hypothesis was rejected at the 0.05 level. Experiments were replicated independently as indicated. All statistical analyses were performed with GraphPad Prism version 4.00 for Windows (GraphPad Software, San Diego California, USA, http://www.graphpad.com).

Results

5.1 Adipocyte characterisation

5.1.1 Adipocyte cell sizes in the study population

Fat cells of 80 patients were isolated and cell size was determined. Mean age of the patients was 41.5 ± 1.5 years and the mean BMI was 25.7 ± 0.5 kg/m^2. Adipocyte cell sizes positively correlated with the BMI (Figure 3). However, although higher BMI resulted in larger fat cell diameters the association levels off at a BMI greater 30 kg/m^2.

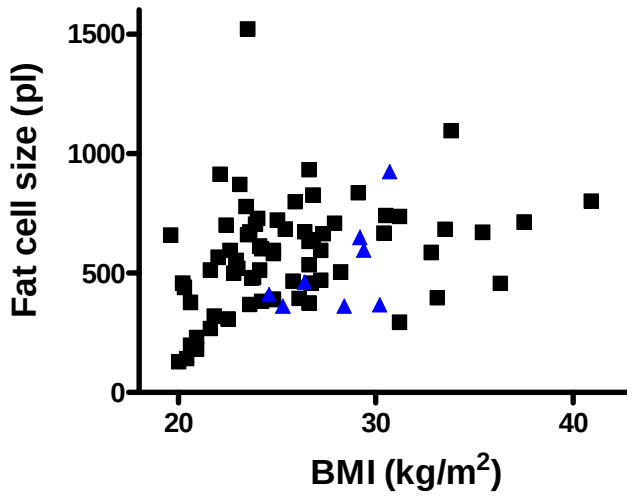

Figure 3: Distribution of mean fat cell size (pl) according to BMI. Adipocyte cell size of 80 patients (72 females (■) and 8 males (▲)) was assessed by microscopically measuring as well as calculating the volume. Adipocyte cell size was plotted in dependence of BMI. (nonparametric correlation; r^2 = 0.1317; ***p < 0.001)

For analysing differences between hypertrophic and non-hypertrophic fat cells isolated adipocytes from 18 subjects (Table 1) were separated into F1 and F4 due to their floating properties. Isolated adipocytes before fractionation are called TF. Mean fat cell sizes significantly differed between the fractions. Fat cells in F4 were 2.4-fold larger compared to fat cells in F1 (Figure 4).

Table 1: Sample characteristics for insulin signaling studies in fractionated adipocytes.

sex	age (y)	BMI (kg/m^2)	F1 cell size (pl)	TF cell size (pl)	F4 cell size (pl)
16 f; 2 m	41.6 ± 3.4	26.7 ± 1.0	343.2 ± 35.2	521.7 ± 73.6	840.4 ± 100.5

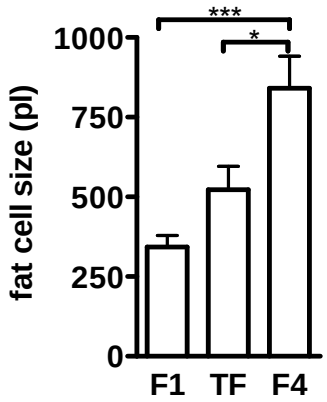

Figure 4: Distribution of adipocytes according to fat cell size (pl). Isolated fat cells of 18 patients were separated into small (F1) and large (F4) adipocytes. Results are means ± SE of fat cell size of F1, TF and F4 (one-way ANOVA followed by Tukey post-test *p<0.05, ***p<0.001).

Collagenase digestion to obtain isolated fat cells causes stress to the cells. In order to avoid influences of this cell stress on further experiments, fat cells were cultured for 32 hours. Consequently, LDH activity was 4.2-fold lower after 32 hours compared to 16 hours of culture (Figure 5).

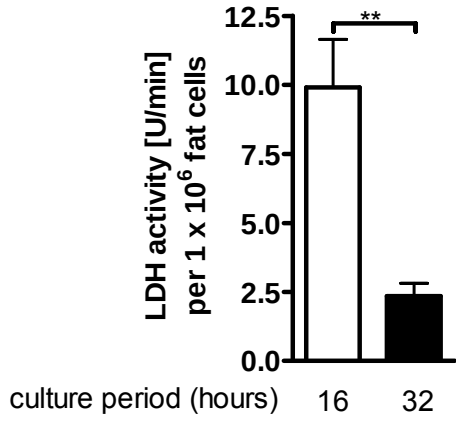

Figure 5: LDH activity of TF in dependence of the fat cell culture period. Isolated fat cells were cultured for 16 hours and 32 hours, respectively prior to the collection of fat cell infranatants. LDH activity was measured as described in Methods. Results are means ± SE of 7 independent experiments (Student's t-test **p<0.01).

5.1.2 Insulin signaling in fractionated adipocytes

Insulin signaling in hypertrophic adipocytes was hypothesised to be impaired compared to those in non-hypertrophic fat cells. To analyse whether insulin sensitivity and fat cell size are interrelated insulin signaling from F1, TF and F4 was investigated.

Fractionated adipocytes were cultured and subsequently stimulated with or without 100 nM insulin for 10 min before protein was isolated. The protein concentration from each cell fraction was measured and an increased protein amount by enlarged adipocyte size was observed. The protein concentration of F4 was 2.2-fold higher compared to F1 normalised for fat cell number (Figure 6).

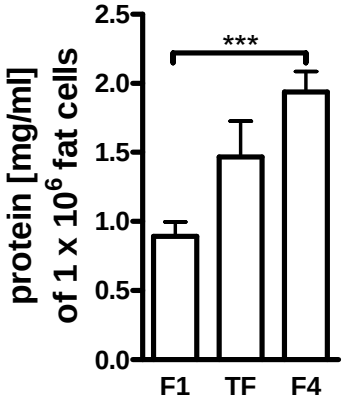

Figure 6: Protein [mg/ml] of 1 x 10^6 adipocytes separated according to cell size. Isolated fat cells of 18 patients were separated into small (F1) and large (F4) adipocytes. Results are means ± SE of protein concentration of 1 x 10^6 fat cells in F1, TF and F4 (statistical analysis between F1 and F4: Student's t-test ***p<0.001).

As protein content of mature adipocytes substantially varied, total as well as activated IRS-1, Akt, Erk 1/2 and c-Cbl were quantified by western blot analysis with GAPDH as internal control (see Methods) [187] and then corrected by protein concentration of 1 x 10^6 fat cells.

The amount of total IRS-1 was 2.5-fold, of Akt 2.6-fold, of Erk 1/2 2.6-fold and of c-Cbl 2.5-fold lower in F4 compared to F1 after adjustment by protein (Figure 7B).

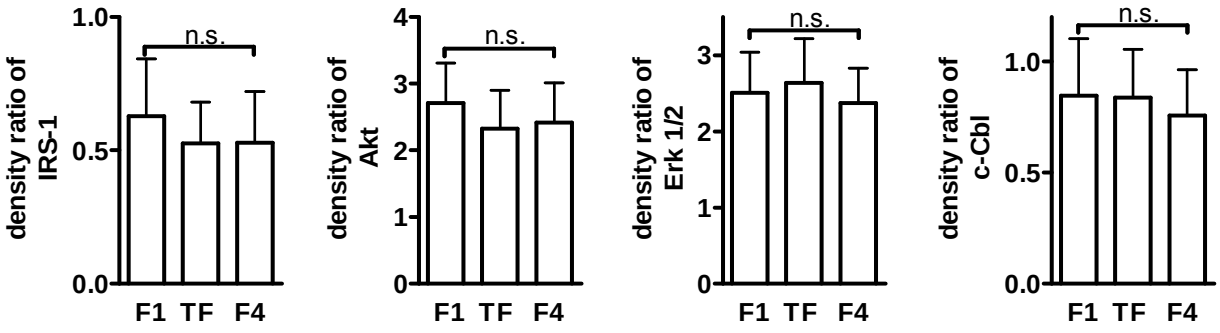

A)

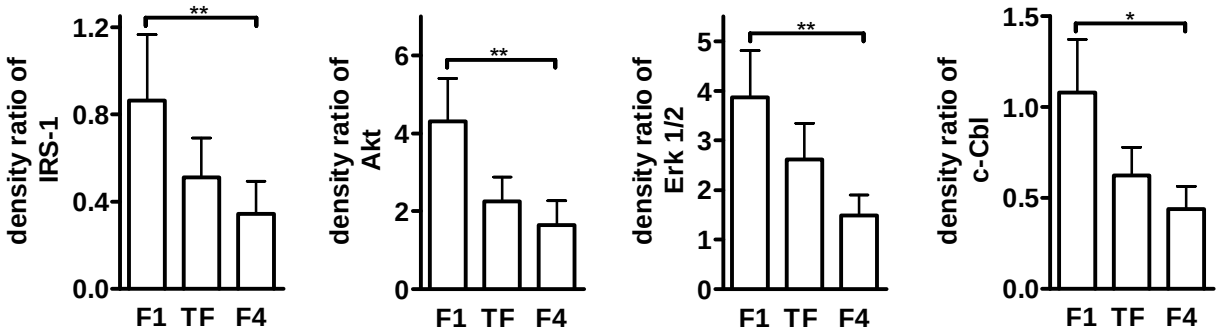

B)

Figure 7: Fat cell size dependent effect on total IRS-1, Akt, Erk 1/2 and c-Cbl. 30 µg of the total protein from F1, TF and F4 was separated by SDS-Page and analysed by western blot with GAPDH as internal control. Quantitative analysis of total IRS-1 (n = 16), Akt (n = 17), Erk 1/2 (n = 17) and c-Cbl (n = 16) before (A) and after (B) adjustment by protein concentration of 1 x 10^6 fat cells is shown as means ± SE (statistical analysis between F1 and F4: Student's t-test *p<0.05; **p<0.01; n.s. means statistically not significant).

Density ratio of both F1 and F4 showed significant activation of p-IRS-1 (F1: 5.4-fold; F4: 4.4-fold), p-Akt (F1: 2.7-fold; F4: 1.9-fold) and p-c-Cbl (F1: 1.2-fold; F4: 1.2-fold) by insulin. Furthermore, in the TF insulin markedly induced phosphorylation of IRS-1 (3.5-fold) as well as of Akt (2.8-fold). Phosphorylation of Erk 1/2 by insulin was 1.4-fold higher in F1 compared to TF. In addition, insulin-stimulated phosphorylation of c-Cbl was 1.2-fold lower in F1 compared to F4 (Figure 8A).

After normalisation of the density ratios by protein concentration of 1 x 10^6 fat cells, the amount of insulin-phosphorylated IRS-1 was 2.5-fold, of Akt 2.6-fold and of Erk 1/2 1.8-fold higher in F1 compared to F4. Moreover, compared to F4 the quantity of phosphorylated c-Cbl was higher in F1 at both before (3.1-fold) and after (2.8-fold) stimulation with insulin. Concerning TF, the amount of insulin-phosphorylated IRS-1, Akt and Erk 1/2 was markedly lower compared to F1 (p-IRS-1: 1.6-fold; p-Akt: 1.9-fold; p-Erk 1/2: 1.7-fold). Furthermore, insulin significantly phosphorylated IRS-1 (5.8-fold) and Akt (4.4-fold) in F1, but not in F4. There was, however, no significant activation of p-Erk 1/2 and p-c-Cbl by insulin in both small and large fat cell fraction (Figure 8B).

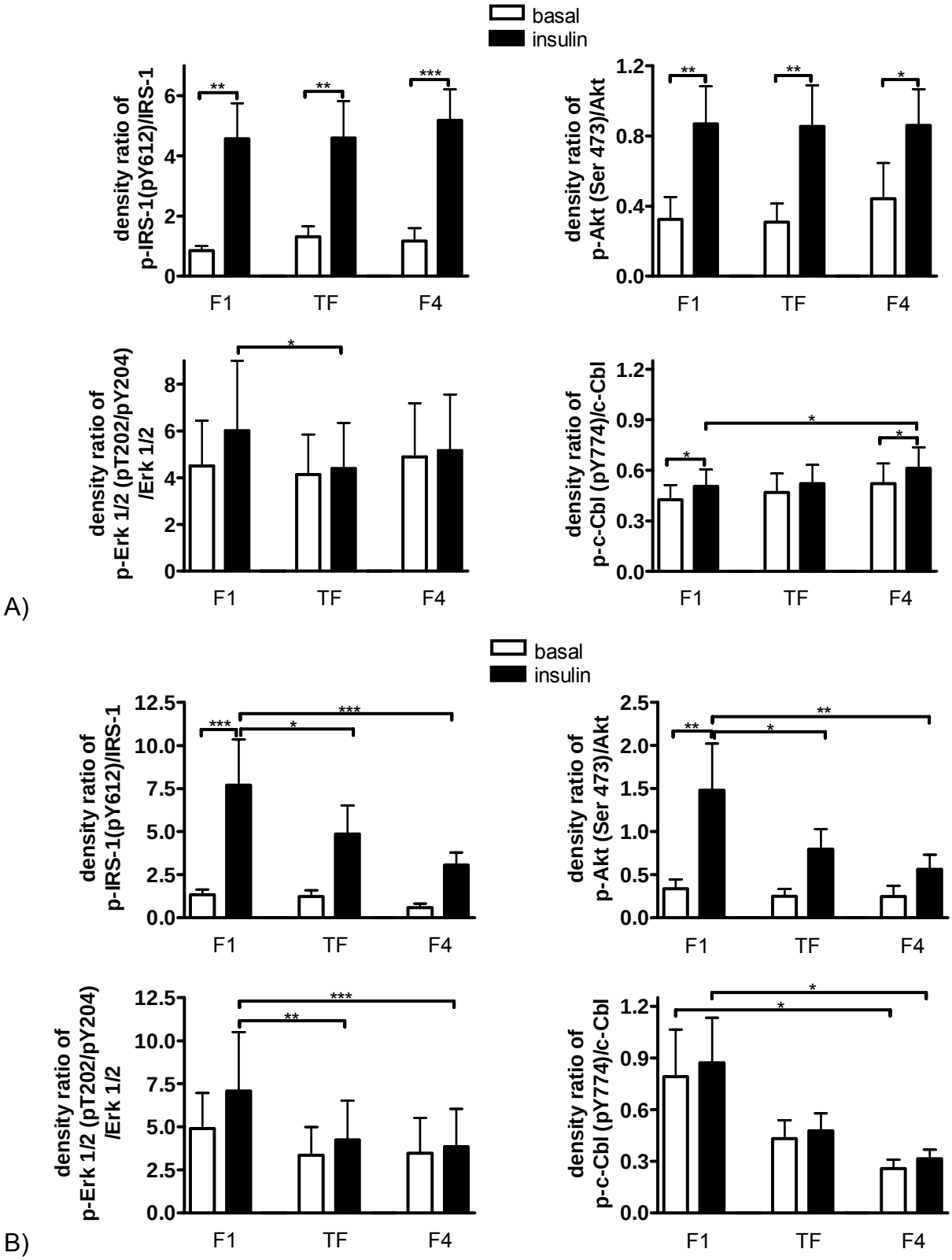

Figure 8: Effect of insulin on phosphorylation of IRS-1, Akt, Erk 1/2 and c-Cbl in dependence of fat cell size. Fractionated fat cells were treated with or without 100 nM insulin for 10min. 30 µg of the total protein was separated by SDS-Page and analysed by western blot with GAPDH as internal control. Quantitative analysis of phosphorylated IRS-1 (n = 16), Akt (n = 17), Erk 1/2 (n = 17) and c-Cbl (n = 12) before (A) and after (B) adjustment by protein concentration of 1 x 10^6 fat cells is shown as means ± SE (two-way ANOVA followed by Bonferroni post test *p<0.05; **p<0.01; ***p<0.001).

As there exists a significant association between BMI and fat cell size in the study population (Figure 3), the amount of insulin-stimulated p-IRS-1, p-Akt, p-Erk 1/2 and p-c-Cbl in dependence of BMI was investigated. The tissue donors were therefore divided into two groups (BMI < 26 kg/m^2 and BMI > 26 kg/m^2) with an approximately similar sample size (Table 2).

Table 2: Characteristics of the samples used for insulin signaling in fractionated adipocytes in dependence of BMI.

Group according to BMI (kg/m^2)	Mean BMI (kg/m^2)	Sex	Age (y)	F1 cell size (pl)	TF cell size (pl)	F4 cell size (pl)	p-value fat cell size F1 vs. F4
< 26 (median: 23.7)	23.4 ± 0.7	6 f; 1 m	42.1 ± 5.5	212.7 ± 20.8	346.3 ± 37.0	622.3 ± 122.0	0.0143
> 26 (median: 27.5)	29.4 ± 1.2	9 f; 1 m	42.3 ± 4.9	418.2 ± 42.1	544.4 ± 64.8	893.2 ± 110.6	0.0006

In F1 of both BMI groups a significantly enhanced phosphorylation of IRS-1 (low BMI: 7.2-fold; high BMI: 3.5-fold) by insulin was identified. In addition, phosphorylation of IRS-1 was significantly increased through the action of insulin in both TF (3.2-fold) and F4 (5.2-fold) of the higher BMI group. Furthermore, independence of BMI, the amount of insulin-stimulated p-IRS-1 was markedly higher in F1 compared to F4 (low BMI: 3.1-fold; high BMI: 1.5-fold) as well as in F1 compared to TF (low BMI: 1.6-fold; high BMI: 1.4-fold) (Figure 9A). After allocation according to BMI, the significant insulin-induced phosphorylation of Akt in F1 (Figure 8B) was only observed in the high BMI group (2.7-fold). Also in this group, the amount of p-Akt by insulin was 1.7-fold higher in F1 compared to TF as well as in F1 compared to F4. However, in the BMI group < 26 kg/m^2, insulin-induced phosphorylation of Akt was 6.7-fold higher in F1 than in F4 (Figure 9B). Compared to F4, insulin-stimulated p-Erk 1/2 was significantly higher in non-hypertrophic adipocytes of both BMI groups (low BMI: 1.9-fold; high BMI: 1.8-fold). In addition, the amount of p-Erk 1/2 was 1.7-fold higher in F1 compared to TF of the high BMI group (Figure 9C). Concerning c-Cbl, in the low BMI group, the amount of p-c-Cbl was higher in F1 compared to F4 at both before (4.0-fold) and after (3.5-fold) treatment with insulin. (Figure 9D).

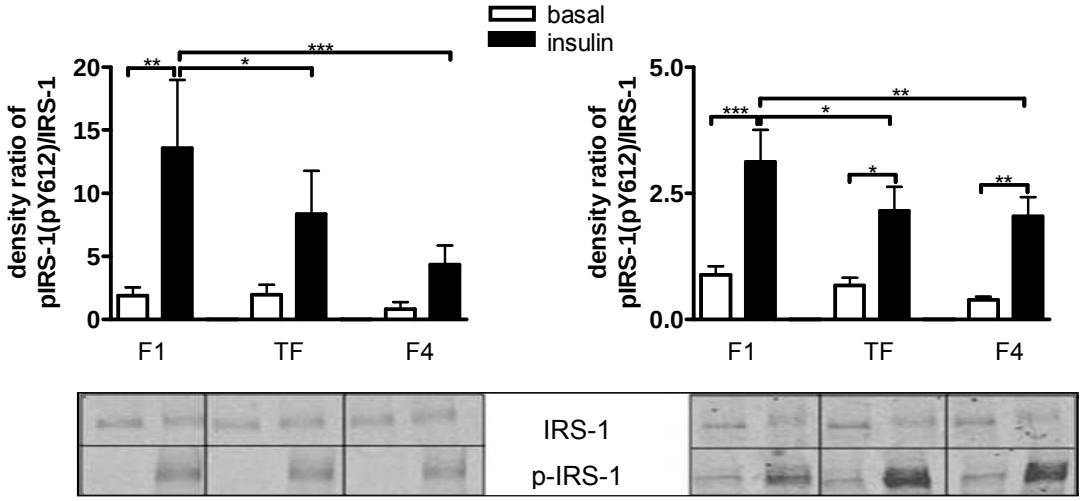

A)

BMI < 26 kg/m^2; n = 7

BMI > 26 kg/m^2; n = 9

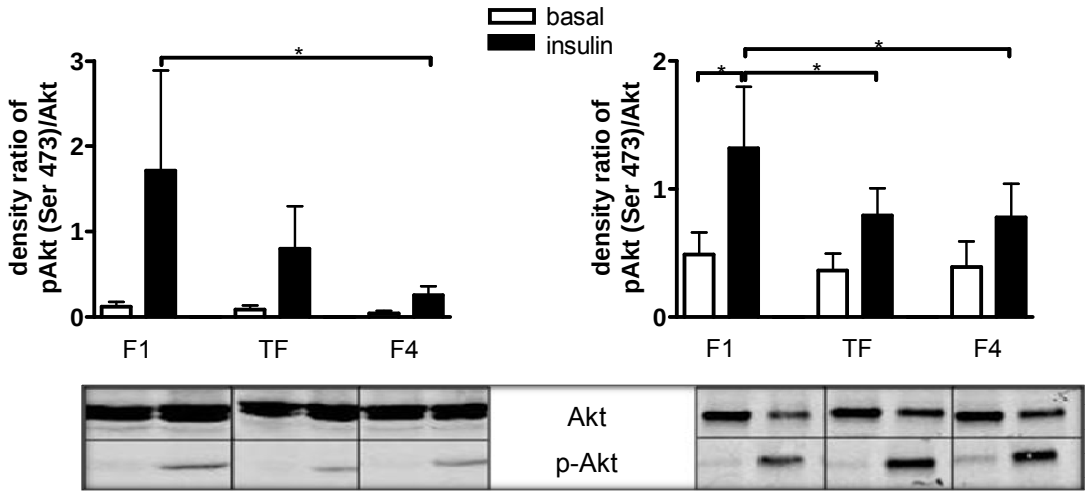

B)

BMI < 26 kg/m^2; n = 7

BMI > 26 kg/m^2; n = 10

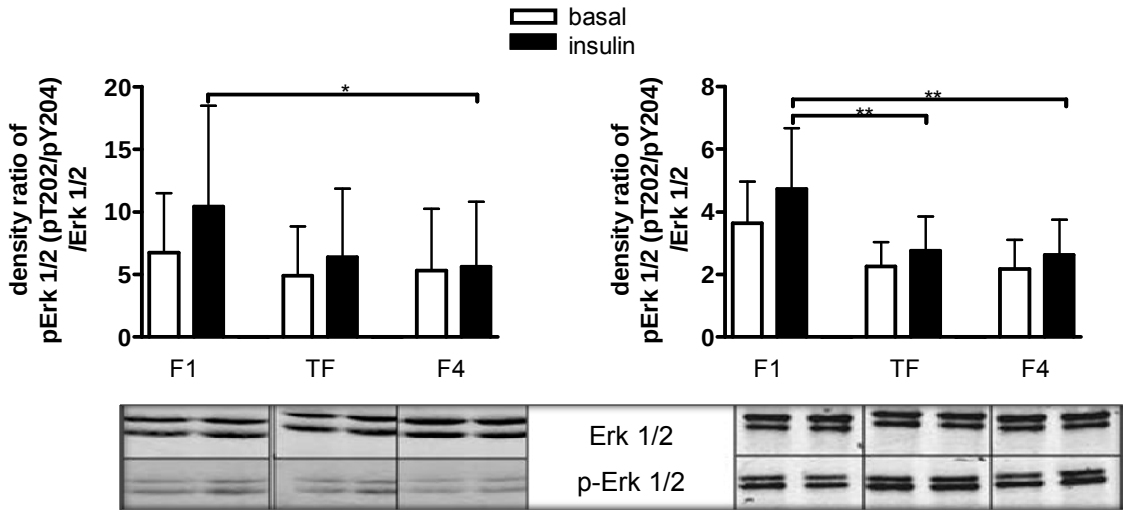

C)

BMI < 26 kg/m^2; n = 7

BMI > 26 kg/m^2; n = 10

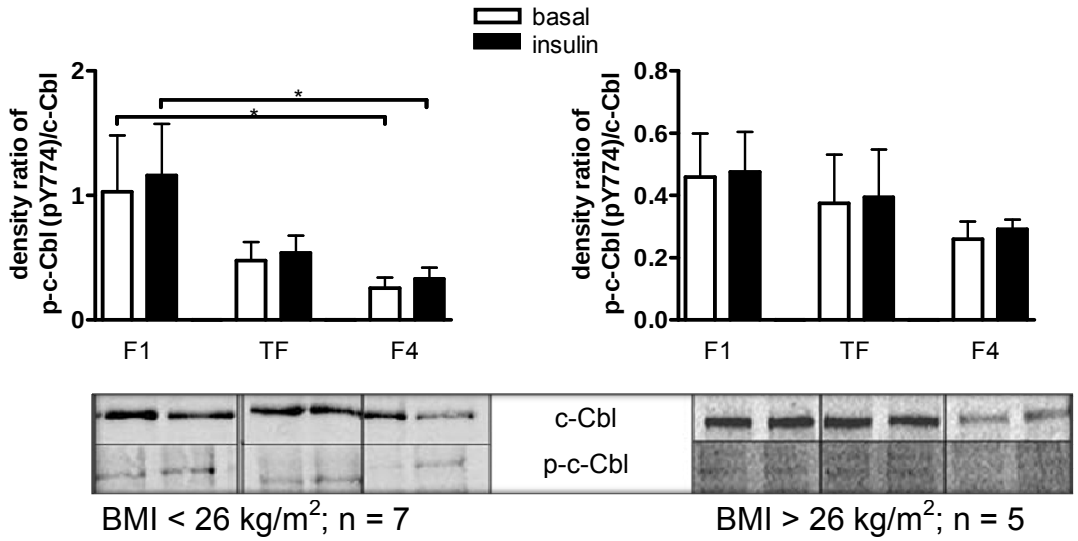

Figure 9: Fat cell size and BMI dependent effects on insulin-stimulated phosphorylation of A) IRS-1, B) Akt, C) Erk 1/2 and D) c-Cbl. Isolated and fractionated fat cells were treated with or without 100 nM insulin for 10 min. 30 µg of the total protein was separated by SDS-Page and analysed by western blot with GAPDH as internal control. Quantitative analysis of phosphorylated IRS-1, Akt, Erk 1/2 and c-Cbl was corrected by protein concentration of 1 x 10^6 fat cells and following separated according to BMI. Results are means ± SE (two-way ANOVA followed by Bonferroni post test *p<0.05; **p<0.01; ***p<0.001).

5.1.3 Proteome and transcriptome of fractionated adipocytes

In order to analyse differences in the proteomic and transcriptomic profile of hypertrophic and non-hypertrophic human adipocytes, protein and RNA of F1 and F4 were extracted as described in Methods. Proteome from five sample pairs were measured by LC-MS/MS. For seven sample pairs the transcriptome was analysed by Affymetrix GeneChip (Table 3).

Table 3: Sample characteristics for LC-MS/MS and microarray analysis, respectively.

Samples used for	BMI (kg/m^2)	sex	age (y)	F1 cell size (pl)	F4 cell size (pl)	p-value fat cell size F1 vs. F4
LC-MS/MS	24.6 ± 0.6	5 f	40.4 ± 7.3	295.6 ± 43.1	903.6 ± 94.4	0.0050
Microarray	24.2 ± 0.8	7 f	41.1 ± 5.0	270.1 ± 36.4	780.0 ± 106.9	0.0021

By LC-MS/MS 2233 protein hits were identified. Ratios between F4 and F1 of each subject were calculated and ratios ≥ 1.3 in at least three of five subjects were used for following analysis. 453 proteins fulfilled these conditions, whereby 290 proteins

were down-regulated and 163 proteins were up-regulated in F4. The statistical analysis with paired t-test ($p<0.05$) exhibited 23 significantly regulated proteins, where 17 proteins are down- and 6 proteins are up-regulated. All proteins found were analysed by PathVisio 2.0.11. [173, 174] according to $p<0.05$ and ratio ≥ 1.3. Six proteins were involved in the main regulated pathways (z score of at least 2) (Table 4).

Table 4: Main regulated pathways and significantly regulated proteins within the pathways in F4 vs. F1 analysed by LC-MS/MS. Proteome of isolated and fractionated fat cells was first analysed by LC-MS/MS and further by PathVisio.

	protein symbol	protein name	ratio	p-value	main regulated pathways	biological process
up-regulated in F4	PSMA4	Proteasome subunit, alpha type, 4	1.45	0.0294	Proteasome degradation	Regulation of cellular amino acid metabolic process
	PSMD8	Proteasome 26S subunit, non-ATPase, 8	1.50	0.0330	Proteasome degradation	Regulation of cellular amino acid metabolic process
	NDUFS4	NADH dehydrogenase (ubiquinone) Fe-S protein 4	49.03	0.0075	Oxidative phosphorylation	ATP synthesis coupled electron transport
down-regulated in F4	GBP1	Guanylate-binding protein 1	0.46	0.0439	Type II interferon signaling (IFNγ)	Cytokine-mediated signaling pathway
	SRSF3	Serine/arginine-rich splicing factor 3	0.51	0.0075	mRNA processing	RNA splicing
	SF3B5	Splicing factor 3b, subunit 5	0.15	0.0069	mRNA processing	RNA splicing

By microarray analysis 29,096 probe sets were found. The statistical analysis (cut of FDR < 10 %) resulted in 358 genes with an at least 1.3 fold different transcriptional rate between F1 and F4. 92 out of these 358 genes were down-regulated and 266 genes were up-regulated in F4 compared to F1. An additional specification of these 358 genes with $p<0.05$ exhibited 130 significantly regulated genes with 34 down-regulated genes and 96 up-regulated genes. All found genes were further analysed by PathVisio 2.0.11. [173, 174] according to $p<0.05$ and ratio ≥ 1.3 (FDR < 10 %). 24 genes were involved in the main regulated pathways (z score of at least 2) (Table 5).

Table 5: Main regulated pathways and significantly regulated genes within the pathways in F4 vs. F1 analysed by microarray. RNA of isolated and fractionated fat cells was first analysed by GeneChip Human Gene 1.0 ST DNA microarrays and further by PathVisio.

	gene symbol	gene name	ratio	p-value	main regulated pathways	biological process
up-regulated in F4	SAA1	Serum amyloid A1	2.29	0.0110	Selenium pathway	acute phase response
	SAA2	Serum amyloid A2	1.90	0.0315	Selenium pathway	acute phase response
	SAA4	Serum amyloid A4	1.86	0.0428	Selenium pathway	acute phase response
	SPS2	Selenophosphate synthetase 2	1.31	0.0483	Selenium pathway	selenocysteine biosynthesis
	FOSL	FOS-like antigen 1	1.32	0.0428	Wnt signaling pathway	response to stress
	JUN	Jun proto-oncogene	1.31	0.0464	Wnt,- MAPK pathway; Apoptosis; Senescence	response to stress
	IGF1	Insulin-like growth factor 1	1.44	0.0428	Apoptosis; Senescence and Autophagy	response to stress
	DDIT3	DNA-damage-inducible transcript 3	1.42	0.0428	Adipogenesis; MAPK signaling pathway	response to stress
	GADD45A	Growth arrest and DNA-damage-inducible, alpha	1.43	0.0428	Adipogenesis; DNA damage response	response to stress
	GADD45B	Growth arrest and DNA-damage-inducible, beta	1.49	0.0497	Adipogenesis; DNA damage response	response to stress
	GPRC5C	G protein-coupled receptor, family C, group 5, member C	1.91	0.0464	GPCRs, Class C Metabotropic glutamate, pheromone	signal transduction
	EGR1	Early growth response 1	1.61	0.0483	Insulin signaling	response to stress
	RRAD	Ras-related associated with diabetes	1.53	0.0464	Insulin signaling	signal transduction
	PLA2G2A	Phospholipase A2, group IIA	1.47	0.0428	Eicosanoid synthesis	response to stress
	MMP19	Matrix metallopeptidase 19	1.67	0.0110	Matrix Metalloproteinases	blood vessel development
down-regulated in F4	SC4MOL	Sterol-C4-methyl oxidase-like	0.65	0.0497	Cholesterol biosynthesis	lipid metabolic process
	CYP51A1	Cytochrome P450, family 51, subfamily A, polypeptide 1	0.73	0.0483	Cholesterol biosynthesis	lipid metabolic process
	G6PD	Glucose-6-phosphate dehydrogenase	0.74	0.0428	Glutathione metabolism	lipid metabolic process
	LAMB1	Laminin, beta 1	0.70	0.0474	Focal adhesion; Inflammatory response pathway	cell development
	ATM	Ataxia telangiectasia mutated	0.73	0.0464	G1 to S cell cycle control	response to stress
	DOCK1	Dedicator of cytokinesis 1	0.73	0.0428	Regulation of actin cytoskeleton	cell development
	IL1R1	Interleukin 1 receptor, type I	0.76	0.0483	Monoamine transport	response to stress
	ZFYVE16	Zinc finger, FYVE domain containing 16	0.72	0.0483	TGF beta signaling pathway	protein targeting to lysosome
	IFIT2	Interferon-induced protein with tetratricopeptide repeats 2	0.74	0.0428	Type II interferon signaling (IFNG)	response to stress

In order to investigate the posttranscriptional regulation in fat cells on adipocyte protein composition, results of both analyses, microarray and LC-MS/MS, were compared using VENNY [188]. All found regulated genes (FDR < 10 %; ratio ≥ 1.3) linked to all found regulated proteins (ratio ≥ 1.3) finally resulted in ten similarities. In each case four of the hits were down- or up-regulated in both transcriptional and protein analyses. Two findings were dissimilarly regulated in microarray vs. LC-MS/MS analyses (Table 6). An additional specification of these comparisons by p<0.05 resulted in no accordances.

Table 6: Genes and proteins which were regulated in both analyses - LC-MS/MS and microarray analysis. All regulated genes (FDR < 10 %; ratio ≥ 1.3) and proteins (ratio ≥ 1.3) were compared by Venn-diagram. Proteins which are regulated by p<0.1 in both analyses are printed in bold. HSPB6: heat shock protein beta-6; GSTM2: glutathione S-transferase mu 2; RAB9A: ras-related protein Rab-9A; PYGM: glycogen phosphorylase, muscle form; ERO1L: endoplasmic oxidoreductin-1-like protein; LMCD1: LIM and cysteine-rich domains 1; COL6A3: collagen type VI alpha 3; NID2: nidogen 2; CTSC: cathepsin C; DPYSL2: dihydropyrimidinase-like 2**.**

	up-regulated in F4 transcriptome (T)			**down-regulated in F4 transcriptome (T)**		
	symbol	**p-value (T; P)**	**ratio (T; P)**	**symbol**	**p-value (T; P)**	**ratio (T; P)**
up-regulated in F4 proteome (P)	**HSPB6**	**0.098; 0.076**	**1.37; 2.59**	ERO1L	0.090; 0.403	0.76; 1.57
	GSTM2	0.085; 0.373	1.45; 1.39			
	RAB9A	0.079; 0.320	1.38; 2.63			
	PYGM	0.061; 0.545	1.59; 2.65			
down-regulated in F4 proteome (P)	LMCD1	0.011; 0.617	1.41; 0.60	COL6A3	0.083; 0.161	0.57; 0.32
				NID2	**0.094; 0.010**	**0.69; 0.61**
				CTSC	**0.073; 0.055**	**0.68; 0.38**
				DPYSL2	0.048; 0.603	0.73; 0.45

5.2 Hepatic glucose production

The rat hepatoma cell line Fao was used for measurements concerning hepatic glucose output. Establishment of the glucose production assay is shown in appendix 8.6. Since hepatic glucose production from Fao cells was reducible by insulin and increasable by cAMP and dexamethasone, the following controls were used to evaluate changes in hepatic glucose output: 1) untreated Fao cells, 2) cells treated with 100 nM insulin and 3) Fao cells treated with 100 µM/100 nM db-CD.

5.2.1 Effect of adipocyte-CM on hepatic glucose production

CM of fractionated adipocytes from five women was obtained as described in Methods. Mean age of the patients was 49.8 ± 6.6 years (range: 31 – 66 years), the mean BMI was 28.3 ± 2.6 kg/m^2 (range: 20.9 – 36.3 kg/m^2) and the mean fat cell size was 403.6 ± 79.1 pl for F1 and 733.8 ± 120.0 pl for F4, respectively.
Compared to untreated cells (100 %) insulin significantly decreased (66.6 ± 6.7 %) and db-CD significantly increased (140.1 ± 7.9 %) hepatic glucose output (Figure 10).

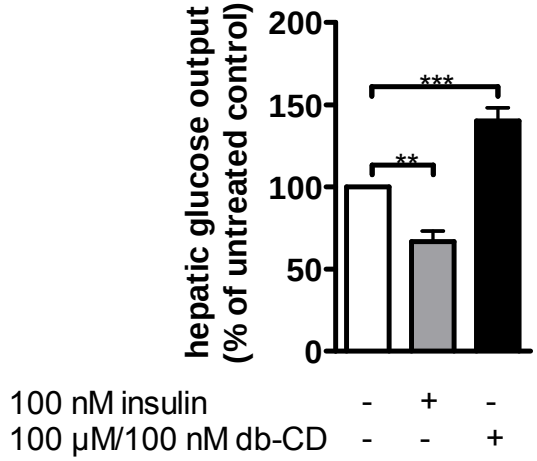

Figure 10: Basal-, insulin- and db-CD-stimulated hepatic glucose output in Fao cells treated with adipocyte culture medium. Fao cell were treated for 20 hours with culture medium for adipocytes prior to incubation in glucose production buffer supplemented with or without insulin or db-CD for 6 hours. Glucose release was measured as described in Methods. Results are means ± SE of 6 independent experiments (one-sample t-test to the untreated control **p<0.01; ***p<0.001).

Hepatic glucose release from Fao cells treated with F1-CM positively correlated with adipocyte cell size. Independent of the fat cell fraction, insulin-suppressed glucose output was attenuated by expanding cell size. In F1- and F4-treated hepatocytes db-CD-stimulated glucose release was unaffected by cell size (Figure 11).

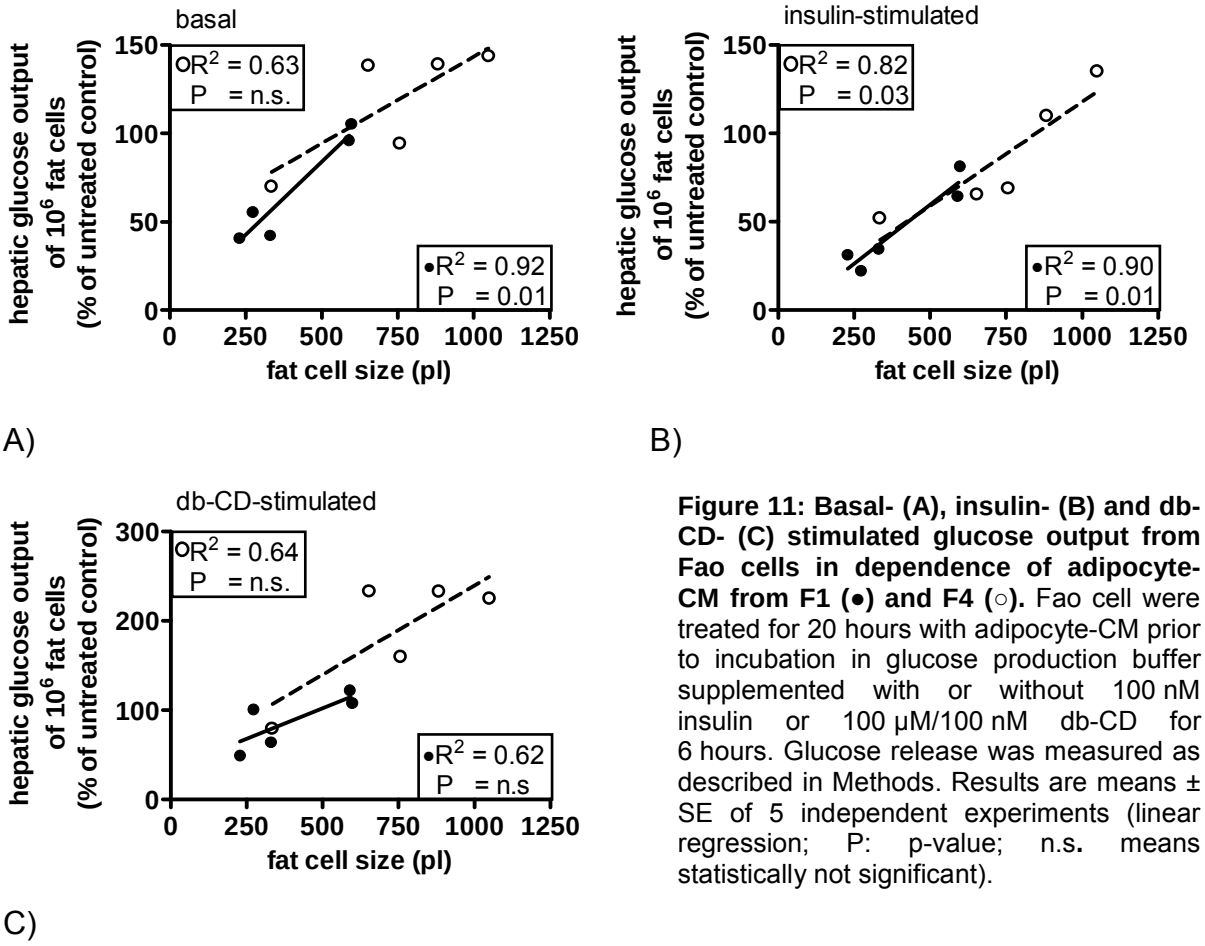

Figure 11: Basal- (A), insulin- (B) and db-CD- (C) stimulated glucose output from Fao cells in dependence of adipocyte-CM from F1 (●) and F4 (○). Fao cell were treated for 20 hours with adipocyte-CM prior to incubation in glucose production buffer supplemented with or without 100 nM insulin or 100 µM/100 nM db-CD for 6 hours. Glucose release was measured as described in Methods. Results are means ± SE of 5 independent experiments (linear regression; P: p-value; n.s**.** means statistically not significant).

5.2.2 Impact of defined adipokines on hepatic gluconeogenesis

In order to specify the effects of adipocyte-CM on hepatic glucose release, seven defined adipokines were selected and analysed according to their influence on hepatic gluconeogenesis. All adipokines were examined regarding their acute (6 hour-treatment) and chronic (30 hour-treatment) effect on hepatic glucose output

as well as their impact on gene expression of the two key enzymes of gluconeogenesis *PEPCK* and *G6Pase*.

Compared to untreated cells (100 %) insulin significantly decreased (65.4 ± 1.8 %) and db-CD significantly increased (141.2 ± 4.9 %) hepatic glucose output from Fao cells (Figure 12). Transcriptional level of *PEPCK* was 5.8-fold decreased by insulin and 5.3-fold increased by db-CD. Concerning *G6Pase* gene expression, it was 20.4-fold reduced by insulin and 2.8-fold enhanced by db-CD (Figure 13).

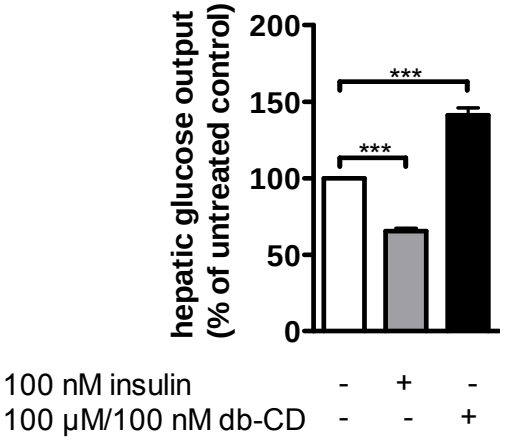

Figure 12: Basal-, insulin- and db-CD-stimulated hepatic glucose output from Fao cells. Fao cell were treated with or without insulin or db-CD for 6 hours. Glucose release was measured as described in Methods. Results are means ± SE of 45 independent experiments (one-sample t-test to the untreated control ***p<0.001).

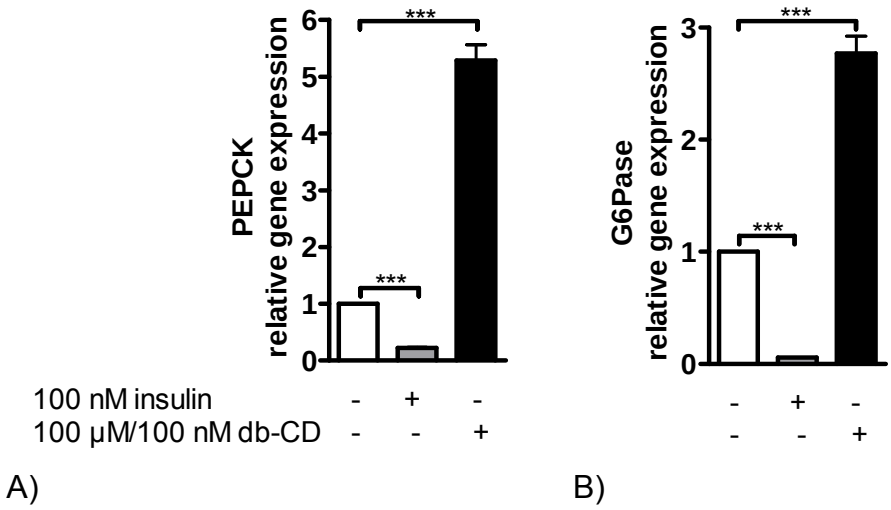

Figure 13: Basal-, insulin- and db-CD-stimulated *PEPCK* (A) and *G6Pase (B)* gene expression in Fao cells. Fao cells were treated with insulin or db-CD for 6 hours. *PEPCK* and *G6Pase* mRNA levels were measured as described in Methods. Results are means ± SE of 40 / 34 independent experiments (one-sample t-test to the untreated control ***p<0.001).

Basal hepatic gluconeogenesis

Basal hepatic glucose release measured by control cells (100 %) was significantly decreased by TNFα (39.6 ± 16.5 %), SDF-1α (68.4 ± 2.2 %) and RANTES (76.7 ± 4.5 %) after 30 hours of incubation (Figure 14).

Basal *PEPCK* gene expression was significantly enhanced by IL6 (1.8-fold) and MCP-1 (1.6-fold), whereas RANTES significantly reduced *PEPCK* mRNA level (1.1-fold) (Figure 15A). *G6Pase* gene expression was significantly down-regulated by both TNFα (4.4-fold) and IL6 (1.4-fold) as well as by the chemokine MCP-1 (1.2-fold) (Figure 15B).

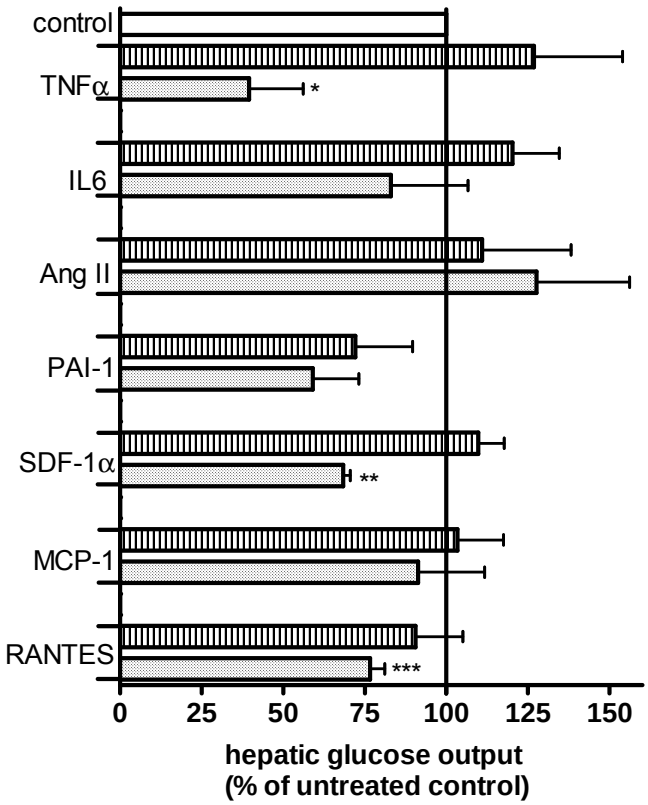

Figure 14: Impact of adipokines on hepatic glucose output from Fao cells. Fao cells were treated for 6 hours (striped) or 30 hours (filled) with 25 ng/ml rrTNFα (n ≥ 4), 200 ng/ml rrIL6 (n ≥ 4), 10^{-5} M rhAng II (n ≥ 5), 100 ng/ml rrPAI-1 (n = 4), 400 ng/ml rrSDF-1α (n ≥ 4), 400 ng/ml rrMCP-1 (n=5) or 100 ng/ml rrRANTES (n ≥ 8). Glucose release was measured as described in Methods. Results are means ± SE (one-sample t-test to the untreated control *p<0.05; **p<0.01; ***p<0.001).

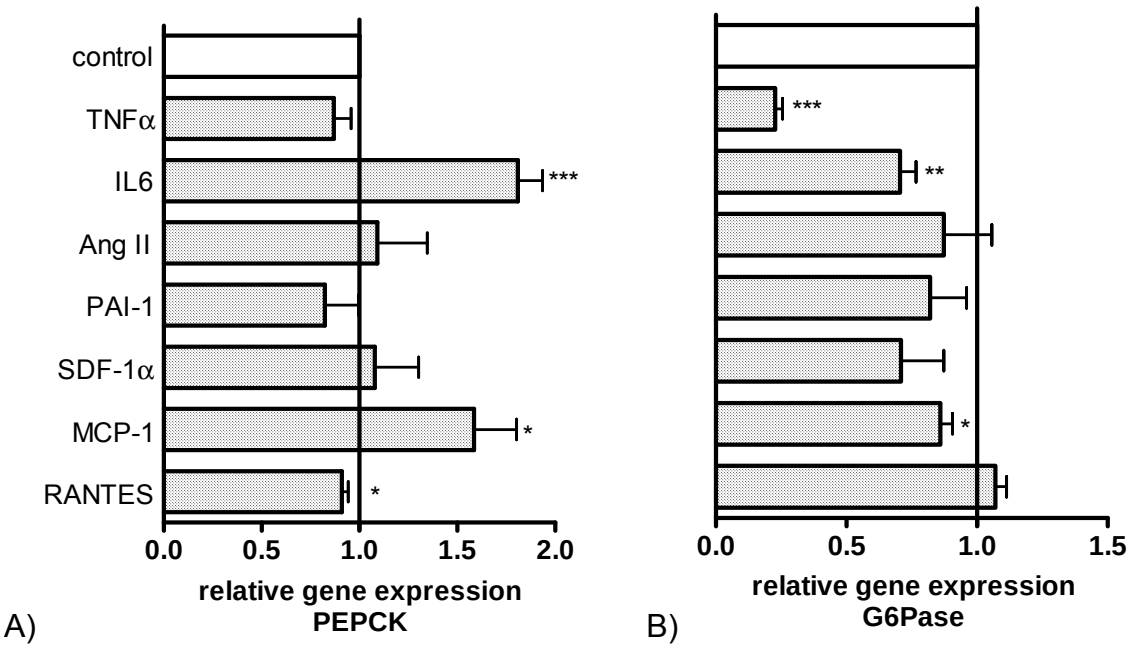

Figure 15: Effect of adipokines on *PEPCK* (A) and *G6Pase* (B) gene expression in Fao cells. Fao cells were treated for 6 hours with 25 ng/ml rrTNFα (n = 5), 200 ng/ml rrIL6 (n ≥ 5), 10^{-5} M rhAng II (n = 4), 100 ng/ml rrPAI-1 (n ≥ 4), 400 ng/ml rrSDF-1α (n = 4), 400 ng/ml rrMCP-1 (n ≥ 4) or 100 ng/ml rrRANTES (n ≥ 9). *PEPCK* and *G6Pase* mRNA levels were measured as described in Methods. Results are means ± SE (one-sample t-test to the untreated control *p<0.05; **p<0.01; ***p<0.001).

Insulin-suppression of hepatic gluconeogenesis

Insulin-suppressed hepatic glucose output (65.4 ± 1.8 %) was significantly impaired by IL6 (98.1 ± 13.0 %) and MCP-1 (82.2 ± 7.4 %) after 6 hours as well as by Ang II (89.7 ± 11.3 %) after 30 hours of treatment. In contrast, after 30 hours of incubation insulin-reduced glucose release was further decreased by TNFα (38.3 ± 15.1 %), PAI-1 (44.2 ± 11.1 %) and RANTES (55.1 ± 3.9 %) (Figure 16).

The insulin-suppressed *PEPCK* gene expression was significantly impaired after treatment with TNFα (1.7-fold), IL6 (1.9-fold), Ang II (1.4-fold), SDF-1α (1.5-fold) and MCP-1 (1.6-fold). In turn, the insulin-stimulated reduction of *PEPCK* mRNA was significantly enhanced by PAI-1 (1.9-fold) and RANTES (2.0-fold) (Figure 17A). Insulin-suppressed *G6Pase* mRNA was only influenced by TNFα and PAI-1. TNFα caused a 2.8-fold and PAI-1 a 1.6-fold enhanced reduction of *G6Pase* gene expression compared to insulin alone (Figure 17B).

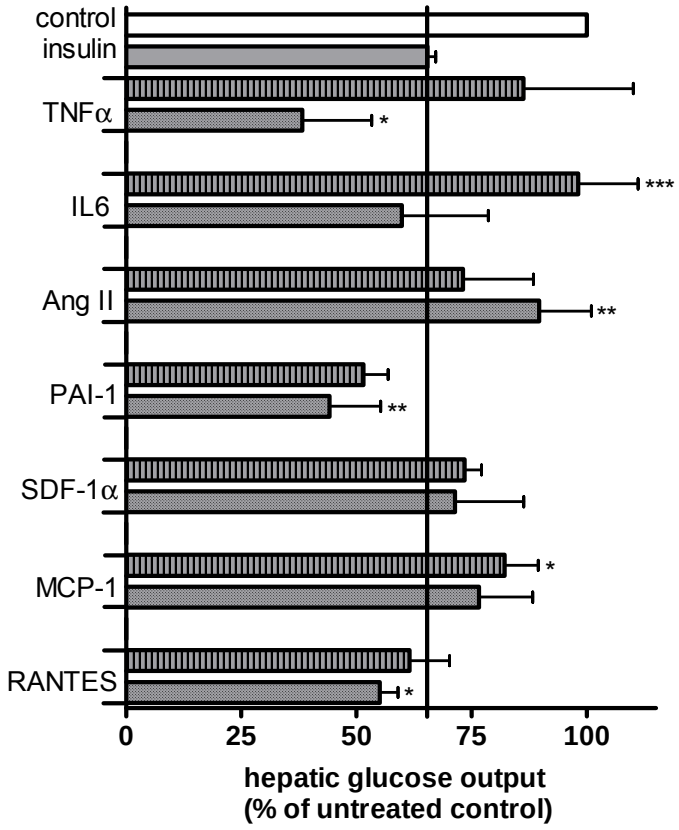

Figure 16: Impact of adipokines on insulin-stimulated hepatic glucose output from Fao cells. Fao cells were treated for 6 hours (striped) or 30 hours (filled) with 25 ng/ml rrTNFα (n ≥ 4), 200 ng/ml rrIL6 (n ≥ 4), 10^{-5} M rhAng II (n ≥ 5), 100 ng/ml rrPAI-1 (n = 4), 400 ng/ml rrSDF-1α (n ≥ 4), 400 ng/ml rrMCP-1 (n = 5) or 100 ng/ml rrRANTES (n ≥ 6) supplemented with 100 nM insulin within the last 6 hours. Glucose release was measured as described in Methods. Results are means ± SE (one-way ANOVA followed by Tukey post-test to the insulin-stimulated control *p<0.05; **p<0.01; ***p<0.001).

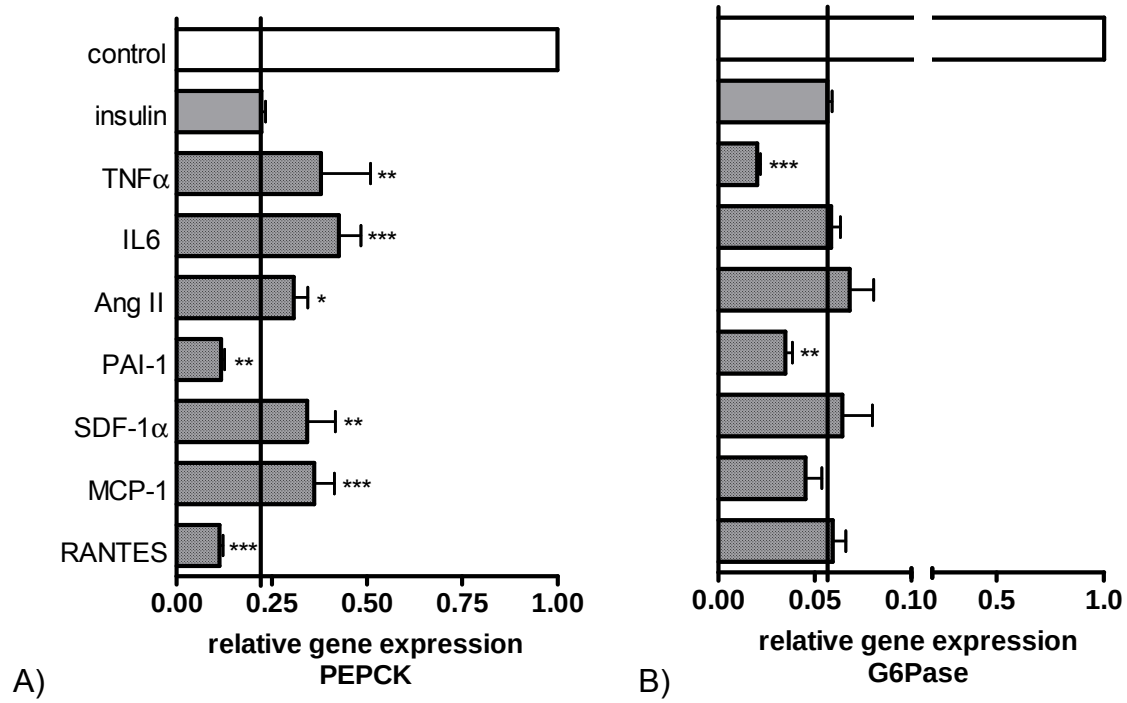

Figure 17: Effect of adipokines on insulin-stimulated *PEPCK* (A) and *G6Pase* (B) gene expression in Fao cells. Fao cells were treated for 6 hours with 25 ng/ml rrTNFα (n = 5), 200 ng/ml rrIL6 (n ≥ 5), 10^{-5} M rhAng II (n = 4), 100 ng/ml rrPAI-1 (n ≥ 4), 400 ng/ml rrSDF-1α (n = 4), 400 ng/ml rrMCP-1 (n ≥ 4) or 100 ng/ml rrRANTES (n ≥ 9) supplemented with 100 nM insulin. *PEPCK* and *G6Pase* mRNA levels were measured as described in Methods. Results are means ± SE (Student's t-test to the insulin-stimulated control *p<0.05; **p<0.01; ***p<0.001).

db-CD-stimulated hepatic gluconeogenesis

All adipokines incubated for 30 hours significantly affected db-CD-stimulated glucose release from Fao cells. The db-CD-stimulated glucose output (141.2 ± 4.9 %) was reduced by TNFα (46.2 ± 6.5 %), IL6 (81.8 ± 27.6 %), PAI-1 (86.7 ± 12.6 %), SDF-1α (91.6 ± 16.4 %), MCP-1 (102.4 ± 20.0 %) and RANTES (116.5 ± 7.8 %). In contrast, Ang II (187.8 ± 35.7 %) further enhanced db-CD-stimulated glucose release (Figure 18).

The db-CD-stimulated transcription of *PEPCK* was significantly reduced by Ang II (1.9-fold) and RANTES (2.3-fold). In contrast, SDF-1α significantly increased (1.4-fold) the db-CD-stimulated *PEPCK* gene expression (Figure 19A).
The db-CD-stimulated *G6Pase* mRNA level was significantly down-regulated by TNFα (2.3-fold), IL6 (2.2-fold), Ang II (2.0-fold), PAI-1 (2.5-fold) and RANTES (2.9-fold). In turn, SDF-1α significantly increased (1.6-fold) db-CD-stimulated gene expression of *G6Pase* (Figure 19B).

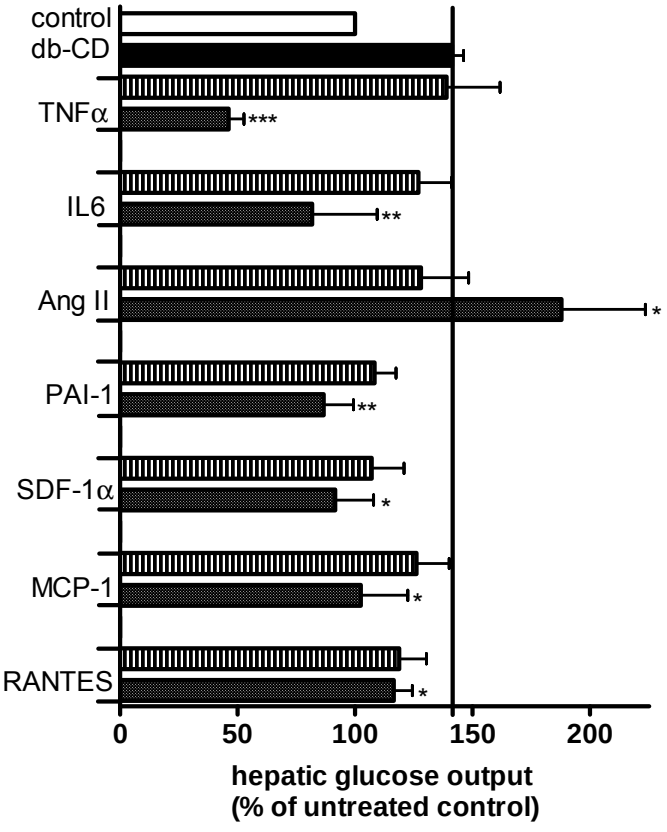

Figure 18: Impact of adipokines on db-CD-stimulated hepatic glucose output from Fao cells. Fao cells were treated for 6 hours (striped) or 30 hours (filled) with 25 ng/ml rrTNFα (n ≥ 4), 200 ng/ml rrIL6 (n ≥ 4), 10^{-5} M rhAng II (n ≥ 5), 100 ng/ml rrPAI-1 (n = 4), 400 ng/ml rrSDF-1α (n ≥ 4), 400 ng/ml rrMCP-1 (n = 5) or 100 ng/ml rrRANTES (n ≥ 7) supplemented with 100 µM/ 100 nM db-CD within the last 6 hours. Glucose release was measured as described in Methods. Results are means ± SE (one-way ANOVA followed by Tukey post-test to the db-CD-stimulated control *p<0.05; **p<0.01; ***p<0.001).

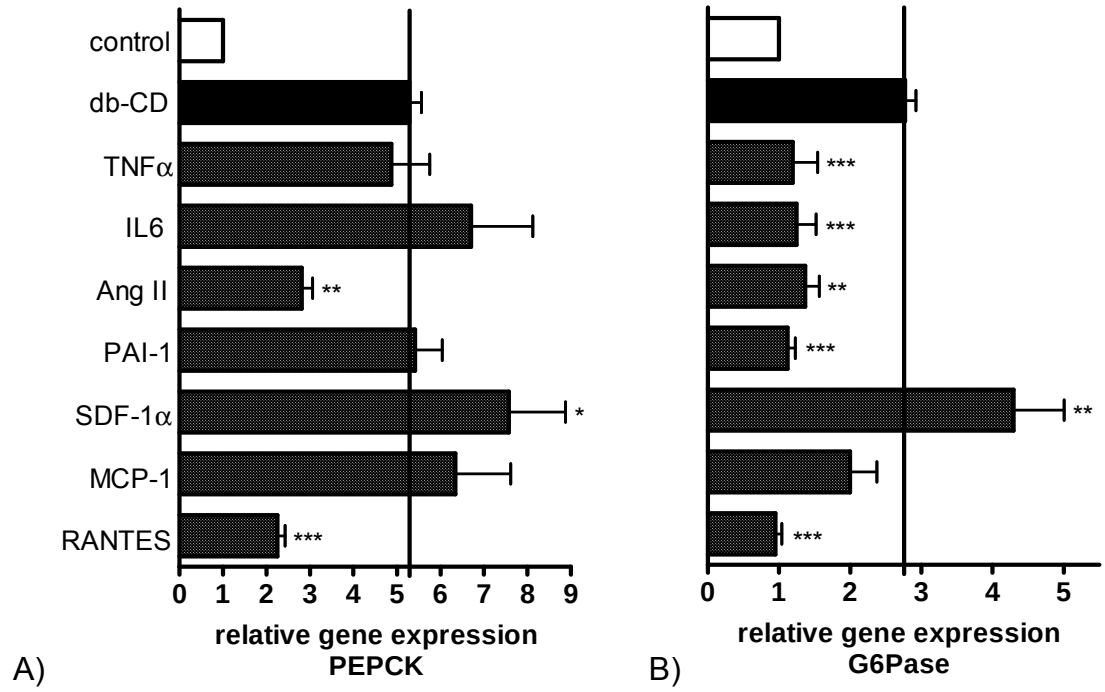

Figure 19: Effect of adipokines on db-CD-stimulated *PEPCK* (A) and *G6Pase* (B) gene expression in Fao cells. Fao cells were treated for 6 hours with 25 ng/ml rrTNFα (n = 5), 200 ng/ml rrIL6 (n ≥ 5), 10^{-5} M rhAng II (n = 4), 100 ng/ml rrPAI-1 (n ≥ 4), 400 ng/ml rrSDF-1α (n = 4), 400 ng/ml rrMCP-1 (n ≥ 4) or 100 ng/ml rrRANTES (n ≥ 9) supplemented with 100 µM/100 nM db-CD. *PEPCK* and *G6Pase* mRNA levels were measured as described in Methods. Results are means ± SE (Student's t-test to the db-CD-stimulated control *p<0.05; **p<0.01; ***p<0.001).

5.3 Impact of RANTES on Fao cells

5.3.1 Expression of receptors for RANTES on Fao cells

RANTES acts mainly through the receptors CCR1 and CCR5. Thus, the existence of both receptors in Fao cells was measured. CCR1 was clearly detectable in Fao cells, whereas CCR5 wasn´t present in these cells. In contrast, both CCR1 and CCR5 were detectable in human primary adipocytes, which served as a positive control (Figure 20).

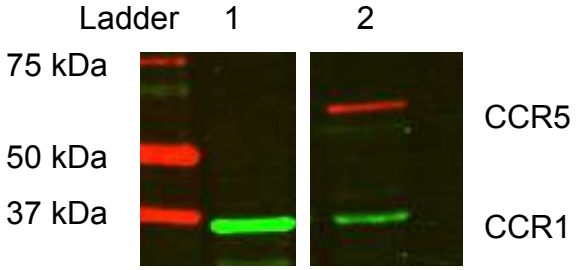

Figure 20: Western blot analysis of CCR1 and CCR5 in Fao cells. 20 µg of total protein of Fao cells (1) as well as primary human adipocytes (2) were separated on SDS-polyacrylamid gels and transferred to a nitrocellulose membrane. CCR1 and CCR5 were detected by western blot analysis as described in Methods. The figure shows one representative blot out of 3 independent experiments.

5.3.2 Impact of RANTES on hepatic gluconeogenesis in Fao cells

After CCR1 was proven in the rat hepatoma cell line Fao, the specificity of the effects of RANTES on hepatic glucose metabolism was investigated by the use of met-RANTES, a CCR1/CCR5 antagonist. Details of effects of different met-RANTES concentrations on gluconeogenesis in Fao cells are shown in appendix 8.8. Met-RANTES at 200 ng/ml was applied on Fao cells 1 hour prior to the treatment with RANTES. The additional administration of met-RANTES was capable to reverse the effects of RANTES on hepatic glucose release as well as *PEPCK* and *G6Pase* mRNA levels (Figure 21).

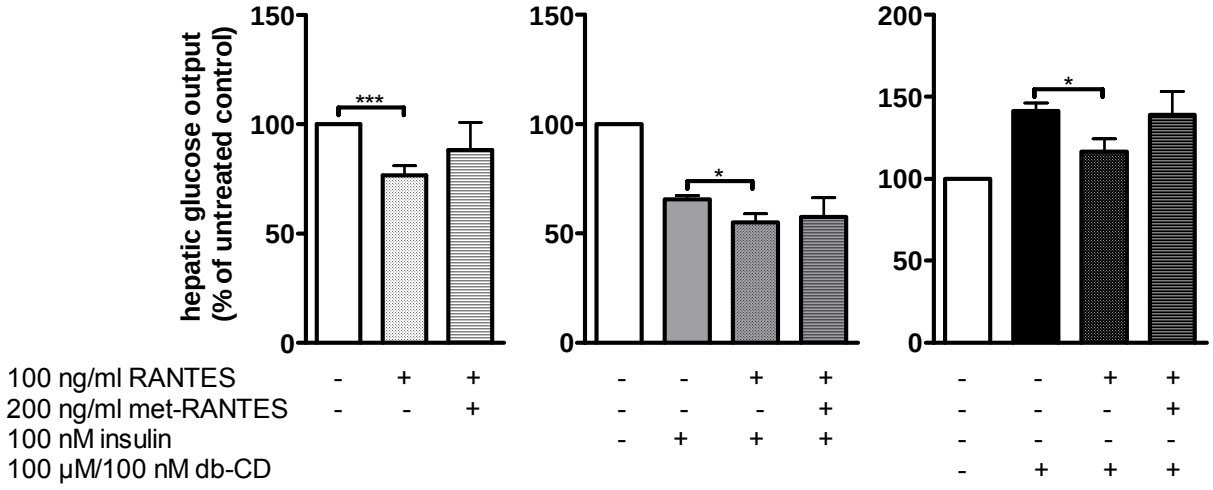

A)

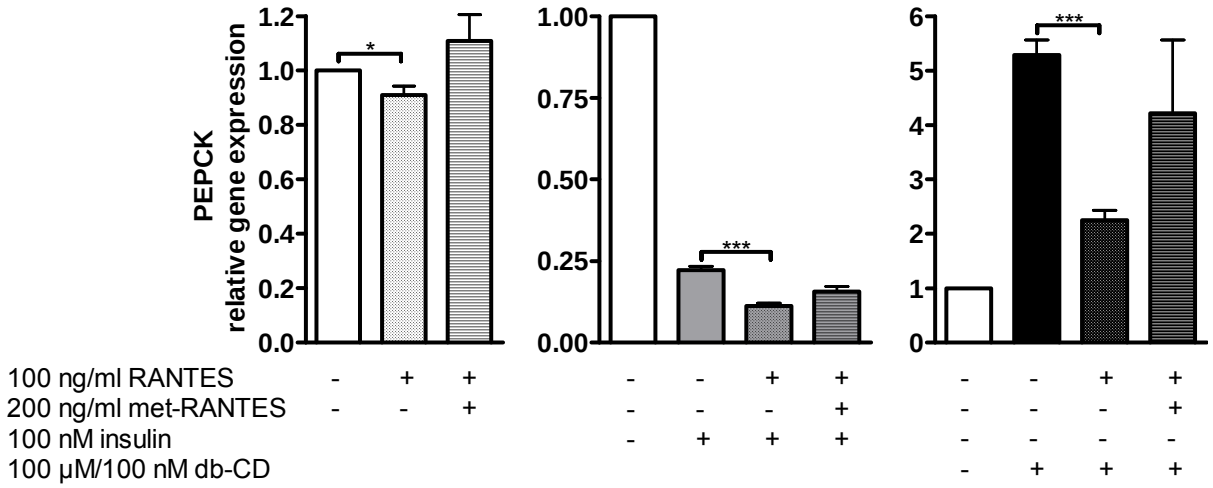

B)

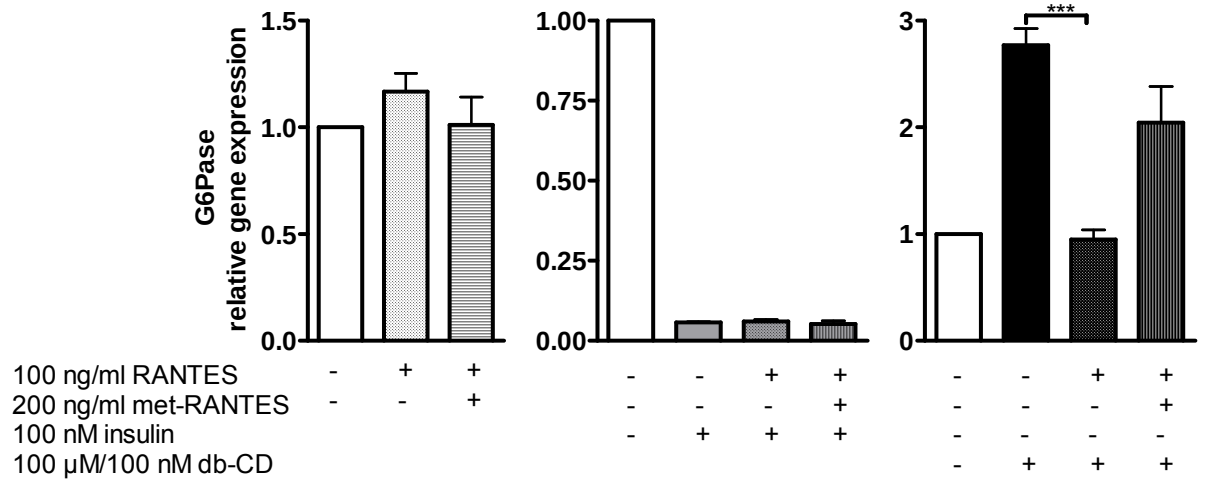

C)

Figure 21: Antagonism of RANTES-induced effects on hepatic glucose output (A) as well as *PEPCK* (B) and *G6Pase* (C) gene expression by met-RANTES. Fao cells were treated with met-RANTES, which was added 1 hour prior to rrRANTES incubation for 30 hours. Both glucose release and gene expression were measured as described in Methods. Results are means ± SE of at least 5 independent experiments (one-sample t-test or one-way ANOVA followed by Tukey post test *p<0.05; ***p<0.001).

5.3.3 Impact of RANTES on hepatic lipid accumulation in Fao cells

To examine the impact of RANTES on hepatic lipid metabolism lipid accumulation in Fao cells was measured after treatment with RANTES. Palmitate (C 16:0), a saturated FA, was used as a positive control for induction of intracellular hepatic lipid accumulation [189]. In result, recombinant RANTES increased hepatic lipid content in

Fao cells by 1.2-fold and palmitate by 1.7-fold when compared to the control cells (Figure 22).

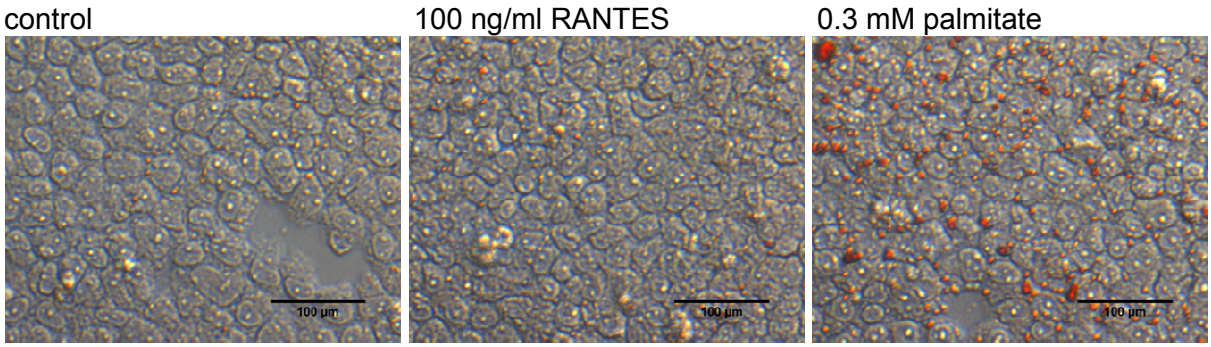

A)

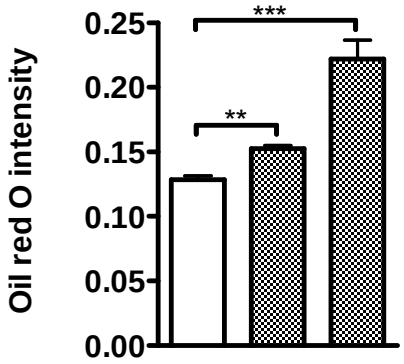

B)

Figure 22: Impact of RANTES and palmitate on hepatic lipid accumulation in Fao cells. Fao cells were treated with rrRANTES or palmitate for 48 hours. Afterwards, hepatocytes were stained with Oil Red O (A) which was further extracted and quantified using spectrometric analysis (B). Black scale bars in pictures indicate 100 µm. Results are means ± SE of 4 - 5 independent experiments (one-way ANOVA followed by Tukey post test **p<0.01; ***p<0.001).

5.4 Impact of RANTES on primary mouse liver

5.4.1 Expression of receptors for RANTES on primary mouse liver

Next to the effect of RANTES on the cell culture model Fao, the impact of RANTES on primary mouse liver was investigated.

First, mice livers were analysed concerning their content of CCR1 and CCR5. In contrast to the rat hepatoma cell line Fao both CCR1 and CCR5 were detectable in

primary mouse liver as well as primary human adipocytes, which served as a positive control (Figure 23).

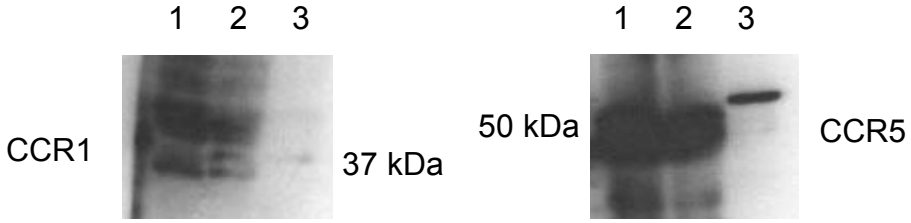

Figure 23: Western blot analysis of CCR1 and CCR5 in mouse liver. 20 µg of total protein of mice livers (1 and 2) as well as primary human adipocytes (3) were separated on SDS-Page and transferred to a PVDF membrane. CCR1 and CCR5 were detected by western blot analysis as described in Methods.

5.4.2 Impact of RANTES on lipid metabolism in mouse liver

In order to analyse the impact of RANTES on hepatic lipid metabolism *in vivo,* TG content in the liver of PBS or RANTES-treated mice was measured as described in Methods. In comparison to livers of PBS-treated mice TG content was 19.9 ± 8.3 % higher in livers of mice treated with RANTES for 4 days (Figure 24).

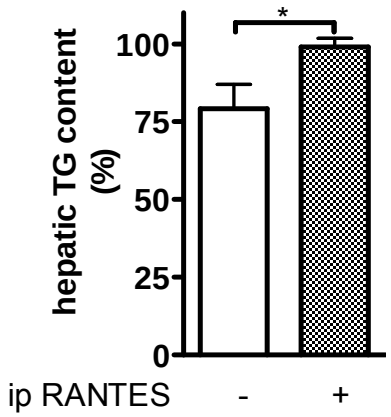

Figure 24: Impact of RANTES on TG accumulation in mouse liver. TG content in the liver of mice treated with PBS (control) or rmRANTES for 4 days. Results are means ± SE of 8 independent liver samples per group (Student's t-test *p<0.05).

Due to the fact that RANTES increased hepatic lipid content *in vitro* and *in vivo*, expression of genes involved in hepatic lipid metabolism was analysed in mice livers. Next to the expression of *Acox 1*, *CPT-1α*, *PPARα*, *PPARγ* and *ACACA* only *SREBP-1c* and *C/EBPα* were significantly affected by RANTES compared to the

control. The transcriptional level of *C/EBPα* and *SREBP-1c* was thereby 1.5-fold and 1.4-fold, respectively, lower in the livers of RANTES-treated mice (Figure 25).

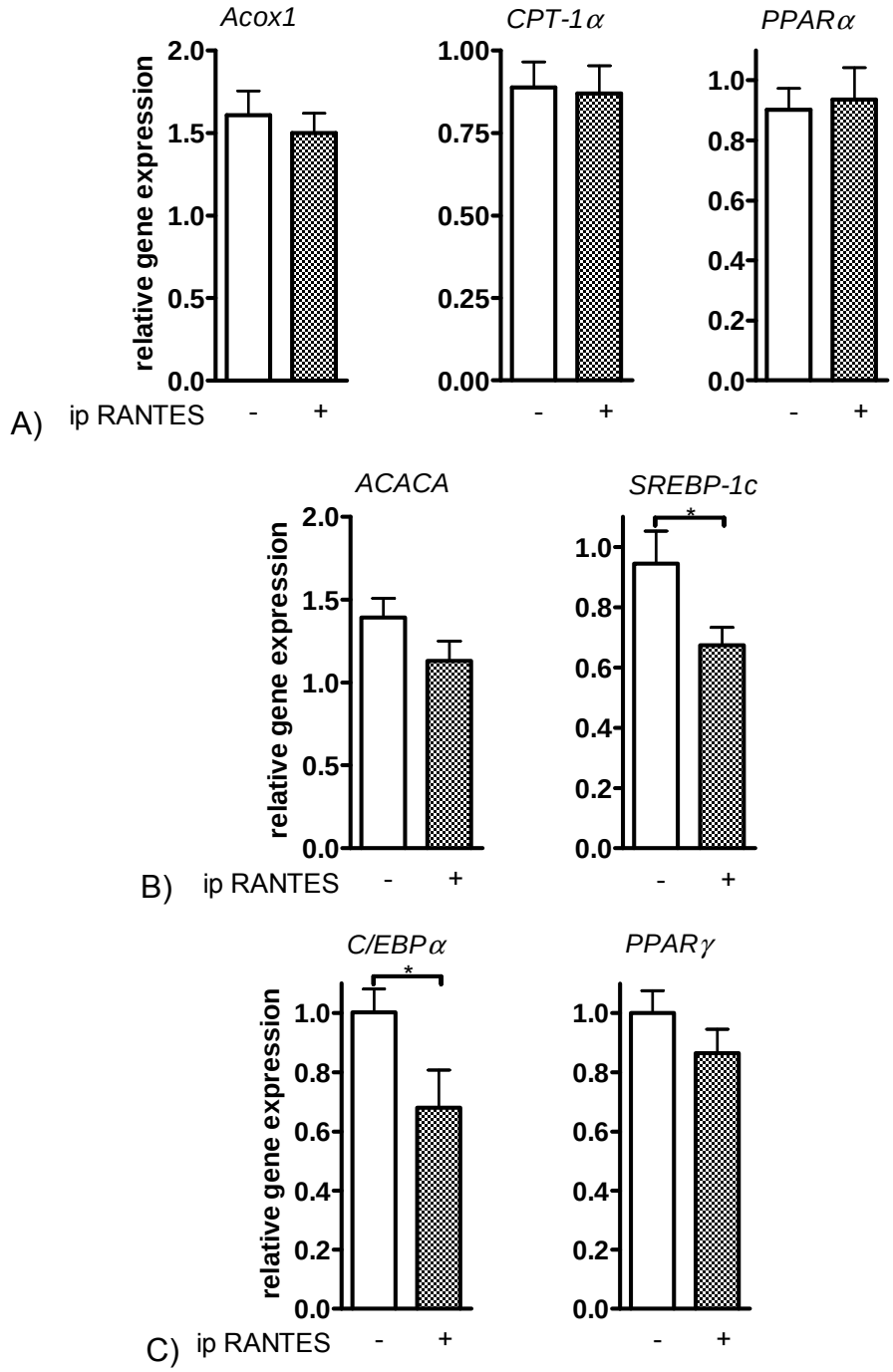

Figure 25: Impact of RANTES on expression of genes associated with hepatic lipid metabolism in mouse liver. Mice were treated with PBS or rmRANTES for 4 days prior to liver isolation. Total RNA from mice without glucose administration was prepared and analysed as described in Methods by using a primer specific to *Acox1*, *CPT-1α*, *PPARα*, *ACACA*, *SREBP-1c*, *C/EBPα* and *PPARγ*. A) genes involved in FA oxidation; B) genes involved in FA synthesis; C) other genes involved in lipid metabolism. Results are means ± SE of 4 - 5 independent liver samples (Student's t-test *p<0.05).

5.4.3 Impact of RANTES on insulin signaling in mouse liver

Insulin has an essential role in maintening glucose and lipid homeostasis and as differences in hepatic glucose and lipid metabolism has been observed by RANTES, the impact of RANTES on insulin signaling was analysed. Insulin acts on the cells via two major pathways: the Akt/PKB pathway and the MAPK pathway. Both, phosphorylation of Akt and Erk 1/2 as part of the MAPK pathway were quantified in mice livers. Although not statistically significant, RANTES decreased activation of Akt (1.4-fold). In contrast, activation of Erk 1/2 was significantly increased due to treatment with RANTES (2.8-fold) (Figure 26).

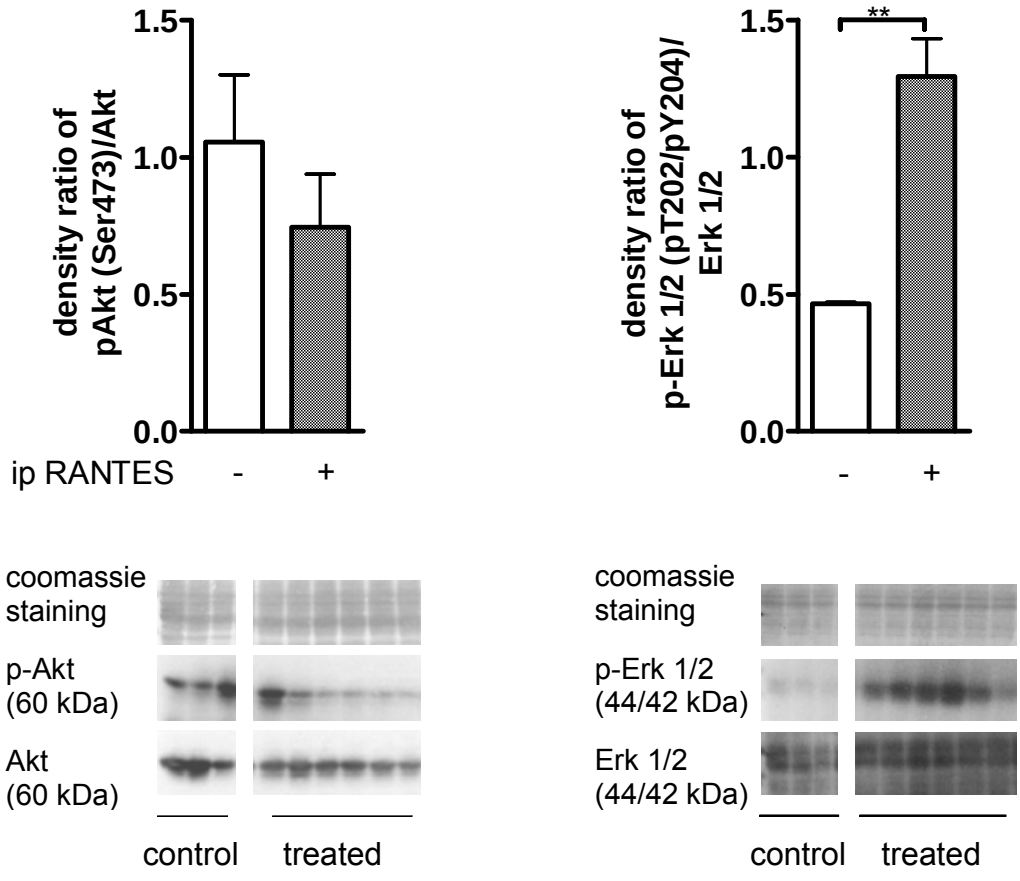

Figure 26: Effect of RANTES on phosphorylation of Akt and Erk1/2 in primary mouse liver. Mice were treated with rmRANTES or PBS for 4 days prior to liver isolation. Liver of mice without glucose administration were lysed and 20 µg of total protein was separated by SDS-Page and analysed by western blot analysis as described in Methods. Results are means ± SE of 3 (control) and 6 (treated), respectively independent liver samples (Student's t-test **p<0.01).

5.4.4 Impact of RANTES on inflammation in mouse liver

As *in vivo* RANTES was recognised to induce phosphorylation of Erk 1/2 in the liver, gene expression of the pro-inflammatory adipokines *TNFα* and *IL6* was investigated. Indeed RANTES increased the transcription of *IL6* (2.1-fold), but the mRNA level of *TNFα* was significantly 1.6-fold reduced by RANTES (Figure 27).

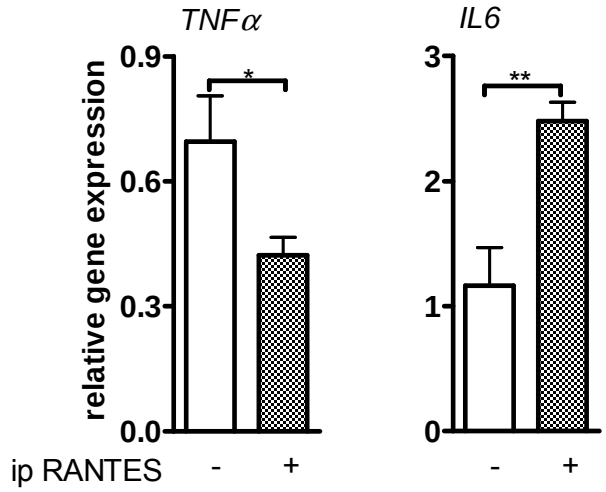

Figure 27: Impact of RANTES on adipokine gene expression in mouse liver. Mice were treated with PBS or rmRANTES for 4 days prior to liver isolation. Total RNA from mice without glucose administration was prepared and analysed as described in Methods by using a primer specific to TNFα and IL6. Results are means ± SE of 3 - 4 independent liver samples (Student's t-test *p<0.05; **p<0.01).

5.5 Impact of RANTES on preadipocyte differentiation

Since RANTES significantly reduced gene expression of *C/EBPα* and *SREBP-1c* the impact of RANTES on adipogenesis was investigated. Primary human preadipocytes from eight healthy subjects were isolated. Mean age of the patients was 42.0 ± 4.2 years and the mean BMI was 23.9 ± 0.6 kg/m^2. Isolated preadipocytes were differentiated until day 18 with or without administration of 100 ng/ml RANTES. Fresh RANTES was given to the cells every third day. GPDH activity as a marker for adipocyte differentiation was determined at day 0, 3, 9 and 18. Compared to control cells RANTES increased adipocyte differentiation activity. This was statistically significant at day nine where GPDH activity was 1.4-fold enhanced by RANTES. Even though adipogenic capacity between RANTES-treated adipocytes and control cells was not significantly different at day 18, mean GPDH activity was furthermore 1.7-fold increased through the incubation with RANTES (Figure 28 and 29).

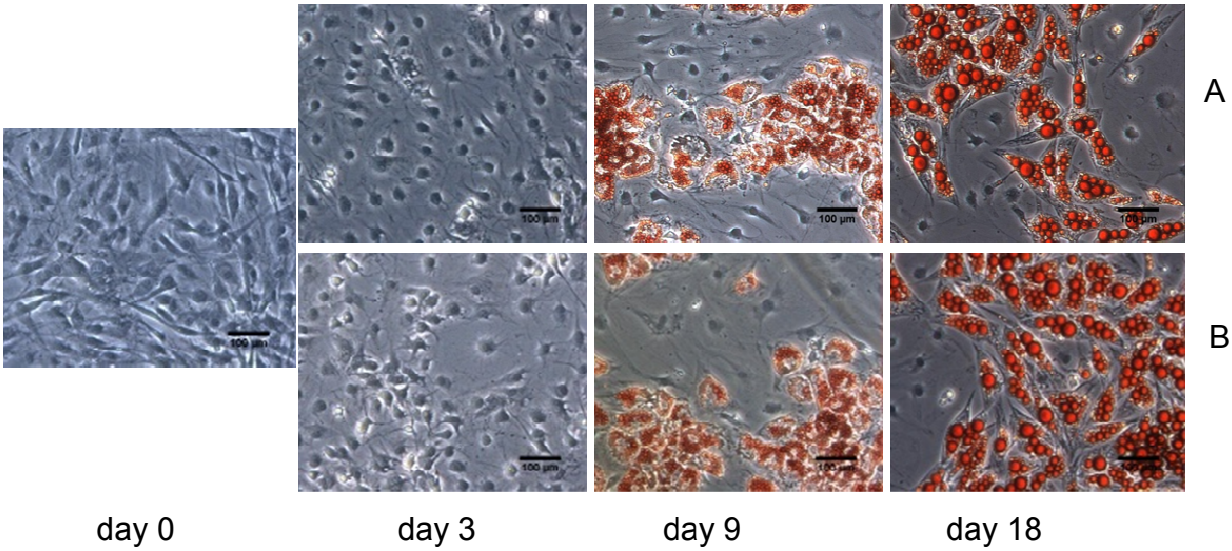

Figure 28: Oil Red O staining of human preadipocytes treated with RANTES during the differentiation period. Primary human preadipocytes were differentiated without (A) or with administration of 100 ng/ml rhRANTES (B) until day 18. Cells were stained with Oil Red O at day 0, 3, 9 and 18. Pictures were taken by light microscopy. Black scale bars in pictures indicate 100 µm.

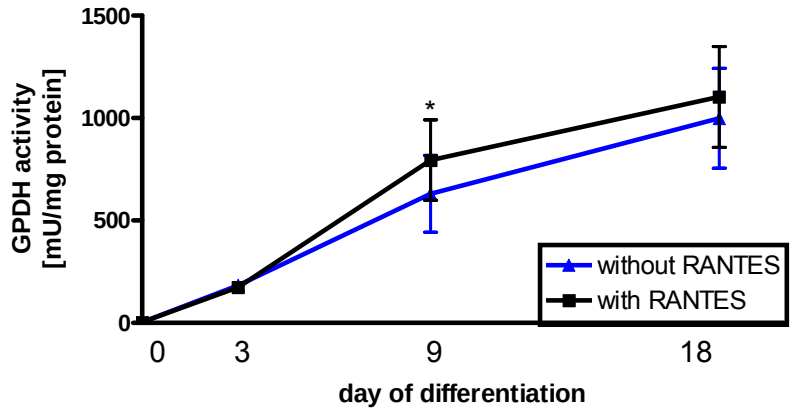

A)

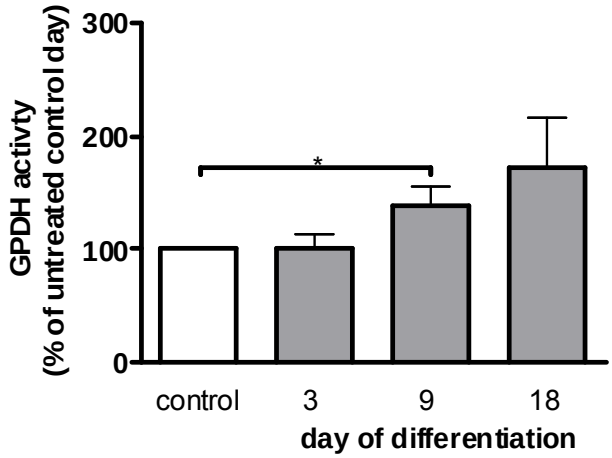

B)

Figure 29: GPDH activity in human maturing preadipocytes treated with RANTES during the differentiation period. Primary human preadipocytes were differentiated without (control) or with 100 ng/ml rhRANTES for time points indicated. At day 0, 3, 9 and 18 cells were harvested and GPDH activity was measured and normalised by total protein. GPDH activity is shown as mU/mg protein (A) and as percent of untreated control day (B). Results are means ± SE of 8 independent experiments (Student's t-test or one-sample t-test to the untreated control day *$p<0.05$).

To exclude alterations in GPDH activity as a result of changes in adipocyte cell number, fat cell number was determined using DAPI staining. Adipocyte cell number was comparable between RANTES-stimulated and unstimulated cells (Figure 30). Higher GPDH activity in RANTES treated cells was therefore not caused by increased proliferation in these cells.

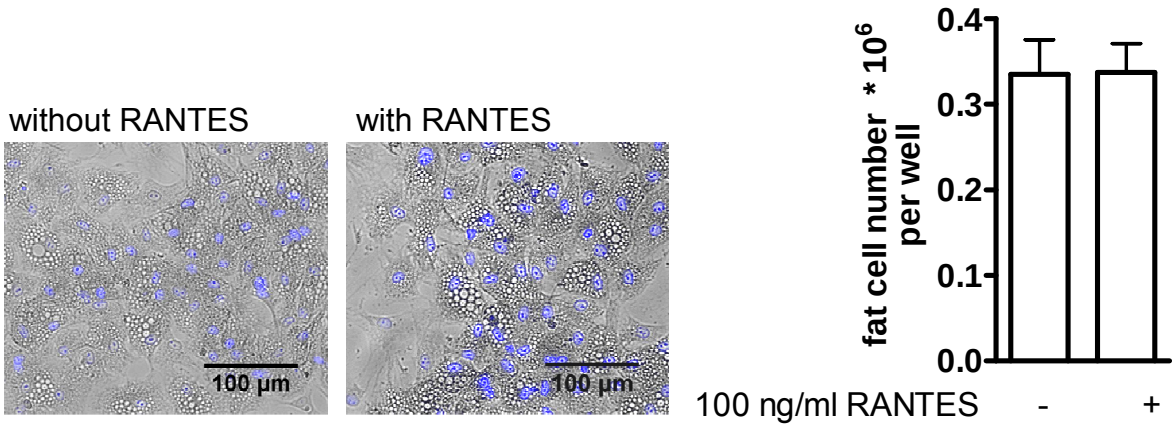

Figure 30: Impact of RANTES on fat cell number of differentiated human adipocytes at day 9. Primary human preadipocytes were differentiated with or without 100 ng/ml rhRANTES. Cells were stained with DAPI (A) and cell number was calculated using Image J (B). Black scale bars in pictures indicate 100 µm. Results are means ± SE of 4 independent experiments.

Adipogenesis is accompanied by changes in the secretory pattern of fat cells. The influence of RANTES on the production of adiponectin, IL6 and leptin during adipocyte differentiation was determined. RANTES had no impact on the secretion of adiponectin, IL6 and leptin during adipogenesis (Figure 31).

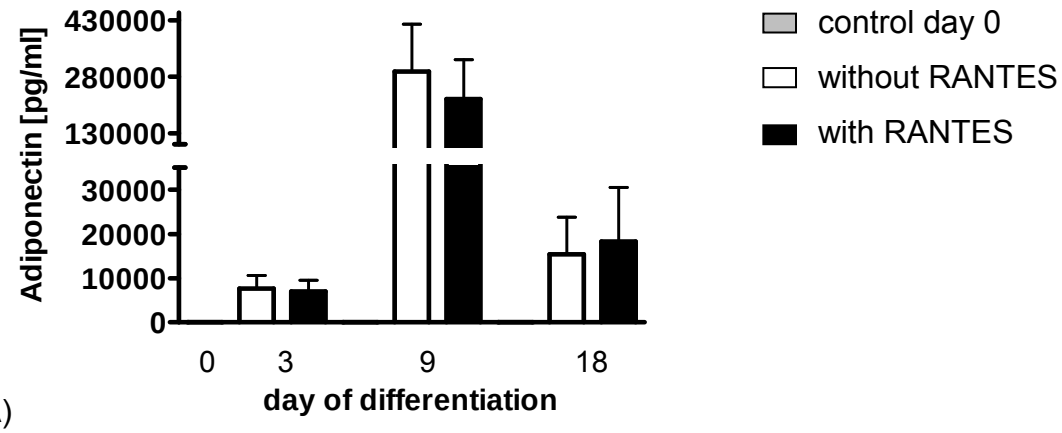

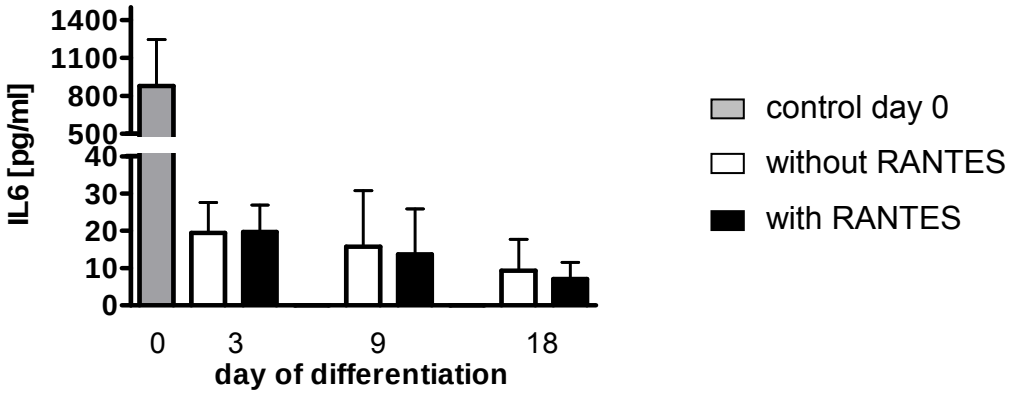

B)

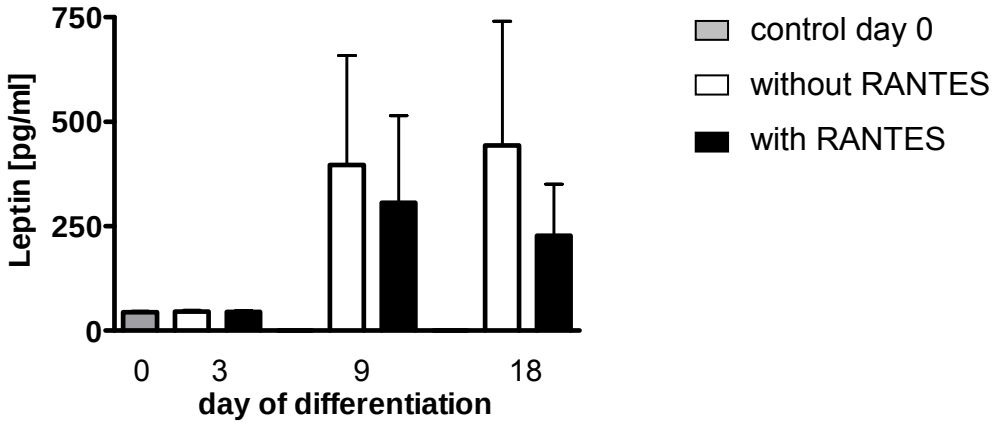

C)

Figure 31: Effect of RANTES on adipokine secretion in human differentiating preadipocytes. Primary human preadipocytes were differentiated without or with 100 ng/ml rhRANTES. Supernatants were harvested at day 0, 3, 9 and 18 and secretion of adiponectin (A), IL6 (B) and leptin (C) was determined by ELISA as described in Methods. Results are means ± SE of 5 independent experiments.

6 Discussion

One of the most common liver diseases is NAFLD. Obesity and type 2 diabetes are closely associated with NAFLD. The exact mechanisms leading to NAFLD are unclear, but there is strong evidence that factors secreted by AT are involved. The aim of this thesis was to obtain a better insight into the relation between adipocytes, especially adipocyte cell size, and NAFLD.

6.1 Metabolic function of adipocytes

The present study was the first one comparing small and large adipocytes from the same subject concerning their insulin sensitivity as well as proteome- and gene expression profile. A major finding was that fat cell size rather than BMI has an impact on adipocyte metabolism, because all differences were observed in normal weight subjects with a significant distinction in fat cell size between small and large adipocytes.

6.1.1 Insulin signaling in small and large adipocytes

In the present study, the amount of total IRS-1, Akt, Erk 1/2 and c-Cbl was reduced in enlarged adipocytes after adjustment by protein. Furthermore, compared to large fat cells, small adipocytes exhibited a significant activation of IRS-1 and Akt by insulin. The stronger insulin-stimulated phosphorylation of IRS-1 in small adipocytes was, in addition, detected in normal weight subjects and overweight subjects. However, the activation of IRS-1 by insulin in small cells of overweight subjects was not as high, as observed in the lean BMI group (7.2-fold vs. 3.5-fold), which could be caused by a higher mean fat cell size of F1 in this BMI group. A similar effect was seen for insulin-stimulated phosphorylation of Akt, although a significant activation of Akt in small adipocytes was only observed in the overweight group. This is based on a high standard of deviation in the normal weight group due to the data of one single person. Exclusion of this person results in a significant insulin-induced

phosphorylation of Akt in small but not in large adipocytes of both BMI groups (data not shown). Thus, adipocyte cell size has an influence on insulin signaling *per se* and, in addition, cell size seems to be a better predictor of insulin sensitivity than BMI. This is in agreement with the finding that obesity by itself does not always lead to diabetes [190]. Furthermore, Kovacs et al. showed that the expression of *IRS1* is markedly lower in obese compared to lean non-diabetic Pima Indians [191]. A reduced amount of IRS-1 is further associated with insulin resistance and low expression of *GLUT4,* contributing to attenuated insulin-induced glucose uptake in fat cells [192]. Frank et al. also compared insulin signaling between small and large adipocytes within the same subjects. Unlike the present work, they found no differences in the amount of IRS-1 as well as in the insulin-stimulated phosphorylation of IRS-1 and Akt 1 in the two cell fractions. On the contrary, GLUT4 translocation was induced by insulin in small but not in enlarged fat cells [26]. Comparison between Franck et al. and the present work exhibited heterogeneities with regard to the study population and analysis. For example, in the current work it was clearly shown that hypertrophic fat cells have twice as much protein as non-hypertrophic adipocytes. The results of the present study were subsequently corrected for protein concentration of 1 x 10^6 fat cells. Both studies are confronted in Table 7.

Table 7: Comparison between the study from Franck et al. [26] and the present work.

Parameter	Present work	Franck et al.
Study population for IRS-1 and Akt analysis	- 18 healthy adults - mean BMI: 27 ± 1 kg/m^2 - mean age: 42 ± 3 y	- 6 medicated adults - mean BMI: 30 ± 6.4 kg/m^2 - mean age: 60 ± 19 y
Adipocyte separation	according to their floating properties	by the use of two different filter pore sizes
Culturing of isolated fat cells	- in culture medium supplemented with biotin and sodium pyruvate - 5 mM glucose - 2 days (37 °C, 5 % CO_2)	- in 1:1 vol/vol culture medium / KRP - 12.5 mM glucose - overnight (37 °C, 10 % CO_2)
Insulin treatment	100 nM for 10 min	10 nM for 10 min

Protein analysis by SDS-Page	- added per lane: equal amounts of total protein - internal control: GAPDH	- added per lane: equal fat cells volumes per fraction - internal control: β-actin

Concerning the Cbl-CAP pathway, which has recently been discussed as an alternative pathway for GLUT4 translocation by insulin, an insulin-induced Cbl-phosphorylation was not detected in primary human fat cells, neither in small nor in enlarged adipocytes. An additional separation according to BMI also showed no activation of c-Cbl by insulin in both fat cell fractions. The results of the present study therefore contradict those of Kimura et al., who exhibited a reduced insulin-stimulated phosphorylation of Cbl and GLUT4 translocation in 3T3-L1 adipocytes over-expressing a CAP mutant [193]. In contrast, the current work is in agreement with the findings from Mitra et al. [194]. A suppression of c-Cbl, CAP and CrkII via siRNAs did not compromise the stimulated effect of insulin on GLUT4 translocation in adipocytes. Furthermore, glucose uptake in primary mouse adipocytes from wild type mice as well as c-Cbl knock-out mice was comparable after stimulation with different insulin concentrations [194]. Cbl can be phosphorylated on four different tyrosine residues: Y371, Y700, Y731 and Y774 [195]. In most studies investigating Cbl-phosphorylation, general tyrosine-phosphorylated proteins are recognised [196, 197]. However, phosphorylation of Cbl on Y700 and Y774 offers docking sites for CrkII [198, 199, 195]. In the present study a Y774 specific antibody was used. In conformity with JeBailey et al. who investigated the time-dependent Y774-phosphorylation of Cbl by insulin in 3T3-L1 cells [200], insulin does not induce Cbl activation. These data propose that in primary human adipocytes, phosphorylation of c-Cbl is not induced by insulin unless the Cbl-CrkII interaction in adipocytes is mediated by other tyrosine residues, as investigated in this work. However, in the present study the amount of basal and insulin-stimulated p-c-Cbl was higher in small than in large fat cells. Moreover, after separation according to BMI this finding was lost in the overweight BMI group, suggesting that the Cbl-CAP pathway plays a role in adipocyte metabolism. In 3T3-L1 preadipocytes, Metformin stimulates an AMPK-mediated Cbl-Cap pathway independently of insulin. This activation results in the translocation of GLUT4 to the plasma membrane [201]. Furthermore, AMPKα2 knock-out mice have enlarged adipocytes and are obese [202]. Thus, the Cbl-CAP

pathway seems to be an insulin-independent alternative pathway for GLUT4 translocation in human adipose tissue.

Another insulin-induced pathway is the MAPK pathway, which was also investigated. MAPKs play an important role in proliferation and differentiation, where Erk 1 especially is important for initiating adipocyte differentiation [203]. Activation of Erk is furthermore associated with insulin resistance. It diminishes the expression of IR, IRS-1 and -2 as well as their phosphorylation [204]. In the present study, Erk 1/2 was not markedly activated by insulin in both fat cell fractions, but the insulin-induced phosphorylation of Erk 1/2 was significantly higher in small compared to large fat cells. In contrast, the basal phosphorylated Erk 1/2 was similar between both cell fractions. Additional separation according to BMI displayed that the differences between small and enlarged adipocytes exist in patients with lower and with higher BMI, suggesting a metabolic involvement of this pathway in adipose tissue metabolism. Activation of Erk signaling is linked to changes in fat cell size [205] and consequently occurs primarily in larger fat cells. Furthermore, fat cells of diabetic patients display enhanced basal phosphorylation of MAPKs compared to healthy controls. In contrast, insulin-induced activation of Erk 1/2 occurs in healthy people, but not in subjects with type 2 diabetes [206]. Thus, the higher insulin-induced phosphorylation of Erk 1/2 in small fat cells could indicate reduced insulin sensitivity with increasing adipocyte cell size.

6.1.2 Proteomic and transcriptomic profile in small and large adipocytes

A relationship between hypertrophic adipocytes and obesity-related dysfunctions has been observed in many studies (chapter 1.2.1), but there is limited knowledge about differences in protein transcription between small and large adipocytes. In this study, 453 proteins and 358 genes were detected at different levels in small compared to large fat cells, demonstrating that cell size *per se* may alter adipocyte function.

In proteomic analysis NDUFS4 was the highest up-regulated protein in large compared to small adipocytes. NDUFS4 is an essential subunit of the mitochondrial membrane respiratory chain complex I [207] and plays a role in oxidative

phosphorylation. It functions in the transfer of energy/electrons from NADH, produced by the oxidation of sugars and fats, to the respiratory chain for ATP synthesis [208]. Increased amounts of NDUFS4 in enlarged adipocytes might therefore be caused by higher energy supply in these cells. However, during oxidative phosphorylation, ROS are produced, which in turn may contribute to oxidative stress and subsequently to the damage of cells and proteins [208]. Damaged or misfolded proteins are further degraded by the proteasome, which seem to be more active in large compared to small fat cells, too. Thus, although increased levels of unfolded proteins and subsequent ER stress were already described for obesity and insulin resistance [209], the present study indicates that fat cell size *per se* is a potential mediator between the link of ER stress and obesity as well as insulin resistance. Furthermore, in the present work a cell size dependent influence on the posttranscriptional regulation through lower amounts of SRSF3 and SF3B5 in enlarged adipocytes was observed. Both splicing factors are implicated in RNA processing and splicing. A potential link between alternative splicing and obesity as well as insulin resistant was already described [210, 211]. The results of the present study now indicate that cell size *per se* might play an important role in the posttranscriptional regulation of genes implicated in human disease.

This finding leads, in turn, to the question of what happens to the gene expression profile. DNA microarray analysis exhibited that more genes were up- than down-regulated in large adipocytes. Moreover, most of them are involved in response to stress. Especially, the acute-phase proteins SAA were highly expressed in enlarged fat cells. SAAs are apolipoproteins produced at high levels in AT [212]. They are elevated in inflamed tissues where they play a role in the recruitment of immune cells to the inflammatory site and they are related to insulin resistance [213, 214]. In 2006, genetic distribution between small and large adipocytes was first analysed by Jernas et al. [215]. They categorised genes which were up-regulated in hypertrophic fat cells and found that most of these genes are involved in inflammatory processes. Moreover, SAA proteins were also in the focus of Jernas et al. and they supposed that SAAs are implicated in the relationship between enlarged adipocytes and type 2 diabetes [215]. Since in the present study, SAAs were in addition highly expressed in large fat cells with impaired insulin sensitivity, the assumptions before are clearly confirmed by our results.

Another finding in the present study was the noticeably higher expression of c-Jun in large compared to small adipocytes. Moreover, c-Jun was represented in most of the up-regulated pathways, like wnt-signaling pathway, MAPK signaling pathway, apoptosis and senescence. c-Jun is a transcription factor activated by the MAPK JNK. JNK, in turn, is implicated in the development of obesity and insulin resistance [216]. Thus, a potential link between hypertrophic adipocytes and type 2 diabetes was further validated.

Although a higher stress level in large compared to small adipocytes was observed by proteomic and transcriptomic analyses, results of both examinations were additionally directly compared. As expected, a higher stress response in large compared to small fat cells was detected. This was shown by elevated levels of HSPB6 protein content and gene expression. HSPB6, also known as HSP20, belongs to the small heat shock proteins and it is highly up-regulated in response to oxidative stress [217, 218]. Furthermore, both gene and protein amount of CTSC were decreased in large compared to small adipocytes. CTSC, also known as dipeptidyl peptidase I, is a protease expressed during adipogenesis and in immune-related cells [219, 220]. It plays an important role in innate and adaptive immune processes and loss of function in CTSC leads to an impaired immune defense [221]. Investigations on AT gene expression in response to short-term overfeeding revealed a decline of CTSC in lean subjects, whereas no changes were observed in obese people. The authors therefore hypothesised that the reduction of CTSC in lean subjects might protect cells in response to an energy excess [222]. Thus, in relation to the present results, a reduced level of CTSC in hypertrophic adipocytes could indicate both a reduced immune defence and lower protection against energy overhang in these cells.

A major finding in this study was a reduction of COL6A3 and NID2 at mRNA and protein level. Both are components of the basal lamina and are therefore involved in ECM remodeling. Obesity seems to be associated with destabilisation of the ECM. Especially obesity-related hypoxia may play an important role in this process, because of its impact on enzymes for ECM-protein-processing [223, 224]. In 3T3-F442A adipocytes hypoxia increases the production of MMPs [225]. MMPs are enzymes that catalyse the splitting of peptide bonds into proteins. They degrade

proteins of the ECM and are important for function of cell surface receptors and cytokine activity [226–228]. In the microarray analysis of the present work, higher expression of *MMP19* in large compared to small adipocytes was observed. Since COL and NID are substrates of MMP19 [224], less amounts of these factors in this study are still in agreement with higher *MMP19* gene expression in F4. Hence, fat cell size *per se* plays a critical role in ECM composition. Furthermore, these results could indicate in turn that hypoxia occurs in enlarged adipocytes. Previously, it was shown that ob/ob mice lacking COL6 exhibit larger adipocytes with improved whole body energy homeostasis [229]. In the present study, COL6 was reduced in the large fat cells of healthy non-obese subjects, but hypertrophic adipocytes were related to enhanced stress response and insulin resistance.

Results of both analyses are summarised in Figure 32.

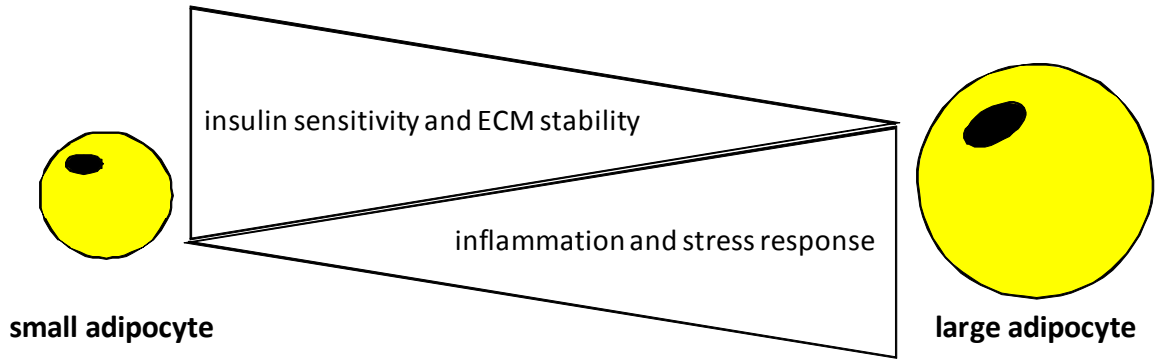

Figure 32: Overview about cell size dependent effects in adipocytes.

6.2 Metabolic function of adipocyte-CM on hepatocytes

In this study, a relationship between stress response and adipocyte cell size was observed by proteomic and transcriptomic analysis. This is in line with findings from fat cell size dependent adipokine secretion, where enlarged adipocytes secrete more pro-inflammatory adipokines [41]. Such a chronic low-grade inflammation caused by AT may influence hepatic and peripheral glucose metabolism.

In the present work, basal hepatic glucose output from Fao cells incubated with CM from small fat cell fraction positively correlated with fat cell size. However, in the large adipocyte group a significant increased glucose release by fat cell size was missing. Interestingly, compared to the basal glucose output in both fat cell fractions, a significant cell size dependent increase of db-CD-stimulated hepatic glucose release was absent. This leads to the assumption that an enhanced adipocyte cell size causes a reduction rather than a stimulation of hepatic glucose output. In contrast, in the present study, independent of the fat cell fraction insulin-suppressed glucose output worsened with enhanced adipocyte cell size. Consequently, fat cell size *per se* is associated with impaired insulin-suppressed glucose release from cultured hepatocytes. In obese non-diabetic subjects, gluconeogenesis is enhanced compared to the leaner ones. The endogenous glucose output is however similar between both obese and lean patients, because of a reduced glycogenolytic flux in obese patients [230]. In contrast, diabetic subjects exhibit hyperglycemia via an increase of both hepatic gluconeogenesis and glycogenolysis [231]. In the current work, the influence of adipocyte-CM on hepatic glycogenolysis was not examined. Nevertheless, alongside reduced insulin sensitivity in adipocytes by increasing cell size, there is evidence to suggest that fat cell size have, in addition, a negative impact on hepatic insulin action and could therefore contribute to hyperglycemia.

6.3 Metabolic function of adipokines on hepatocytes

Since in the present study hepatic glucose release from Fao cells treated with adipocyte-CM from large fat cell fraction did not markedly correlate with increasing cell size, an enhanced glucose output by pro-inflammatory adipokines was not assumed. Indeed, in the present study basal hepatic glucose release was rather reduced after incubation with TNFα, IL6, PAI-1, SDF-1α, MCP-1 and RANTES for 30 hours. However, basal effects of adipokines were not always statistically significant. Db-CD-stimulated hepatic glucose output was additively used to examine the effects of adipokines on hepatic glucose production. In that case, all effects on basal glucose production became significant by additionally treating with db-CD. Thus, the pro-inflammatory adipokines TNFα, IL6, PAI-1, SDF-1α, MCP-1 and RANTES led to a significant reduction of hepatic glucose output. Ang II was the only one which showed an increased hepatic glucose production in a time-dependent manner. These results are in line with previous publications. While TNFα and SDF-1α suppress hepatic gluconeogenesis [232, 233], Ang II was shown to induce it [234, 235].

An important finding was that most of the adipokines-induced impact on hepatic glucose output was especially combined with a reduction of *G6Pase* mRNA level. G6Pase is a gluconeogenic key enzyme that catalyses the conversion of glucose-6-phosphate (G6P) into free glucose. Its transcription is induced by glucagon (via cAMP) as well as glucocorticoids (dexamethasone) and in contrast, is inhibited by insulin [162]. A TNFα-induced suppression of *G6Pase* mRNA was already shown, but it was indicated that this inhibition is not mediated by the insulin-induced pathways [236]. TNFα rather suppresses the G6Pase promoter activity by temporary over-expression of NF_KB [236] and can thereby lead to an impaired hepatic glucose production. Furthermore, depletion of *G6Pase* gene expression by TNFα was described to be combined with enhanced glycogenolysis [237], which might in turn increase hepatic glucose output. It is however assumed that the produced glucose-6-phosphate (G6P) is used for FA synthesis [237]. Glycogenolytic activity was also described for IL6 [238] and Ang II [239] which exhibited a reduced db-CD-stimulated *G6Pase* mRNA level as well. Ang II induced hyperglycemia [240] might therefore be caused by enhanced gluconeogenesis and glycogenolysis.

In the present study, SDF-1α was the only adipokine, which caused an increased db-CD-stimulated expression of *G6Pase* with distinctly reduced hepatic glucose production in parallel. A reduced db-CD-stimulated gluconeogenesis by SDF-1 was previously shown, but this was associated with additional suppression of both *PEPCK* and *G6Pase* transcription [233]. A reason for this disagreement could be that in the current study Fao cells were used to investigate hepatic gluconeogenesis, whereas Liu et al. analysed the impact of SDF-1 on primary hepatocytes [233]. The amount of CXCR4, a SDF-1α specific receptor, was not measured in Fao cells of this study, but it was published that these cells express low amounts of CXCR4 [241]. Thus, the differences could be caused by the reduced responsiveness of the hepatoma cells used in the present study.

Next to the db-CD-stimulated glucose release from Fao hepatoma cells, the insulin-suppressed hepatic glucose output was also investigated in the current work. Since in this study fat cell size correlates with an impaired insulin suppression of glucose release, an impact of pro-inflammatory adipokines on insulin-stimulated glucose output was assumed. Indeed, in the present study TNFα, IL6, Ang II, SDF-1α and MCP-1 attenuated insulin action in hepatocytes measured by *PEPCK* gene expression. The impairment of insulin action was thereby mostly reflected by elevated glucose production after 6 hours of adipokine exposure. An exception represented again Ang II, where the significant inhibition of insulin-reduced glucose release occurred after an incubation of 30 hours. Interestingly, compared to the observation that the adipokine-affected db-CD-stimulated glucose release was primarily related to changes in the *G6Pase* gene expression, effects on insulin-induced hepatic glucose output were mostly associated with *PEPCK* gene transcription. PEPCK is a gluconeogenic key enzyme in the earlier stage of gluconeogenesis. It converts oxaloacetate into phosphoenolpyruvate and CO_2 [162].
For some of the investigated adipokines an impact on insulin-suppressed hepatic gluconeogenesis was already published. For example, TNFα and Ang II were shown to debilitate insulin-induced Akt phosphorylation in hepatocytes [161, 242]. SDF-1 was reported to activate insulin- independent Akt/PKB, contributing to decreased *PEPCK* and *G6Pase* gene expression [233]. Up to now and to the best of our knowledge, there are no data concerning the direct effect of SDF-1α on insulin-inhibited gluconeogenesis. In this study both *PEPCK* and *G6Pase* mRNA levels

were, however, also not decreased by SDF-1α alone, which might be, as mentioned above, caused by less responsiveness of the FAO cells. Thus, the SDF-1α attenuated insulin action should be confirmed by the use of other hepatocyte cell models. Little investigation has been made concerning the impact of MCP-1 on insulin-stimulated hepatic glucose production. It is known, that mice that over-express MCP-1 in AT are insulin resistant and have higher liver TG content compared to control mice [243]. Moreover, MCP-1 induced steatosis is associated with higher hepatic *G6Pase* and *PEPCK* gene expression [243, 244]. Thus, an impaired insulin-suppressed hepatic gluconeogenesis by MCP-1 is in line with earlier publications.
The effect of IL6 on hepatic insulin action is still controversially described. While Inoue et al. showed an IL6-mediated improvement of hepatic glucose production [245], Kim et al. observed an impaired insulin-suppressed hepatic glucose output by IL6 [246] and is therefore in agreement with the results of the present work.

Unlike the other adipokines, PAI-1 and RANTES caused a further reduction in both, insulin-suppressed *PEPCK* gene expression and hepatic glucose output. To the best of my knowledge the direct effects of both PAI-1 and RANTES on hepatic gluconeogenesis were currently not investigated. Since RANTES is markedly up-regulated in patients with NAFLD [108, 247] the effect of RANTES on liver metabolism was analysed in a more detailed way (chapter 6.3.1).

In view of the data presented in this study so far, the following working hypothesis concerning the influence of both adipocyte-CM and adipokines on liver metabolism was developed (Figure 33).

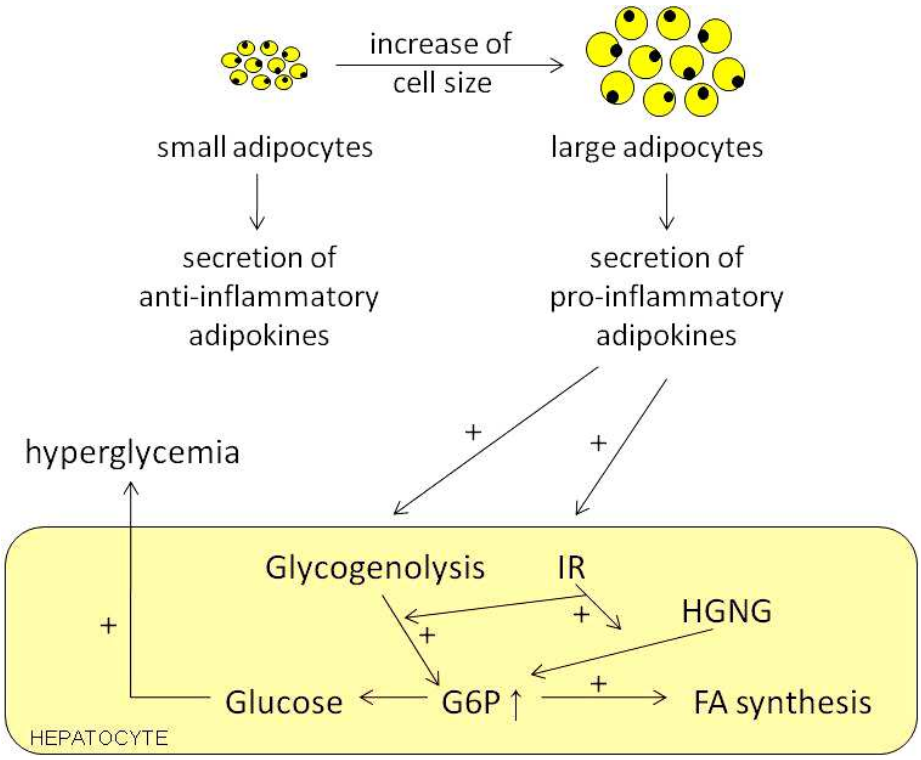

Figure 33: Working hypothesis of the influence of hypertrophic fat cells on liver metabolism. Hypertrophic adipocytes secrete pro-inflammatory adipokines which stimulate (+) glycogenolysis and induce insulin resistance (IR) in hepatocytes. Insulin resistance in turn attenuates insulin-suppressed hepatic gluconeogenesis (HGNG). Thus, both increased glycogenolysis and HGNG lead to an enhanced amount of glucose-6-phosphate (G6P) in hepatocytes. The produced G6P is further used for FA synthesis or converts to glucose, which can be released into the circulation contributing to higher blood glucose level.

6.3.1 Metabolic function of RANTES on hepatic metabolism

In the current study, it was shown that RANTES incubation for 30 hours resulted in decreased hepatic glucose release independent of co-incubation with insulin or db-CD. Moreover, the stronger reduction of insulin-suppressed glucose output by RANTES was linked to lower *PEPCK* mRNA levels. Accordingly, based on the previous results, where changes in db-CD-stimulated hepatic glucose output were linked to *G6Pase* gene expression and insulin affected glucose production to *PEPCK* gene transcription, RANTES seems to improve the insulin effect on hepatocytes. However, phosphorylation of Akt was unaffected by RANTES in the current work. Another signaling pathway of insulin in the liver involves the phosphorylation of Erk 1/2. It was described that activation of ERK1/2 in hepatocytes is negatively controlled

by cAMP [248]. Since in the present study RANTES significantly decreased db-CD-stimulated glucose output, an enhanced activation of Erk 1/2 was expected. Indeed, compared to the control mice, RANTES significantly increased phosphorylation of Erk 1/2 in mice livers.

In astrocytes, RANTES decreases the amount of intracellular cAMP and activates Erk 1/2 followed by the production of pro-inflammatory mediators like TNFα and IL6 [249]. The enhanced phosphorylation of Erk 1/2 in the current study was, however, combined with a significantly decreased expression of *TNFα*. TNFα induces the production of RANTES in the liver [250]. The suppressed transcription of TNFα by RANTES could therefore be caused by a negative feedback mechanism. In contrast, RANTES-induced activation of Erk 1/2 in the present work was related to an increased *IL6* mRNA level, which in turn could influence the hepatic glucose production. In the present *in vitro* study, IL6 treatment for 6 hours attenuated insulin action on both hepatic glucose output and *PEPCK* gene expression. Hence, impaired insulin sensitivity in the liver could also be secondarily induced by RANTES through the synthesis of IL6. Furthermore, the expression of *IL6* is up-regulated in patients with NASH compared to those with simple steatosis or normal biopsies [251]. Moreover, IL6 has direct effects on lipid metabolism in hepatocytes by decreasing gene expression of the transcription factor *SREBP-1c* [252].

Normally, SREBP-1c regulates FA synthesis and is therefore expressed at elevated levels in fatty liver [253, 254]. An advanced NASH is, however, rather associated with a reduction of *SREBP-1c* gene [255]. In this study, RANTES treated mice showed increased hepatic TG content with enhanced expression of *IL6* and, in addition, decreased levels of *SREBP-1c* mRNA. Thus, RANTES might play an important role in an advanced NASH and subsequent fibrosis.
Furthermore, a suppressed expression of *SREBP-1c* is associated with the absence of C/EBPα [256]. Disruption of C/EBPα increases the risk of fibrosis through activating hepatic stellate cells (HSCs) [257], which in addition, express RANTES in order to prompt their proliferation and migration [258]. Activated HSCs, in turn, produce components of the extracellular matrix contributing to fibrosis [259]. Moreover, a reduced *C/EBPα* gene expression induces hypoglycemia and decreases the expression of both *PEPCK* and *liver glycogen synthase (GS)* [260]. In the present

study, *C/EBPα* mRNA level in the mouse liver as well as hepatic glucose production and *PEPCK* gene expression in the Fao cells were significantly reduced following RANTES treatment. Thus, a potential link between RANTES and the progression towards liver fibrosis is further supported.

Next, C/EBPα is an adipogenic key factor and plays an essential role in lipid metabolism. Ablation of C/EBPα in adult mice caused the development of a fatty liver due to decreased rates of hepatic FA oxidation and apolipoprotein synthesis [261]. In this study TG content in the liver of RANTES treated mice was increased, but this was not associated with changes in the expression of genes involved in FA oxidation. In contrast, RANTES increased differentiation of primary human preadipocytes. The exact mechanism for RANTES-induced TG accumulation could not be explained by the present study. One possibility could be, however, a decreased hepatic lipid release by diminished ApoB secretion upon RANTES treatment. Further study is necessary to investigate the impact of RANTES on hepatic TG accumulation in more detail.

7 Conclusion and Outlook

The present study confirms that rather fat cell size than obesity *per se* plays an important role in the development of metabolic dysfunction. Adipocyte hypertrophy causes an impairment of insulin signaling, which is predominantly mediated through the IRS-1 / Akt-pathway in human adipocytes. Furthermore, enlargement of adipocytes is associated with a higher stress response and changes in the ECM composition, which may lead to disturbances also in other organs. We therefore tested whether fat cell size affects glucose production in the liver. To the best of our knowledge, this study was the first to demonstrate a direct effect of fat cell size on db-CD- and insulin-stimulated hepatic glucose output. Contrary to our expectations, hepatic glucose production did not increase with growing fat cell volume as well as after treatment with pro-inflammatory adipokines. However, due to our results an enhanced hepatic glycogen breakdown is assumed and an impaired insulin suppressed glucose production was observed by both expanding adipocyte cell size and pro-inflammatory adipokines. We therefore suggest that fat cell size rather than obesity *per se* positively correlates with hepatic insulin resistance and consequently with hepatic de novo lipogenesis as well as elevated blood glucose levels. Nevertheless, in order to get evidence the results have to be replicated by the use of selective antagonists and with regard to the glycogen content.

In the present work it was also demonstrated for the first time that both PAI-1 and RANTES have a direct impact on hepatic glucose metabolism. Their effect was moreover unlike to the other adipokines. Both seem to enhance the insulin-suppressed effect on hepatic glucose production. RANTES was selected and investigated in more detail. Interestingly, RANTES affected both hepatic lipid and glucose metabolism. Hepatic lipid content was increased *in vivo* and *in vitro* after treatment with RANTES and this was associated with the induction of Erk 1/2 phosphorylation in the liver. An increased activation of Erk 1/2 was further combined with the production of *IL6* as well as a decreased gene expression of *C/EBPα* and *SREBP-1c*, which could indicate an increased risk for the progression of fibrosis due to RANTES treatment. Since circulating RANTES levels are increased in obese and NAFLD patients, this chemokine could contribute to the progression of liver disease and serves therefore as a potential target for NAFLD therapy.

In conclusion, these results enable more insights into the relationship between fat cell size and obesity related diseases, like NASH. Fat cell size *per se* was thereby shown to be a better predictor than BMI. Although, measurement of BMI is still easier compared to the determination of fat cell size, these results can be helpful for the development of new diagnostic tools.

8. Appendix

8.1 List of Figures

8.2 List of Tables

8.3 Chemicals

Acetic Acid	Carl Roth, Karlsruhe, Germany
Acetonitrile	Rathburn, Walkerburn, Scotland
Agarose	PEQLAB, Erlangen, Germany
Ammonium Persulfate	Sigma-Aldrich, Steinheim, Germany
BioRad lysis buffer	BioRad, Munich, Germany
Biotin	Carl Roth, Karlsruhe, Germany
Boric acid	Merck, Darmstadt, Germany
Bromphenol blue	VWR, Darmstadt, Germany
BSA fraction V	Sigma-Aldrich, Steinheim, Germany
$CaCl_2$	Merck, Darmstadt, Germany
Chloroform	Carl Roth, Karlsruhe, Germany
Collagenase	Biochrom, Berlin, Germany
Coomassie Brilliant Blue G-250	Serva, Heidelberg, Germany
Complete Mini	Roche, Grenzach-Wyhlen, Germany
DAPI	Sigma-Aldrich, Steinheim, Germany
db-cAMP	Sigma-Aldrich, Steinheim, Germany
Deoxycholat	Sigma-Aldrich, Steinheim, Germany
Dexamethasone	Sigma-Aldrich, Steinheim, Germany
DHAP	Sigma-Aldrich, Steinheim, Germany
DMEM (no glucose, 5.6 mM and 25 mM glucose)	Invitrogen, Karlsruhe, Germany
DMEM / F12 (1:1) (17.5 mM glucose)	Invitrogen, Karlsruhe, Germany
DMSO	Carl Roth, Karlsruhe, Germany
DNA loading dy	Promega, Mannheim, Germany
D-panthotenate	Sigma-Aldrich, Steinheim, Germany
DTT	Omnilab, Bremen, Germany
ECL	Amersham, Freiburg, Germany
ECL Advanced solution	GE Healthcare, Munich, Germany
EDTA	Merck, Darmstadt, Germany
EGF	ImmunoTools, Friesoythe, Germany
Ethanol	J.T.Baker, Deventer, Netherlands
Etidiumbromid	Omnilab, Bremen, Germany
FCS-F	Invitrogen, Karlsruhe, Germany
FCS-Gold	PAA, Cölbe, Germany
FGF	ImmunoTools, Friesoythe, Germany
Formaldehyd	Carl Roth, Karlsruhe, Germany
glucose-free DMEM	Sigma-Aldrich, Steinheim, Germany
Glycin	Merck, Darmstadt, Germany
Glycerin	Merck, Darmstadt, Germany
Goat serum	PAA, Cölbe, Germany
HamF12	Invitrogen, Karlsruhe, Germany
HEPES	Sigma-Aldrich, Steinheim, Germany

Hydrocortison	Sigma-Aldrich, Steinheim, Germany
IBMX	Serva, Heidelberg, Germany
Insulin	Sigma-Aldrich, Steinheim, Germany
Iodacetamid	Sigma-Aldrich, Steinheim, Germany
Isopropanol	Merck, Darmstadt, Germany
KCL	Merck, Darmstadt, Germany
KOH	VWR, Darmstadt, Germany
Mercaptoethanol	Sigma-Aldrich, Steinheim, Germany
Methanol	Riedel-de Haën, Seelze, Germany
$MgSO_4$	Merck, Darmstadt, Germany
NaCl	Merck, Darmstadt, Germany
NaCl 0.9 %	B. Braun Melsungen AG, Melsungen, Germany
NADH	Applichem, Darmstadt, Germany
NaH_2PO_4	Merck, Darmstadt, Germany
NaOH	J.T.Baker, Deventer, Netherlands
NP-40	Sigma-Aldrich, Steinheim, Germany
NuPage Sample buffer & Bis Tris Gel	Invitrogen, Karlsruhe, Germany
Oil Red O	Serva, Heidelberg, Germany
PAA/BisAA	Carl Roth, Karlsruhe, Germany
Palmitic Acid	Sigma-Aldrich, Steinheim, Germany
PBS	Biochrom, Berlin, Germany
PCR water (Nuclease-free water)	Sigma-Aldrich, Steinheim, Germany
Pen/Strep	PAA, Cölbe, Germany
PhosSTOP	Roche, Grenzach-Wyhlen, Germany
Phenylmethanesulfonylfluoride (PMSF)	Sigma-Aldrich, Steinheim, Germany
Protein ladder	BioRad, Munich, Germany
Rosiglitazone	Sigma-Aldrich, Steinheim, Germany
SDS	Omnilab, Bremen, Germany
Skin milk	Carl Roth, Karlsruhe, Germany
Sodium-lactate	Sigma-Aldrich, Steinheim, Germany
Sodium-pyruvate	Sigma-Aldrich, Steinheim, Germany
SYBR green ROX Mix	Thermo Scientific, Schwerte, Germany
T3	Sigma-Aldrich, Steinheim, Germany
TEMED	Carl Roth, Karlsruhe, Germany
Transferrin	Sigma-Aldrich, Steinheim, Germany
Triethanolamin-HCL	Sigma-Aldrich, Steinheim, Germany
Tris-Hcl	Sigma-Aldrich, Steinheim, Germany
Trizol	Invitrogen, Karlsruhe, Germany
Trypsin	Promega, Mannheim, Germany
Trypsin/EDTA	PAA, Cölbe, Germany
Tween 20	Sigma-Aldrich, Steinheim, Germany

8.4 Set-ups for LC-MSMS

mass analysis

- MS1 active gain control	1.000,000 per injection time 100 ms
- MS2 active gain control	10,000 per injection time 100 ms
- MS1 resolution	30,000 (at 400 m/z)
- MS2 resolution	15,000
- Precursor selection method	top 15

protein identification

- Database	IPI_v3_68_PFAM FASTA
- Enzyme	Trypsin
- Max. missed cleavage sites	2
- Fixed modifications	Carbamyidomethyl
- Variable modifications	Oxidation (Met), Acetyl (N-terminus)
- Quantification	None
- Peptide tolerance	± 10 ppm
- #13C	1
- MS2 tolerance	± 0.02 Da
- Peptide charge	2+, 3+
- Mass value	Monoisotopic
- Instrument	ESI-FTICR

Scaffold filter criteria

- Minimum identification percentage for protein	80 %
- Number of unique peptides required	2
- Minimum identification percentage for peptides	50 %

8.5 LC-MS/MS and microarray data

Table 8: Results from LC-MS/MS and microarray study. All regulated proteins (ratio ≥ 1.3) and all regulated genes (FDR < 10 %; ratio > 1.3) were summarised and confronted.

Gene ID	Description	LC-MS/MS		Microarray	
		p-value	ratio	p-value	ratio
4938	2',5'-oligoadenylate synthetase 1, 40/46kDa			0.051	0.65
622	3-hydroxybutyrate dehydrogenase, type 1	0.455	0.56		
26873	5-oxoprolinase (ATP-hydrolysing)	0.914	0.56		
55347	Abhydrolase domain containing 10	0.274	2.12		
116236	Abhydrolase domain containing 15	0.146	2.15		
48	Aconitase 1, soluble	0.377	1.81		
70	Actin, alpha, cardiac muscle 1	0.146	3.41		
60	Actin, beta	0.520	0.56		
467	Activating transcription factor 3			0.069	1.48
23237	Activity-regulated cytoskeleton-associated protein			0.048	1.37
55856	Acyl-CoA thioesterase 13	0.867	0.42		
56999	ADAM metallopeptidase with thrombospondin type 1 motif, 9			0.079	0.73
130340	Adaptor-related protein complex 1, sigma 3 subunit			0.045	1.91
1176	Adaptor-related protein complex 3, sigma 1 subunit	0.183	0.51		
118	Adducin 1 (alpha)	0.926	0.49		
120	Adducin 3 (gamma)	0.280	0.33		
353	Adenine phosphoribosyltransferase	0.318	0.50		
159	Adenylosuccinate synthase	0.078	0.55		
122622	Adenylosuccinate synthase like 1			0.087	1.32
22850	ADNP homeobox 2			0.062	1.35
375	ADP-ribosylation factor 1	0.300	0.52		
378	ADP-ribosylation factor 4	0.683	0.57		
381	ADP-ribosylation factor 5	0.637	0.59		
382	ADP-ribosylation factor 6	0.601	0.38		
10124	ADP-ribosylation factor-like 4A, transcript variant 1			0.051	1.57
23204	ADP-ribosylation factor-like 6 interacting protein 1	0.234	2.20		
79026	AHNAK nucleoprotein	0.289	0.60		
87769	AIG2-like domain 1	0.227	0.15		
290	Alanyl (membrane) aminopeptidase	0.213	0.33		
10840	Aldehyde dehydrogenase 1 family, member L1	0.200	2.04		
8659	Aldehyde dehydrogenase 4 family, member A1			0.087	1.32
5832	Aldehyde dehydrogenase 18 family, member A1	0.722	0.58		
316	Aldehyde oxidase 1	0.405	0.41		
231	Aldo-keto reductase family 1, member B1 (aldose reductase)	0.137	0.54		
230	Aldolase C, fructose-bisphosphate	0.458	3.89		
54518	Amyloid beta (A4) precursor protein-binding, family B, member 1 interacting protein	0.612	1.88		
154796	Angiomotin			0.063	1.36
51421	Angiomotin like 2			0.086	1.38
25841	Ankyrin repeat and BTB (POZ) domain containing 2			0.074	1.32
27063	Ankyrin repeat domain 1 (cardiac muscle)			0.046	1.66
55608	Ankyrin repeat domain 10			0.048	1.39
57730	Ankyrin repeat domain 36B			0.093	0.68
306	Annexin A3	0.125	0.39		
63982	Anoctamin 3			0.060	1.46
196527	Anoctamin 6	0.252	1.39		
336	Apolipoprotein A-II	0.377	0.39		
338	Apolipoprotein B (including Ag(x) antigen)			0.087	1.58
345	Apolipoprotein C-III	0.387	0.13		
79135	Apolipoprotein O	0.262	1.71		
65117	Arginine/serine-rich coiled-coil 2			0.063	1.44
445	Argininosuccinate synthetase 1	0.157	1.65		
8874	ARHGEF7; Rho guanine nucleotide exchange factor (GEF) 7	0.713	0.62		
10097	ARP2 actin-related protein 2 homolog (yeast)	0.208	0.70		
91947	Arrestin domain containing 4			0.043	1.45
57491	Aryl-hydrocarbon receptor repressor; programmed cell death 6	0.051	0.58		
29929	Asparagine-linked glycosylation 6, alpha-1,3-glucosyltransferase homolog (S. cerevisiae)			0.058	0.76
443	Aspartoacylase (Canavan disease)	0.182	1.82		
472	Ataxia telangiectasia mutated			0.046	0.73
51062	Atlastin GTPase 1			0.073	1.34
25923	Atlastin GTPase 3	0.086	1.45		
522	ATP synthase, H+ transporting, mitochondrial F0 complex, subunit F6	0.745	0.38		
10632	ATP synthase, H+ transporting, mitochondrial F0 complex, subunit G	0.236	3.41		
513	ATP synthase, H+ transporting, mitochondrial F1 complex, delta subunit	0.806	0.43		
23250	ATPase, class VI, type 11A			0.093	0.76
9550	ATPase, H+ transporting, lysosomal 13kDa, V1 subunit G1	0.672	0.31		
9296	ATPase, H+ transporting, lysosomal 14kDa, V1 subunit F	0.085	0.20		
9114	ATPase, H+ transporting, lysosomal 38kDa, V0 subunit d1			0.061	1.35

Gene ID	Description	LC-MS/MS		Microarray	
		p-value	ratio	p-value	ratio
476	ATPase, Na+/K+ transporting, alpha 1 polypeptide	0.432	0.56		
483	ATPase, Na+/K+ transporting, beta 3 polypeptide	0.168	0.70		
23460	ATP-binding cassette, sub-family A (ABC1), member 6			0.048	0.67
225	ATP-binding cassette, sub-family D (ALD), member 2	0.196	2.75		
23	ATP-binding cassette, sub-family F (GCN20), member 1	0.636	2.80		
475	ATX1 antioxidant protein 1 homolog (yeast)	0.373	0.24		
79365	Basic helix-loop-helix family, member e41			0.046	2.01
689	BTF3; basic transcription factor 3	0.344	0.52		
148789	Beta-1,3-N-acetylgalactosaminyltransferase 2			0.048	1.33
567	Beta-2-microglobulin	0.828	0.30		
670	Biphenyl hydrolase-like (serine hydrolase)	0.342	3.25		
10409	Brain abundant, membrane attached signal protein 1	0.716	0.39		
9577	Brain and reproductive organ-expressed (TNFRSF1A modulator)			0.048	1.34
51660	Brain protein 44-like	0.195	3.02		
153579	Butyrophilin-like 9	0.314	0.30		
55845	C3orf10 Isoform 1 of Probable protein BRICK1	0.446	0.28		
1012	Cadherin 13, H-cadherin (heart)	0.307	0.40		
794	Calbindin 2	0.069	2.18		
781	Calcium channel, voltage-dependent, alpha 2/delta subunit 1	0.908	1.83		
824	Calpain 2, (m/II) large subunit	0.088	0.70		
25927	Cannabinoid receptor interacting protein 1	0.257	0.28		
10487	CAP, adenylate cyclase-associated protein 1 (yeast)	0.084	0.50		
761	Carbonic anhydrase III, muscle specific	0.142	0.42		
873	Carbonyl reductase 1	0.123	1.45		
1066	Carboxylesterase 1 (monocyte /macrophage serine esterase 1)	0.059	1.68		
1359	Carboxypeptidase A3 (mast cell)	0.318	0.54		
202333	Cardiomyopathy associated 5			0.092	1.37
1499	Catenin (cadherin-associated protein), beta 1, 88kDa	0.415	0.41		
1500	Catenin (cadherin-associated protein), delta 1	0.486	0.30		
1075	Cathepsin C	0.055	0.38	0.073	0.68
1514	Cathepsin L1	0.260	1.87		

Gene ID	Description	LC-MS/MS		Microarray	
		p-value	ratio	p-value	ratio
4435	Cbp/p300-interacting transactivator, with Glu/Asp-rich carboxy-terminal domain,1			0.088	1.59
25819	CCR4 carbon catabolite repression 4-like (S. cerevisiae)			0.048	1.56
80381	CD276 molecule	0.685	0.43		
960	CD44 molecule (Indian blood group)	0.198	0.28		
966	CD59 molecule, complement regulatory protein	0.683	0.47		
9308	CD83 molecule			0.063	1.43
1164	CDC28 protein kinase regulatory subunit 2			0.054	1.41
57396	CDC-like kinase 4			0.080	1.59
55847	CDGSH iron sulfur domain 1	0.305	0.64		
10752	Cell adhesion molecule with homology to L1CAM (close homolog of L1)			0.058	0.63
53405	Chloride intracellular channel 5	0.174	0.55		
1119	Choline kinase alpha			0.063	1.59
57053	Cholinergic receptor, nicotinic, alpha 10			0.043	1.31
1464	Chondroitin sulfate proteoglycan 4	0.532	0.47		
148523	Chromosome 1 open reading frame 51			0.047	2.22
148423	Chromosome 1 open reading frame 52			0.093	1.31
57035	Chromosome 1 open reading frame 63			0.076	1.54
440574	Chromosome 1 open reading frame 151	0.288	58.72		
126868	Chromosome 1 open reading frame 161			0.091	1.38
388701	Chromosome 1 open reading frame 189			0.048	1.49
440957	Chromosome 3 open reading frame 78			0.087	1.45
55286	Chromosome 4 open reading frame 19			0.069	1.56
201725	Chromosome 4 open reading frame 46			0.043	1.83
4883	Chromosome 5 open reading frame 23			0.051	1.64
153222	Chromosome 5 open reading frame 41			0.051	1.39
222166	Chromosome 7 open reading frame 41	0.252	8.73		
286006	Chromosome 7 open reading frame 53			0.046	1.91
79846	Chromosome 7 open reading frame 63			0.067	1.42
10974	Chromosome 10 open reading frame 116	0.808	0.49		
28971	Chromosome 11 open reading frame 67	0.415	7.45		
81892	Chromosome 14 open reading frame 156	0.122	0.40		
80072	Chromosome 15 open reading frame 34			0.043	1.61
57020	Chromosome 16 open reading frame 62	0.112	3.94		
83636	Chromosome 19 open reading frame 12			0.073	1.42
58509	Chromosome 19 open reading frame 29			0.059	1.36
284424	Chromosome 19 open reading frame 30			0.057	1.96
114036	Chromosome 21 open reading frame 82			0.081	0.70
9076	Claudin 1			0.031	1.63
9002	Coagulation factor II (thrombin) receptor-like 3			0.094	0.72

Gene ID	Description	LC-MS/MS		Microarray	
		p-value	ratio	p-value	ratio
2162	Coagulation factor XIII, A1 polypeptide	0.203	0.20		
26958	Coatomer protein complex, subunit gamma 2	0.619	0.51		
28952	Coiled-coil domain containing 22	0.183	1.45		
79140	Coiled-coil domain containing 28B			0.096	1.40
83643	Coiled-coil domain containing 3			0.034	1.39
54520	Coiled-coil domain containing 93			0.058	1.32
1291	Collagen, type VI, alpha 1	0.371	0.33		
1292	Collagen, type VI, alpha 2	0.385	0.24		
1293	Collagen, type VI, alpha 3	0.161	0.32	0.083	0.57
23412	COMM domain containing 3	0.501	0.43		
170622	COMM domain containing 6	0.590	0.07		
708	Complement component 1, q subcomponent binding protein	0.313	2.76		
735	Complement component 9			0.057	1.39
50813	COPS7A; COP9 signalosome subunit 7A	0.091	1.88		
23242	Cordon-bleu homolog (mouse)			0.043	1.40
57175	Coronin, actin binding protein, 1B	0.015	0.66		
2017	Cortactin	0.879	0.48		
1160	Creatine kinase, mitochondrial 2 (sarcomeric)	0.384	2.70		
200186	CREB regulated transcription coactivator 2			0.050	1.45
1407	Cryptochrome 1 (photolyase-like)			0.048	1.47
1408	Cryptochrome 2 (photolyase-like)			0.061	1.46
1410	Crystallin, alpha B	0.155	1.61		
64478	CUB and Sushi multiple domains 1			0.069	1.31
60677	CUGBP, Elav-like family member 6			0.046	1.34
8454	Cullin 1	0.569	0.58		
8450	Cullin 4B	0.199	0.40		
8065	Cullin 5	0.075	1.53		
898	Cyclin E1			0.096	1.38
57018	Cyclin L1			0.058	1.53
1031	Cyclin-dependent kinase inhibitor 2C (p18, inhibits CDK4)	0.111	0.46		
1540	Cylindromatosis (turban tumor syndrome)			0.048	1.31
1475	Cystatin A (stefin A)	0.494	0.43		
1476	Cystatin B (stefin B)	0.343	0.22		
64651	Cysteine-serine-rich nuclear protein 1			0.079	1.65
51727	Cytidine monophosphate (UMP-CMP) kinase 1, cytosolic	0.353	1.90		
1727	Cytochrome b5 reductase 3	0.230	1.58		
1528	Cytochrome b5 type A (microsomal)	0.391	1.71		
80777	Cytochrome b5 type B (outer mitochondrial membrane)	0.512	957.21		
1327	Cytochrome c oxidase subunit IV isoform 1	0.202	0.32		
9377	Cytochrome c oxidase subunit Va	0.290	0.17		
1329	Cytochrome c oxidase subunit Vb	0.092	4.17		
1340	Cytochrome c oxidase subunit Vib polypeptide 1 (ubiquitous)	0.917	3.02		
1583	Cytochrome P450, family 11, subfamily A, polypeptide 1			0.050	1.39
1576	Cytochrome P450, family 3, subfamily A, polypeptide 4			0.092	1.38
1577	Cytochrome P450, family 3, subfamily A, polypeptide 5			0.059	1.32
1595	Cytochrome P450, family 51, subfamily A, polypeptide 1			0.048	0.73
23191	Cytoplasmic FMR1 interacting protein 1	0.220	0.48		
10970	Cytoskeleton-associated protein 4	0.216	0.62		
1652	D-dopachrome tautomerase	0.097	2.55		
1654	DEAD (Asp-Glu-Ala-Asp) box polypeptide 3, X-linked	0.367	0.49		
1655	DEAD (Asp-Glu-Ala-Asp) box polypeptide 5	0.232	0.37		
10521	DEAD (Asp-Glu-Ala-Asp) box polypeptide 17	0.153	0.63		
1660	DEAH (Asp-Glu-Ala-His) box polypeptide 9	0.238	0.58		
1665	DEAH (Asp-Glu-Ala-His) box polypeptide 15	0.519	1.63		
28960	Decapping enzyme, scavenger	0.372	0.59		
1793	Dedicator of cytokinesis 1			0.043	0.73
1603	Defender against cell death 1	0.650	0.43		
400830	Defensin, beta 132			0.061	2.07
79154	Dehydrogenase/reductase (SDR family) member 11	0.179	1.53		
1854	Deoxyuridine triphosphatase	0.255	0.47		
79139	Der1-like domain family, member 1	0.273	2.73		
117159	Dermcidin	0.127	0.39		
1829	Desmoglein 2			0.076	0.76
1808	Dihydropyrimidinase-like 2	0.603	0.45	0.048	0.73
23576	Dimethylarginine dimethylaminohydrolase 1	0.375	0.58		
29958	Dimethylglycine dehydrogenase	0.068	1.94		
1649	DNA-damage-inducible transcript 3			0.043	1.42
3301	DnaJ (Hsp40) homolog, subfamily A, member 1	0.152	0.60		
9829	DnaJ (Hsp40) homolog, subfamily C, member 6			0.096	1.59
1816	Dopamine receptor D5			0.087	1.38
1850	Dual specificity phosphatase 8			0.048	1.35
11221	Dual specificity phosphatase 10			0.093	1.53
8632	Dynein, axonemal, heavy chain 17			0.043	1.60
140735	Dynein, light chain, LC8-type 2	0.143	0.18		

Gene ID	Description	LC-MS/MS		Microarray	
		p-value	ratio	p-value	ratio
6990	Dynein, light chain, Tctex-type 3	0.369	1.77		
8291	Dysferlin, limb girdle muscular dystrophy 2B (autosomal recessive)	0.473	0.41		
1605	Dystroglycan 1 (dystrophin-associated glycoprotein 1)	0.345	0.41		
1958	Early growth response 1			0.048	1.61
1960	Early growth response 3			0.074	1.32
2009	Echinoderm microtubule associated protein like 1	0.036	0.38		
256364	Echinoderm microtubule associated protein like 3	0.363	2.25		
5167	Ectonucleotide pyrophosphatase/phosphodiesterase 1	0.629	2.57		
10085	EGF-like repeats and discoidin I-like domains 3			0.048	0.52
25975	EGF-like-domain, multiple 6			0.011	2.00
255520	ELMO/CED-12 domain containing 2	0.192	1.99		
9343	Elongation factor Tu GTP binding domain containing 2	0.258	0.44		
64834	Elongation of very long chain fatty acids; ELOVL1	0.024	0.60		
2010	Emerin	0.801	3.81		
2022	Endoglin	0.941	0.35		
64167	Endoplasmic reticulum aminopeptidase 2			0.076	0.71
90952	Endothelial cell adhesion molecule	0.473	0.41		
80314	Enhancer of polycomb homolog 1 (Drosophila)			0.094	1.46
2079	Enhancer of rudimentary homolog (Drosophila)	0.595	0.23		
79746	Enoyl Coenzyme A hydratase domain containing 3	0.271	2.17		
1892	Enoyl Coenzyme A hydratase, short chain, 1, mitochondrial	0.270	2.90		
1969	EPH receptor A2			0.048	1.40
1948	Ephrin-B2			0.043	1.56
58513	Epidermal growth factor receptor pathway substrate 15-like 1	0.309	1.93		
30001	ERO1-like (S. cerevisiae)	0.403	1.57	0.090	0.76
2035	Erythrocyte membrane protein band 4.1 (elliptocytosis 1, RH-linked)			0.087	1.33
26298	Ets homologous factor			0.077	1.52
9521	Eukaryotic translation elongation factor 1 epsilon 1	0.145	1.95		
1965	Eukaryotic translation initiation factor 2, subunit 1 alpha, 35kDa	0.115	0.67		
8668	Eukaryotic translation initiation factor 3, subunit I	0.498	0.68		
9775	Eukaryotic translation initiation factor 4A, isoform 3	0.309	0.55		
1983	Eukaryotic translation initiation factor 5	0.423	0.67		
2107	Eukaryotic translation termination factor 1	0.507	0.68		
2130	EWS RNA-binding protein 1	0.140	0.54		
55770	Exocyst complex component 2	0.597	2.51		
11260	Exportin, tRNA (nuclear export receptor for tRNAs)	0.194	0.63		
113115	Family with sequence similarity 54, member A			0.083	1.38
55177	Family with sequence similarity 82, member A2	0.313	1.65		
92689	Family with sequence similarity 114, member A1	0.073	1.70		
115572	Family with sequence similarity 46, member B			0.048	1.42
54629	Family with sequence similarity 63, member B			0.050	0.74
8880	Far upstream element (FUSE) binding protein 1	0.677	0.53		
2224	Farnesyl diphosphate synthase; FDPS	0.125	0.59		
2167	Fatty acid binding protein 4, adipocyte	0.159	0.55		
3992	Fatty acid desaturase 1			0.081	0.67
55711	Fatty acyl CoA reductase 2			0.096	0.74
114907	F-box protein 32			0.094	1.47
2200	Fibrillin 1			0.031	0.63
10818	Fibroblast growth factor receptor substrate 2			0.080	1.32
11259	Filamin A interacting protein 1-like			0.043	1.40
2316	Filamin A, alpha (actin binding protein 280)	0.982	0.45		
2287	FK506 binding protein 3, 25kDa	0.230	2.87		
2314	Flightless I homolog (Drosophila)	0.356	0.49		
441310	FLJ00290 protein			0.050	1.82
11167	Follistatin-like 1	0.104	0.70		
8061	FOS-like antigen 1			0.043	1.32
24147	Four jointed box 1 (Drosophila)			0.083	1.35
2517	Fucosidase, alpha-L- 1, tissue			0.073	0.66
65991	FUN14 domain containing 2	0.624	10.53		
85476	G elongation factor, mitochondrial 1	0.213	1.55		
55890	G protein-coupled receptor, family C, group 5, member C			0.046	1.91
29094	Galectin-related protein			0.068	1.35
2625	GATA binding protein 3			0.054	1.82
10985	GCN1 general control of amino-acid synthesis 1-like 1 (yeast)	0.625	0.67		
2934	Gelsolin (amyloidosis, Finnish type)	0.192	0.60		
152007	GLI pathogenesis-related 2	0.149	6.17		
8521	Glial cells missing homolog 1 (Drosophila)			0.057	1.54

Gene ID	Description	LC-MS/MS		Microarray	
		p-value	ratio	p-value	ratio
2539	Glucose-6-phosphate dehydrogenase			0.043	0.74
2745	Glutaredoxin (thioltransferase)	0.505	0.65		
51218	Glutaredoxin 5	0.225	0.05		
2944	Glutathione S-transferase mu 1			0.087	1.31
2946	Glutathione S-transferase mu 2 (muscle)	0.373	1.39	0.085	1.45
57678	Glycerol-3-phosphate acyltransferase, mitochondrial	0.510	2.29		
2653	Glycine cleavage system protein H (aminomethyl carrier)	0.299	0.03		
10249	Glycine-N-acyltransferase			0.074	1.94
2997	Glycogen synthase 1 (muscle)	0.966	2.46		
8908	Glycogenin 2	0.147	2.72		
2995	Glycophorin C (Gerbich blood group)	0.301	5.55		
79709	Glycosyltransferase 25 domain containing 1	0.469	0.44		
2239	Glypican 4			0.068	0.75
2803	Golgin A4			0.048	1.34
29841	Grainyhead-like 1 (Drosophila)			0.048	1.67
1647	Growth arrest and DNA-damage-inducible, alpha			0.043	1.43
4616	Growth arrest and DNA-damage-inducible, beta			0.050	1.49
2669	GTP binding protein overexpressed in skeletal muscle			0.070	1.37
2644	GTP cyclohydrolase I feedback regulator	0.134	0.16		
10399	Guanine nucleotide binding protein (G protein), beta polypeptide 2-like 1	0.181	0.49		
54331	Guanine nucleotide binding protein (G protein), gamma 2	0.541	0.28		
2791	Guanine nucleotide binding protein (G protein), gamma 11	0.899	0.15		
55970	Guanine nucleotide binding protein (G protein), gamma 12	0.646	0.37		
2633	Guanylate binding protein 1, interferon-inducible, 67kDa	0.044	0.46		
3005	H1 histone family, member 0	0.770	0.11		
51020	HD domain containing 2	0.446	0.47		
10808	Heat shock 105kDa/110kDa protein 1	0.642	0.39		
3336	Heat shock 10kDa protein 1 (chaperonin 10)	0.411	0.42		
27129	Heat shock 27kDa protein family, member 7 (cardiovascular)			0.068	1.54
3306	Heat shock 70kDa protein 2	0.530	1.72		
126393	Heat shock protein, alpha-crystallin-related, B6	0.076	2.59	0.098	1.37
10075	HECT, UBA and WWE domain containing 1	0.221	0.46		

Gene ID	Description	LC-MS/MS		Microarray	
		p-value	ratio	p-value	ratio
3162	Heme oxygenase (decycling) 1	0.165	0.45		
3039	Hemoglobin, alpha 2; hemoglobin, alpha 1	0.609	0.09		
3043	Hemoglobin, beta	0.625	0.13		
3045	Hemoglobin, delta	0.814	0.43		
3339	Heparan sulfate proteoglycan 2	0.234	0.50		
84868	Hepatitis A virus cellular receptor 2			0.060	0.73
3068	Hepatoma-derived growth factor (high-mobility group protein 1-like)	0.257	0.57		
3182	Heterogeneous nuclear ribonucleoprotein A/B	0.103	0.50		
3183	Heterogeneous nuclear ribonucleoprotein C (C1/C2)	0.086	0.33		
3184	Heterogeneous nuclear ribonucleoprotein D (AU-rich element RNA binding protein 1, 37kDa)	0.054	0.61		
9987	Heterogeneous nuclear ribonucleoprotein D-like	0.016	0.67		
3190	Heterogeneous nuclear ribonucleoprotein K	0.233	2.50		
10236	Heterogeneous nuclear ribonucleoprotein R	0.502	0.41		
3192	Heterogeneous nuclear ribonucleoprotein U (scaffold attachment factor A)	0.295	1.61		
221092	Heterogeneous nuclear ribonucleoprotein U-like 2	0.365	0.37		
8479	HIRA interacting protein 3			0.051	1.32
84681	Histidine triad nucleotide binding protein 2	0.110	5.58		
3006	Histone cluster 1, H1c	0.325	0.22		
3010	Histone cluster 1, H1t			0.068	1.33
3012	Histone cluster 1, H2ae; histone cluster 1, H2ab	0.368	3.74		
8343	Histone cluster 1, H2bf			0.064	1.49
8339	Histone cluster 1, H2bg			0.079	1.47
8970	Histone cluster 1, H2bj			0.048	1.46
8365	Histone cluster 1, H4h			0.046	1.43
8349	Histone cluster 2, H2be			0.046	1.41
440689	Histone cluster 2, H2bf			0.043	1.76
7919	HLA-B associated transcript 1	0.053	0.51		
7917	HLA-B associated transcript 3	0.319	0.52		
26959	HMG-box transcription factor 1			0.081	1.35
79663	HSPB (heat shock 27kDa) associated protein 1			0.062	1.49
3145	Hydroxymethylbilane synthase	0.180	1.94		
81888	Hydroxypyruvate isomerase homolog (E. coli)	0.203	1.87		
51144	Hydroxysteroid (17-beta) dehydrogenase 12	0.179	1.75		
7923	Hydroxysteroid (17-beta) dehydrogenase 8	0.228	1.89		
284837	Hypothetical LOC284837			0.046	1.99

Gene ID	Description	LC-MS/MS		Microarray	
		p-value	ratio	p-value	ratio
388796	Hypothetical LOC388796			0.054	1.33
401281	Hypothetical LOC401281			0.059	1.55
402483	Hypothetical LOC402483			0.050	1.33
5928	Hypothetical LOC642954; retinoblastoma binding protein 4	0.187	0.51		
29058	Hypothetical LOC642975; chromosome 20 open reading frame 30	0.522	0.26		
654433	Hypothetical LOC654433			0.096	1.50
8028117	Hypothetical protein			0.094	1.40
6637	Hypothetical protein LOC100132425; similar to small nuclear ribonucleoprotein polypeptide G	0.657	0.13		
55737	Hypothetical protein LOC100133770; vacuolar protein sorting 35 homolog (S. cerevisiae)	0.527	1.44		
100506809	Hypothetical protein LOC100506809			0.090	1.48
84772	Hypothetical protein MGC13008			0.096	1.33
9592	Immediate early response 2			0.043	1.49
3615	IMP (inosine monophosphate) dehydrogenase 2	0.086	0.58		
10526	Importin 8			0.043	0.73
54556	Inhibitor of growth family, member 3			0.059	1.39
3479	Insulin-like growth factor 1 (somatomedin C)			0.043	1.44
3482	Insulin-like growth factor 2 receptor	0.504	2.11		
55656	Integrator complex subunit 8			0.056	0.75
3678	Integrin, alpha 5 (fibronectin receptor, alpha polypeptide)	0.319	0.45		
3659	Interferon regulatory factor 1			0.094	1.94
3394	Interferon regulatory factor 8			0.043	1.35
2537	Interferon, alpha-inducible protein 6			0.073	0.72
3433	Interferon-induced protein with tetratricopeptide repeats 2			0.043	0.74
3437	Interferon-induced protein with tetratricopeptide repeats 3			0.057	0.67
3475	Interferon-related developmental regulator 1			0.061	1.33
3554	Interleukin 1 receptor, type I			0.048	0.76
3606	Interleukin 18 (interferon-gamma-inducing factor)			0.051	1.39
3608	Interleukin enhancer binding factor 2, 45kDa	0.303	0.62		
3609	Interleukin enhancer binding factor 3, 90kDa	0.211	1.62		
9118	Internexin neuronal intermediate filament protein, alpha			0.043	1.62
8826	IQ motif containing GTPase activating protein 1	0.282	0.56		
51015	Isochorismatase domain containing 1	0.169	1.84		
3420	Isocitrate dehydrogenase 3 (NAD+) beta	0.489	0.50		

Gene ID	Description	LC-MS/MS		Microarray	
		p-value	ratio	p-value	ratio
55699	Isoleucyl-tRNA synthetase 2, mitochondrial	0.659	0.58		
3727	Jun D proto-oncogene			0.060	1.32
3725	Jun proto-oncogene			0.046	1.31
3728	Junction plakoglobin			0.043	0.70
340359	Kelch-like 38 (Drosophila)			0.046	1.61
55958	Kelch-like 9 (Drosophila)			0.043	0.74
3848	Keratin 1	0.712	2.12		
3849	Keratin 2	0.847	3.30		
3856	Keratin 8			0.048	1.45
3857	Keratin 9	0.933	2.80		
284827	Keratin associated protein 13-4			0.051	1.76
23392	KIAA0368	0.463	2.06		
22889	KIAA0907			0.046	1.38
57495	KIAA1239			0.043	1.71
284058	KIAA1267			0.056	1.39
57805	KIAA1967	0.129	0.59		
25959	KN motif and ankyrin repeat domains 2	0.382	0.65		
163782	KN motif and ankyrin repeat domains 4	0.149	1.46		
7071	Kruppel-like factor 10			0.051	1.45
8462	Kruppel-like factor 11			0.057	1.44
9314	Kruppel-like factor 4 (gut)			0.078	1.36
497048	KU-MEL-3			0.096	2.88
114294	Lactamase, beta	0.178	2.05		
51110	Lactamase, beta 2	0.114	2.09		
4000	Lamin A/C	0.844	0.61		
84823	Lamin B2	0.238	0.51		
3910	Laminin, alpha 4	0.081	0.61		
3912	Laminin, beta 1			0.047	0.70
3915	Laminin, gamma 1 (formerly LAMB2)	0.160	0.72		
56925	Latexin	0.407	0.46		
26524	LATS, large tumor suppressor, homolog 2 (Drosophila)			0.062	1.31
3956	Lectin, galactoside-binding, soluble, 1	0.947	0.21		
3954	Leucine zipper-EF-hand containing transmembrane protein 1	0.310	1.87		
10128	Leucine-rich PPR-motif containing	0.623	1.73		
120892	Leucine-rich repeat kinase 2			0.096	0.76
4012	Leucyl/cystinyl aminopeptidase	0.672	0.71		
51520	Leucyl-tRNA synthetase	0.394	0.63		
29995	LIM and cysteine-rich domains 1	0.617	0.60	0.011	1.41
51474	LIM domain and actin binding 1	0.730	0.55		
55180	Lines homolog (Drosophila)			0.061	1.35
3988	Lipase A, lysosomal acid, cholesterol esterase			0.087	0.64

Gene ID	Description	LC-MS/MS		Microarray	
		p-value	ratio	p-value	ratio
3991	Lipase, hormone-sensitive	0.523	1.71		
3929	Lipopolysaccharide binding protein			0.078	1.71
9361	Lon peptidase 1, mitochondrial	0.694	1.70		
91355	Low density lipoprotein receptor-related protein 5-like			0.048	1.33
4035	Low density lipoprotein-related protein 1 (alpha-2-macroglobulin receptor)	0.127	0.56		
51691	LSM8 homolog, U6 small nuclear RNA associated (S. cerevisiae)	0.537	0.35		
3936	Lymphocyte cytosolic protein 1 (L-plastin)	0.570	0.46		
23135	Lysine (K)-specific demethylase 6B			0.071	1.50
3916	Lysosomal-associated membrane protein 1	0.190	1.63		
114569	Mal, T-cell differentiation protein 2	0.194	2.49		
4190	Malate dehydrogenase 1, NAD (soluble)			0.096	1.33
9761	Malectin	0.344	3.23		
10873	Malic enzyme 3, NADP(+)-dependent, mitochondrial			0.063	1.38
256714	MAP7 domain containing 2			0.046	2.22
8649	MAPK scaffold protein 1	0.646	0.04		
4321	Matrix metallopeptidase 12 (macrophage elastase)			0.069	1.58
4327	Matrix metallopeptidase 19			0.011	1.67
4161	Melanocortin 5 receptor			0.043	1.67
10916	Melanoma antigen family D, 2			0.058	0.76
154141	Membrane bound O-acyltransferase domain containing 1			0.048	0.70
4311	Membrane metallo-endopeptidase	0.292	1.65		
4354	Membrane protein, palmitoylated 1, 55kDa			0.083	0.74
115123	Membrane-associated ring finger (C3HC4) 3			0.069	1.32
7873	Mesencephalic astrocyte-derived neurotrophic factor	0.467	0.34		
4501	Metallothionein 1X			0.064	1.32
56922	Methylcrotonoyl-Coenzyme A carboxylase 1 (alpha)	0.907	1.57		
4522	Methylenetetrahydrofolate dehydrogenase (NADP+ dependent) 1, methenyltetrahydro-folate cyclohydrolase, formyltetrahydrofolate synthetase	0.238	2.30		
8076	Microfibrillar associated protein 5			0.050	1.36
406937	MicroRNA 145			0.075	0.71
4259	Microsomal glutathione S-transferase 3	0.835	1.78		
4281	Midline 1 (Opitz/BBB syndrome)			0.096	1.46
92259	Mitochondrial ribosomal protein S36	0.998	0.13		
51102	Mitochondrial trans-2-enoyl-CoA reductase	0.096	1.56		

Gene ID	Description	LC-MS/MS		Microarray	
		p-value	ratio	p-value	ratio
9927	Mitofusin 2	0.245	3.58		
11343	Monoglyceride lipase	0.240	1.50		
56180	Motile sperm domain containing 1			0.062	1.33
4436	MutS homolog 2, colon cancer, nonpolyposis type 1 (E. coli)			0.080	0.76
26579	Myeloma overexpressed			0.051	1.39
4208	Myocyte enhancer factor 2C			0.066	0.70
4641	Myosin IC	0.262	0.65		
4642	Myosin ID			0.046	0.56
79784	Myosin, heavy chain 14	0.156	1.65		
4627	Myosin, heavy chain 9, non-muscle	0.868	0.57		
10627	Myosin, light chain 12A, regulatory, non-sarcomeric	0.614	15.17		
10398	Myosin, light chain 9, regulatory	0.214	0.51		
4082	Myristoylated alanine-rich protein kinase C substrate	0.224	0.48		
4668	N-acetylgalactosaminidase, alpha-			0.046	0.72
79158	N-acetylglucosamine-1-phosphate transferase, alpha and beta subunits			0.050	0.74
50814	NAD(P) dependent steroid dehydrogenase-like	0.353	0.63		
1728	NAD(P)H dehydrogenase, quinone 1	0.103	1.77		
4695	NADH dehydrogenase (ubiquinone) 1 alpha subcomplex, 2, 8kDa	0.077	0.41		
4702	NADH dehydrogenase (ubiquinone) 1 alpha subcomplex, 8, 19kDa	0.652	0.61		
4710	NADH dehydrogenase (ubiquinone) 1 beta subcomplex,4	0.013	0.46		
4724	NADH dehydrogenase (ubiquinone) Fe-S protein 4, 18kDa (NADH-coenzyme Q reductase)	0.007	49.03		
4726	NADH dehydrogenase (ubiquinone) Fe-S protein 6, 13kDa (NADH-coenzyme Q reductase)	0.270	1.81		
4666	Nascent polypeptide-associated complex alpha subunit	0.213	0.65		
57701	NCK-associated protein 5-like			0.075	1.32
57447	NDRG family member 2	0.366	1.49		
10763	Nestin	0.405	0.17		
4905	N-ethylmaleimide-sensitive factor			0.058	0.72
4741	Neurofilament, medium polypeptide			0.043	1.46
10316	Neuromedin U receptor 1			0.062	1.33
4897	Neuronal cell adhesion molecule			0.043	1.51
4886	Neuropeptide Y receptor Y1			0.082	1.70

Gene ID	Description	LC-MS/MS		Microarray	
		p-value	ratio	p-value	ratio
50863	Neurotrimin			0.048	1.60
4809	NHP2 non-histone chromosome protein 2-like 1 (S. cerevisiae)	0.219	2.74		
4811	Nidogen 1	0.870	0.69		
22795	Nidogen 2 (osteonidogen)	0.010	0.61	0.094	0.69
10577	Niemann-Pick disease, type C2	0.483	4.10		
91754	NIMA (never in mitosis gene a)-related kinase9	0.473	0.44		
4814	Ninjurin 1			0.057	1.32
4671	NLR family, apoptosis inhibitory protein			0.096	0.75
112597	Non-protein coding RNA 152			0.046	1.31
64168	N-terminal EF-hand calcium binding protein 1			0.043	2.05
81788	NUAK family, SNF1-like kinase, 2			0.050	2.67
4686	Nuclear cap binding protein subunit 1, 80kDa	0.130	0.42		
4793	Nuclear factor of kappa light polypeptide gene enhancer in B-cells inhibitor, beta			0.054	1.43
84807	Nuclear factor of kappa light polypeptide gene enhancer in B-cells inhibitor, delta			0.062	1.44
4794	Nuclear factor of kappa light polypeptide gene enhancer in B-cells inhibitor, epsilon			0.088	2.02
9572	Nuclear receptor subfamily 1, group D, member 1			0.043	1.72
4929	Nuclear receptor subfamily 4, group A, member 2			0.080	1.73
4691	Nucleolin	0.090	0.55		
4860	Nucleoside phosphorylase	0.273	0.43		
80224	Nucleotide binding protein-like	0.202	3.69		
134492	NudC domain containing 2	0.469	0.09		
11164	Nudix (nucleoside diphosphate linked moiety X)-type motif 5	0.098	1.59		
57451	Odz, odd Oz/ten-m homolog 2 (Drosophila)			0.043	1.41
64859	Oligonucleotide/oligosaccharide-binding fold containing 2A			0.057	1.44
26578	Osteoclast stimulating factor 1	0.442	0.75		
5007	Oxysterol binding protein	0.739	0.48		
23022	Palladin, cytoskeletal associated protein			0.083	1.32
445815	PALM2-AKAP2 readthrough	0.459	0.62		
119548	Pancreatic lipase-related protein 3			0.080	1.84
5763	Parathymosin	0.213	2.48		
23047	PDS5, regulator of cohesion maintenance, homolog B (S. cerevisiae)			0.048	0.76
10611	PDZ and LIM domain 5	0.171	0.43		
10105	Peptidylprolyl isomerase F	0.267	2.23		
5187	Period homolog 1 (Drosophila)			0.053	2.43

Gene ID	Description	LC-MS/MS		Microarray	
		p-value	ratio	p-value	ratio
8864	Period homolog 2 (Drosophila)			0.084	1.44
25824	Peroxiredoxin 5	0.393	0.50		
23082	Peroxisome proliferator-activated receptor gamma, coactivator-related 1			0.064	1.41
79142	PHD finger protein 23			0.083	1.31
10026	Phosphatidylinositol glycan anchor biosynthesis, class K			0.043	0.75
93183	Phosphatidylinositol glycan anchor biosynthesis, class M			0.048	0.76
23556	Phosphatidylinositol glycan anchor biosynthesis, class N			0.043	0.71
23761	Phosphatidylserine decarboxylase			0.051	1.32
5153	Phosphodiesterase 1B, calmodulin-dependent			0.071	0.72
5211	Phosphofructokinase, liver	0.292	1.33		
5214	Phosphofructokinase, platelet	0.356	0.47		
29085	Phosphohistidine phosphatase 1	0.406	13200.62		
5295	Phosphoinositide-3-kinase, regulatory subunit 1 (alpha)	0.310	0.23		
5320	Phospholipase A2, group IIA (platelets, synovial fluid)			0.043	1.47
5321	Phospholipase A2, group IVA (cytosolic, calcium-dependent)	0.511	2.29		
23236	Phospholipase C, beta 1 (phosphoinositide-specific)			0.054	0.69
201164	Phospholipase D family, member 6			0.080	1.45
64077	Phospholysine phosphohistidine inorganic pyrophosphate phosphatase	0.327	4.01		
8682	Phosphoprotein enriched in astrocytes 15	0.091	0.53		
5634	Phosphoribosyl pyrophosphate synthetase 2			0.060	0.74
5836	Phosphorylase, glycogen, liver	0.358	2.00		
5837	Phosphorylase, glycogen, muscle	0.545	2.65	0.061	1.59
9317	Phosphotriesterase related	0.425	0.64		
27445	Piccolo (presynaptic cytomatrix protein)			0.046	1.54
5292	Pim-1 oncogene			0.048	1.61
11040	Pim-2 oncogene			0.061	1.45
5358	Plastin 3 (T isoform)	0.301	0.59		
5175	Platelet/endothelial cell adhesion molecule	0.663	0.28		
23612	Pleckstrin homology-like domain, family A, member 3	0.801	0.18		
5339	Plectin 1, intermediate filament binding protein 500kDa	0.118	0.59		
5817	Poliovirus receptor	0.196	0.41		

Gene ID	Description	LC-MS/MS		Microarray	
		p-value	ratio	p-value	ratio
115207	Potassium channel tetramerisation domain containing 12	0.304	0.35		
57326	Pre-B-cell leukemia homeobox interacting protein 1	0.193	1.64		
5204	Prefoldin subunit 5	0.811	0.50		
5672	Pregnancy specific beta-1-glycoprotein 4			0.094	1.35
200373	Primary ciliary dyskinesia protein 1			0.058	1.66
5351	Procollagen-lysine 1, 2-oxoglutarate 5-dioxygenase 1			0.096	0.76
5216	Profilin 1	0.876	0.36		
5217	Profilin 2	0.489	3.42		
5245	Prohibitin	0.315	4.21		
8974	Prolyl 4-hydroxylase, alpha polypeptide II			0.087	0.73
5034	Prolyl 4-hydroxylase, beta polypeptide	0.125	1.47		
5660	Prosaposin	0.354	4.73		
542767	Prostate collagen triple helix			0.073	1.44
5714	Proteasome (prosome, macropain) 26S subunit, non-ATPase, 8	0.033	1.50		
5685	Proteasome (prosome, macropain) subunit, alpha type, 4	0.029	1.45		
5693	Proteasome (prosome, macropain) subunit, beta type, 5	0.677	0.63		
5694	Proteasome (prosome, macropain) subunit, beta type, 6	0.484	0.35		
5699	Proteasome (prosome, macropain) subunit, beta type, 10	0.073	0.41		
5577	Protein kinase, cAMP-dependent, regulatory, type II, beta	0.069	1.31		
5514	Protein phosphatase 1, regulatory (inhibitor) subunit 10			0.048	1.47
23645	Protein phosphatase 1, regulatory (inhibitor) subunit 15A			0.043	1.39
84919	Protein phosphatase 1, regulatory (inhibitor) subunit 15B			0.043	1.34
5537	Protein phosphatase 6, catalytic subunit	0.042	0.55		
8493	Protein phosphatase, Mg2+/Mn2+ dependent, 1D			0.080	1.33
8073	Protein tyrosine phosphatase type IVA, member 2	0.270	0.57		
201562	Protein tyrosine phosphatase-like (proline instead of catalytic arginine), member b	0.015	0.59		
5101	Protocadherin 9			0.060	1.42
56121	Protocadherin beta 15			0.030	0.71
57717	Protocadherin beta 16			0.053	0.75
56133	Protocadherin beta 2			0.059	0.73
56132	Protocadherin beta 3			0.087	0.72
5092	Pterin-4 alpha-carbinolamine dehydratase /dimerization cofactor of hepatocyte nuclear factor 1 alpha	0.125	0.41		
84105	Pterin-4 alpha-carbinolamine dehydratase /dimerization cofactor of hepatocyte nuclear factor 1 alpha (TCF1) 2	0.162	0.31		
8495	PTPRF interacting protein, binding protein 2 (liprin beta 2)			0.083	1.44
400952	Putative uncharacterized protein UNQ6975 /PRO21958			0.082	1.39
5464	Pyrophosphatase (inorganic) 1	0.136	1.40		
27068	Pyrophosphatase (inorganic) 2	0.359	1.96		
55066	Pyruvate dehydrogenase phosphatase regulatory subunit	0.385	0.62		
5315	Pyruvate kinase, muscle	0.567	0.56		
23637	RAB GTPase activating protein 1	0.099	0.41		
5861	RAB1A, member RAS oncogene family	0.023	39.27		
22930	RAB3 GTPase activating protein subunit 1 (catalytic)	0.570	2.08		
5878	RAB5C, member RAS oncogene family	0.862	0.72		
5870	RAB6C, member RAS oncogene family	0.066	0.55		
9367	RAB9A, member RAS oncogene family	0.320	2.63	0.079	1.38
130132	Raftlin family member 2			0.043	0.59
23180	Raftlin, lipid raft linker 1	0.067	0.72		
57186	Ral GTPase activating protein, alpha subunit 2 (catalytic)			0.043	0.74
202151	RAN binding protein 3-like			0.096	1.46
5912	RAP2B, member of RAS oncogene family	0.273	0.51		
83937	Ras association (RalGDS/AF-6) domain family member 4			0.057	1.62
387	Ras homolog gene family, member A	0.883	0.66		
391	Ras homolog gene family, member G (rho G)	0.335	1.41		
9462	RAS protein activator like 2			0.087	1.31
6251	Ras suppressor protein 1	0.245	2.02		
153020	RasGEF domain family, member 1B			0.046	1.39
6236	Ras-related associated with diabetes			0.046	1.53
10231	Regulator of calcineurin 2			0.096	1.59
11079	RER1 retention in endoplasmic reticulum 1 homolog (S. cerevisiae)	0.126	0.54		

Gene ID	Description	LC-MS/MS		Microarray	
		p-value	ratio	p-value	ratio
5954	Reticulocalbin 1, EF-hand calcium binding domain	0.782	0.70		
57333	Reticulocalbin 3, EF-hand calcium binding domain	0.027	0.49		
57142	Reticulon 4	1.000	1.99		
146760	Reticulon 4 receptor-like 1			0.073	1.43
5959	Retinol dehydrogenase 5 (11-cis/9-cis)	0.256	1.50		
25996	REX2, RNA exonuclease 2 homolog (S. cerevisiae)	0.285	1.96		
27289	Rho family GTPase 1			0.096	1.55
390	Rho family GTPase 3	0.123	0.60		
9475	Rho-associated, coiled-coil containing protein kinase 2	0.225	0.55		
84659	Ribonuclease, RNase A family, 7			0.051	1.85
6124	Ribosomal protein L4	0.378	0.35		
6125	Ribosomal protein L5	0.222	0.38		
6135	Ribosomal protein L11	0.239	0.27		
6136	Ribosomal protein L12	0.192	0.42		
6143	Ribosomal protein L19	0.366	0.27		
6169	Ribosomal protein L38	0.133	0.02		
6205	Ribosomal protein S11	0.298	0.24		
6206	Ribosomal protein S12	0.242	0.61		
6217	Ribosomal protein S16	0.205	0.40		
6222	Ribosomal protein S18	0.315	0.09		
6223	Ribosomal protein S19	0.065	0.43		
6233	Ribosomal protein S27a	0.907	0.38		
6189	Ribosomal protein S3A	0.233	0.44		
6196	Ribosomal protein S6 kinase, 90kDa, polypeptide 2			0.059	0.74
6201	Ribosomal protein S7	0.214	0.41		
6203	Ribosomal protein S9	0.140	0.38		
3921	Ribosomal protein SA	0.131	0.52		
6181	Ribosomal protein, large, P2	0.084	0.48		
255488	Ring finger protein 144B			0.057	1.33
23429	RING1 and YY1 binding protein			0.067	1.32
5935	RNA binding motif (RNP1, RRM) protein 3	0.182	53.53		
10432	RNA binding motif protein 14			0.084	1.33
8607	RuvB-like 1 (E. coli)	0.131	0.73		
6275	S100 calcium binding protein A4	0.500	0.40		
6277	S100 calcium binding protein A6	0.759	0.24		
6281	S100 calcium binding protein A10	0.535	0.26		
6284	S100 calcium binding protein A13	0.552	0.37		
140576	S100 calcium binding protein A16	0.349	0.55		

Gene ID	Description	LC-MS/MS		Microarray	
		p-value	ratio	p-value	ratio
6285	S100 calcium binding protein B	0.949	0.30		
949	Scavenger receptor class B, member 1	0.199	0.40		
11196	SEC23 interacting protein	0.090	0.60		
11231	SEC63 homolog (S. cerevisiae)	0.079	2.67		
6400	Sel-1 suppressor of lin-12-like (C. elegans)	0.744	1.55		
22928	Selenophosphate synthetase 2			0.048	1.31
6697	Sepiapterin reductase (7,8-dihydrobiopterin: NADP+ oxidoreductase)	0.046	1.59		
10801	Septin 9	0.217	0.48		
63826	Serine racemase	0.044	1.67		
5272	Serpin peptidase inhibitor, clade B (ovalbumin), member 9	0.164	0.52		
6288	Serum amyloid A1			0.011	2.29
6289	Serum amyloid A2			0.031	1.90
6291	Serum amyloid A4, constitutive			0.043	1.86
375035	SFT2 domain containing 2			0.046	0.76
6727	Signal recognition particle 14kDa (homologous Alu RNA binding protein)	0.028	0.42		
6748	Signal sequence receptor, delta (translocon-associated protein delta)	0.364	0.51		
6742	Single-stranded DNA binding protein 1	0.335	5.61		
6741	Sjogren syndrome antigen B (autoantigen La)	0.421	0.71		
6636	Small nuclear ribonucleoprotein polypeptide F	0.894	0.10		
140775	Smith-Magenis syndrome chromosome region, candidate 8			0.035	1.43
6574	Solute carrier family 20 (phosphate transporter), member 1			0.048	1.45
291	Solute carrier family 25 (mitochondrial carrier; adenine nucleotide translocator),member 4	0.179	0.72		
8402	Solute carrier family 25 (mitochondrial carrier; oxoglutarate carrier), member11	0.187	1.41		
114789	Solute carrier family 25 (mitochondrial carrier; phosphate carrier), member 25			0.080	1.67
1836	Solute carrier family 26 (sulfate transporter), member 2			0.066	0.76
1318	Solute carrier family 31 (copper transporters), member 2			0.011	1.42
55238	Solute carrier family 38, member 7			0.056	1.33
6717	Sorcin	0.760	0.55		
6272	Sortilin 1	0.229	2.20		
51375	Sorting nexin 7			0.092	0.73
23224	Spectrin repeat containing, nuclear envelope 2			0.057	0.76
200162	Sperm associated antigen 17			0.043	1.69

Gene ID	Description	LC-MS/MS		Microarray	
		p-value	ratio	p-value	ratio
6723	Spermidine synthase	0.293	0.49		
10291	Splicing factor 3a, subunit 1, 120kDa	0.596	0.31		
83443	Splicing factor 3b, subunit 5, 10kDa	0.007	0.15		
6428	Splicing factor, arginine/serine-rich 3	0.008	0.51		
8935	Src kinase associated phosphoprotein2			0.043	0.73
6480	ST6 beta-galactosamide alpha-2,6-sialyl-tranferase 1			0.096	0.68
134429	StAR-related lipid transfer (START) domain containing 4			0.056	0.66
219285	Sterile alpha motif domain containing 9-like			0.062	0.59
6342	Sterol carrier protein 2	0.268	5.78		
6307	Sterol-C4-methyl oxidase-like			0.050	0.65
2040	Stomatin	0.359	0.46		
3703	STT3A, subunit of the oligosaccharyl-transferase complex (catalytic)	0.194	0.61		
10923	SUB1 homolog (S. cerevisiae)	0.348	0.46		
6390	Succinate dehydrogenase complex, subunit B, iron sulfur (Ip)	0.090	1.74		
6391	Succinate dehydrogenase complex, subunit C, integral membrane protein, 15kDa	0.129	4.34		
6821	Sulfite oxidase	0.141	1.68		
6818	Sulfotransferase family, cytosolic, 1A, phenol-preferring, member 3	0.488	0.40		
9899	Synaptic vesicle glycoprotein 2B			0.096	0.60
55333	Synaptojanin 2 binding protein	0.034	0.38		
8773	Synaptosomal-associated protein, 23kDa	0.122	0.37		
6386	Syndecan binding protein (syntenin)	0.319	0.63		
23336	Synemin, intermediate filament protein	0.132	3.10		
6809	Syntaxin 3			0.031	1.47
6875	TAF4b RNA polymerase II, TATA box binding protein (TBP)-associated factor, 105kDa			0.031	1.40
54885	TBC1 domain family, member 8B (with GRAM domain)			0.056	0.74
25976	TCDD-inducible poly(ADP-ribose) polymerase			0.043	1.48
64102	Tenomodulin			0.098	1.48
54881	Testis expressed 10			0.081	1.34
200424	Tet oncogene family member 3			0.053	1.76
9881	Tetratricopeptide repeat and ankyrin repeat containing 1			0.048	0.75
60436	TGFB-induced factor homeobox 2			0.049	1.75
7064	Thimet oligopeptidase 1	0.431	0.71		
1890	Thymidine phosphorylase	0.236	0.59		
9168	Thymosin beta 10	0.292	0.26		

Gene ID	Description	LC-MS/MS		Microarray	
		p-value	ratio	p-value	ratio
7116	Thymosin beta 4, X-linked pseudogene 2	0.236	0.08		
10131	TNF receptor-associated protein 1	0.254	1.54		
8041170	Trafficking protein particle complex subunit, putative			0.046	1.38
6921	Transcription elongation factor B(SIII), polypeptide 1 (15kDa, elongin C)	0.063	0.17		
8407	Transgelin 2	0.826	0.48		
26521	Translocase of inner mitochondrial membrane 8 homolog B (yeast)	0.033	0.34		
26520	Translocase of inner mitochondrial membrane 9 homolog (yeast)	0.937	0.32		
26517	Translocase of inner mitochondrial membrane 13 homolog (yeast)	0.827	0.26		
7108	Transmembrane 7 superfamily member 2	0.708	0.72		
10959	Transmembrane emp24 domain trafficking protein 2	0.021	0.36		
11018	Transmembrane emp24 protein transport domain containing 1	0.252	2.19		
51014	Transmembrane emp24 protein transport domain containing 7	0.257	1.38		
389208	Transmembrane protease, serine 11F			0.087	1.64
135932	Transmembrane protein 139			0.096	1.35
374882	Transmembrane protein 205	0.220	0.60		
54968	Transmembrane protein 70			0.069	1.58
84910	Transmembrane protein 87B			0.079	0.69
92162	Transmembrane protein 88			0.053	1.63
10345	Triadin			0.035	1.59
7227	Trichorhinophalangeal syndrome I			0.063	0.74
10612	Tripartite motif-containing 3			0.051	1.44
7706	Tripartite motif-containing 25	0.142	0.45		
55521	Tripartite motif-containing 36			0.057	1.35
7174	Tripeptidyl peptidase II	0.812	2.23		
441250	tRNA-yW synthesizing protein 1 homolog B (S. cerevisiae)			0.069	1.46
7170	Tropomyosin 3	0.558	0.42		
7453	Tryptophanyl-tRNA synthetase	0.453	0.50		
6902	Tubulin folding cofactor A	0.441	15.56		
6904	Tubulin folding cofactor D	0.161	0.57		
7286	Tuftelin 1			0.062	1.58
8743	Tumor necrosis factor (ligand) superfamily, member 10			0.096	0.61

Gene ID	Description	LC-MS/MS		Microarray	
		p-value	ratio	p-value	ratio
7128	Tumor necrosis factor, alpha-induced protein 3			0.062	1.73
7529	Tyrosine 3-monooxygenase/tryptophan 5-monooxygenase activation protein, beta polypeptide	0.127	3.85		
7531	Tyrosine 3-monooxygenase/tryptophan 5-monooxygenase activation protein, epsilon polypeptide	0.092	1.46		
7532	Tyrosine 3-monooxygenase/tryptophan 5-monooxygenase activation protein, gamma polypeptide	0.240	2.44		
29796	Ubiquinol-cytochrome c reductase complex (7.2 kD)	0.484	0.42		
9097	Ubiquitin specific peptidase 14 (tRNA-guanine transglycosylase)	0.891	1.50		
84640	Ubiquitin specific peptidase 38			0.096	1.33
25862	Ubiquitin specific peptidase 49			0.078	1.37
9354	Ubiquitination factor E4A (UFD2 homolog, yeast)	0.635	2.63		
7335	Ubiquitin-conjugating enzyme E2 variant 1	0.150	2.77		
7329	Ubiquitin-conjugating enzyme E2I (UBC9 homolog, yeast)	0.518	0.18		
51569	Ubiquitin-fold modifier 1	0.534	0.35		
51506	Ubiquitin-fold modifier conjugating enzyme 1	0.837	0.32		
55236	Ubiquitin-like modifier activating enzyme 6	0.388	0.61		
91373	UDP-N-acteylglucosamine pyrophosphorylase 1-like 1			0.077	1.77
55325	UFM1-specific peptidase 2	0.976	0.59		
11045	Uroplakin 1A			0.093	1.31
55697	Vac14 homolog (S. cerevisiae)	0.166	1.60		
54832	Vacuolar protein sorting 13 homolog C (S. cerevisiae)			0.050	0.75
112936	Vacuolar protein sorting 26 homolog B (S. pombe)	0.167	0.60		
51699	Vacuolar protein sorting 29 homolog (S. cerevisiae)	0.893	0.59		
7407	Valyl-tRNA synthetase	0.289	0.57		
10490	Vesicle transport through interaction with t-SNAREs homolog 1B (yeast)	0.076	1.65		
4097	V-maf musculoaponeurotic fibrosarcoma oncogene homolog G (avian)			0.052	1.34
79084	WD repeat domain 77	0.036	0.71		
23286	WW and C2 domain containing 1			0.061	1.38
388403	Yippee-like 2 (Drosophila)			0.067	1.51
284273	Zinc binding alcohol dehydrogenase domain containing 2			0.046	0.75
57621	Zinc finger and BTB domain containing 2			0.043	1.60
7538	Zinc finger protein 36, C3H type, homolog (mouse)			0.067	1.68
126295	Zinc finger protein 57			0.062	1.47
7710	Zinc finger protein 154			0.061	1.52
7569	Zinc finger protein 182			0.066	1.58
129025	Zinc finger protein 280A			0.031	1.65
27309	Zinc finger protein 330			0.065	1.34
22891	Zinc finger protein 365			0.050	1.33
25946	Zinc finger protein 385A			0.057	1.41
133923	Zinc finger protein 474			0.031	1.82
148254	Zinc finger protein 555			0.046	1.49
284309	Zinc finger protein 776			0.061	1.43
163131	Zinc finger protein 780B			0.066	0.74
344787	Zinc finger protein 860			0.087	0.76
54503	Zinc finger, DHHC-type containing 13			0.073	0.71
9765	Zinc finger, FYVE domain containing 16			0.048	0.72
	AY358103			0.059	1.65
	ENST00000363158			0.096	1.36
	ENST00000364578			0.087	1.62
	ENST00000365159			0.095	1.31
	ENST00000413930			0.043	1.34
	ENST00000436576			0.062	0.72
	ENST00000462868			0.043	0.74
	ENST00000466667			0.046	1.79
	ENST00000471045			0.081	0.70
	ENST00000478633			0.078	1.37
	ENST00000489347			0.071	0.76
	ENST00000489584			0.058	1.64
	ENST00000495608			0.056	0.75
	ENST00000498263			0.073	1.42
	ENST00000517226			0.046	1.32

8.6 Establishment of the glucose production assay

Three different cell culture models - human hepatoma cell line HepG2 and Huh7 as well as rat hepatoma cell line Fao - were tested regarding their potency for hepatic glucose production. Only the rat hepatoma cell line Fao showed expressive glucose release and was therefore chosen for the experiments.

To optimize the glucose production assay, Fao cells were pre-treated in DMEM for 24 hours with different glucose concentrations supplemented with 0.5 % BSA. Glucose production was determined after an additional incubation in glucose production buffer for 2, 4, 6, 9 or 24 hours. Pre-incubation with a glucose concentration of 5.6 mM resulted in the best time-dependent increase in glucose output and was therefore used for the experiments (Figure 34).

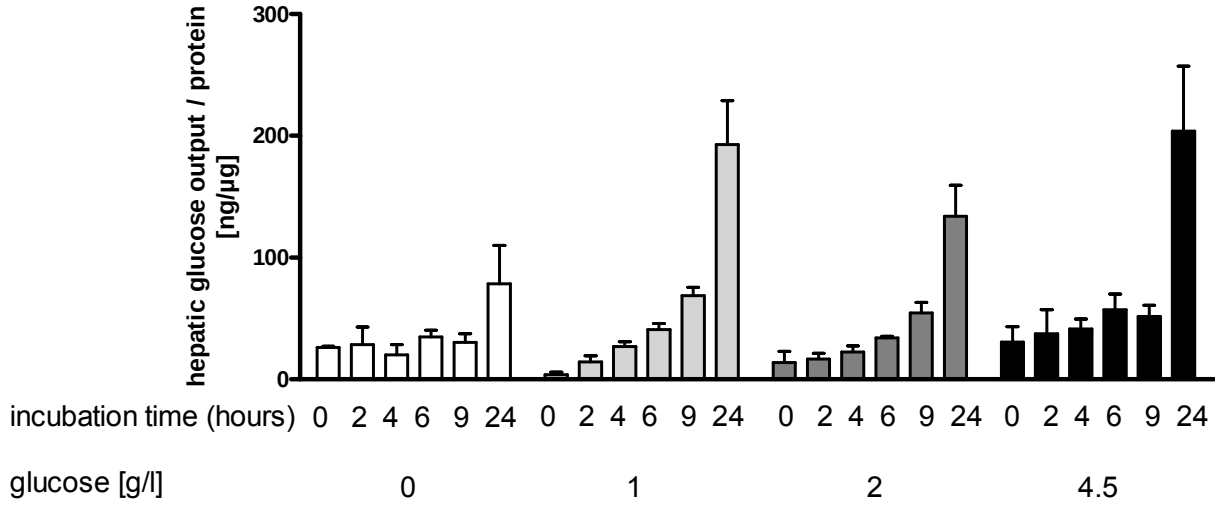

Figure 34: Time dependent hepatic glucose output in Fao cells after pre-incubation with different glucose concentrations. Fao cells were incubated in a culture medium containing 0, 1, 2 or 4.5 g/l glucose supplemented with 0.5 % BSA for 24 hours. Cells were washed and were further cultured in glucose production buffer for 0, 2, 4, 6, 9 or 24 hours. Glucose release was measured and normalised by protein content. Each column represents the mean ± SE of 3 independent experiments.

For maximum effects of insulin and db-CD on hepatic glucose output, Fao cells were incubated for 4 different time points in glucose production buffer supplemented with or without insulin or db-CD prior to the measurement of glucose output calculated as absolute values or as percentage of untreated control (Figure 35).

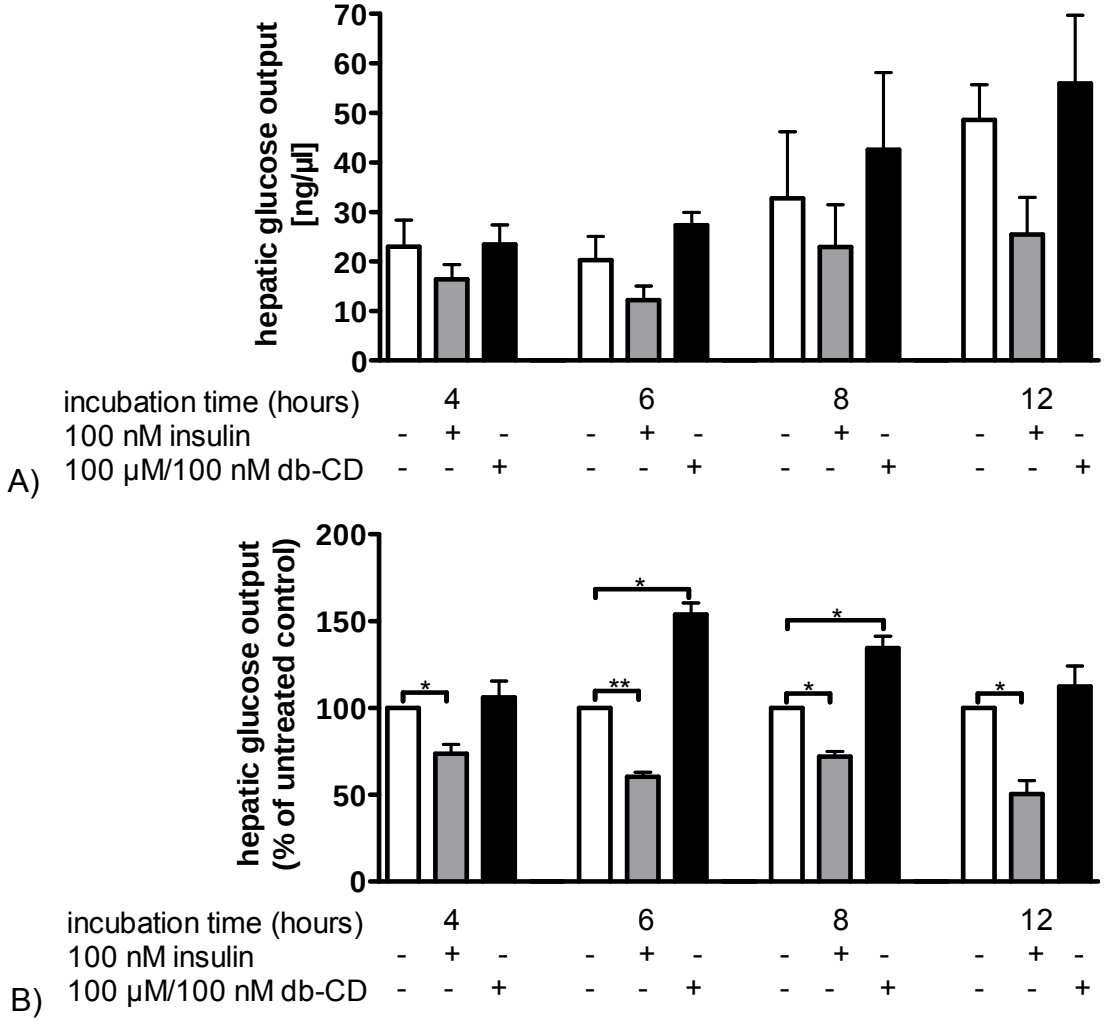

Figure 35: Time dependent effect of insulin and db-CD on hepatic glucose output. Fao cells were incubated in DMEM (5.6 mM glucose) plus 0.5 % BSA for 24 hours. Cells were washed and further treated with or without insulin and db-CD, respectively in glucose production buffer for 4, 6, 8 or 12 hours. Glucose release was measured and normalised by protein content. Data are shown as absolute values (A) or as percentage of untreated control cells (B). Results are means ± SE of 3 independent experiments (one-sample t-test *p<0.05; **p<0.01).

After 6 hours and 8 hours hepatic glucose output in Fao cells was significantly decreased by insulin (60.3 ± 2.6 %; 71.9 ± 3.0 %) and significantly increased by db-CD (153.9 ± 6.6 %; 134.4 ± 6.9 %) . However, the relatively effects of insulin and db-CD on hepatic glucose release were higher after 6 hours compared to 8 hours (Figure 35). For further experiments cells were incubated for 6 hours in glucose production buffer with or without insulin and db-CD, respectively.

8.7 Fao cell viability in dependence of adipokines

Cell viability was tested for all adipokines prior to the experiments and calculated as changes compared to the untreated control in percent. The cell viability of untreated control cells were set to 100 %. None of these adipokines showed toxic effects in the respective range tested (Figure 36).

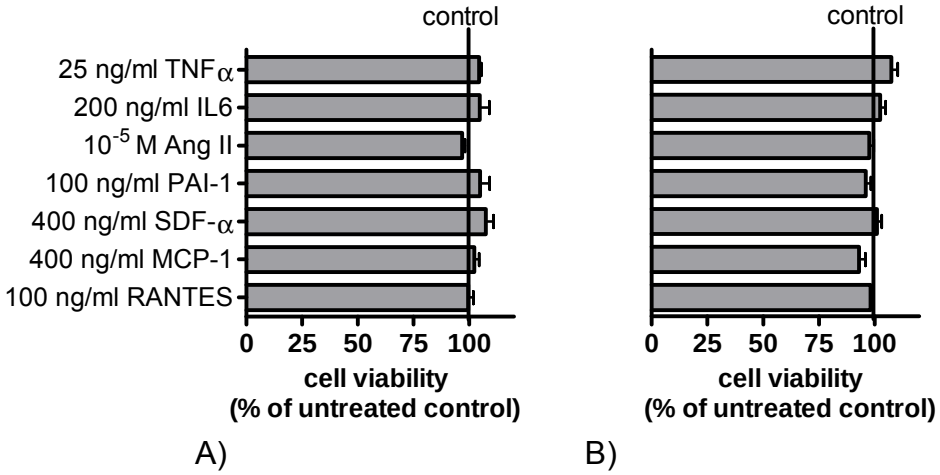

Figure 36: Cell viability of Fao hepatoma cells after treatment with different adipokines. Fao cells were incubated with adipokines for 6 hours (A) and 30 hours (B), respectively. Cell viability was measured by MTS-assay and was calculated as percentage of untreated control (100 %). Results are means ± SE of 3 independent experiments.

8.8 Effect of met-RANTES on hepatic gluconeogenesis

In order to exclude self-standing effects of met-RANTES three different concentrations of met-RANTES were tested regarding their impact on hepatic glucose output as well as on gene expression of *PEPCK* and *G6Pase*, respectively (Figure 37). 200 ng/ml met-RANTES had no effect on hepatic glucose release as well as *PEPCK* and *G6Pase* mRNA and was therefore used to confirm the influence of RANTES on hepatic gluconeogenesis.

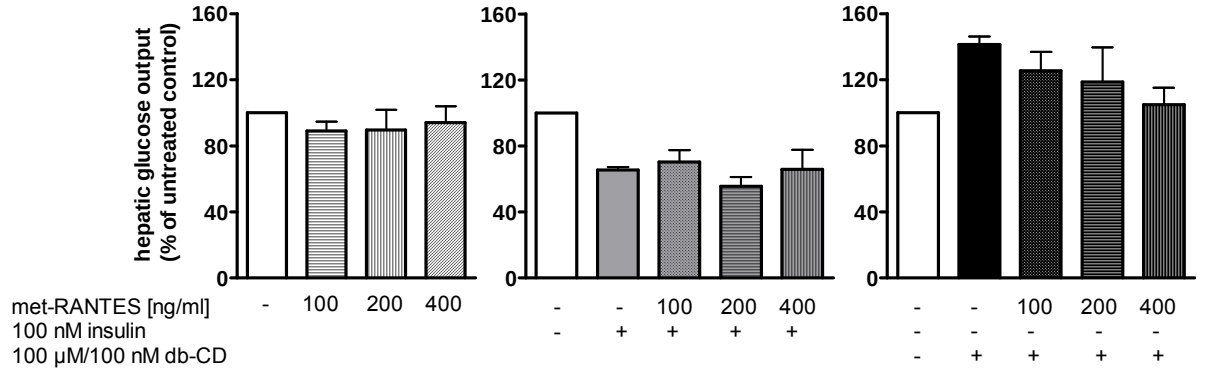

A)

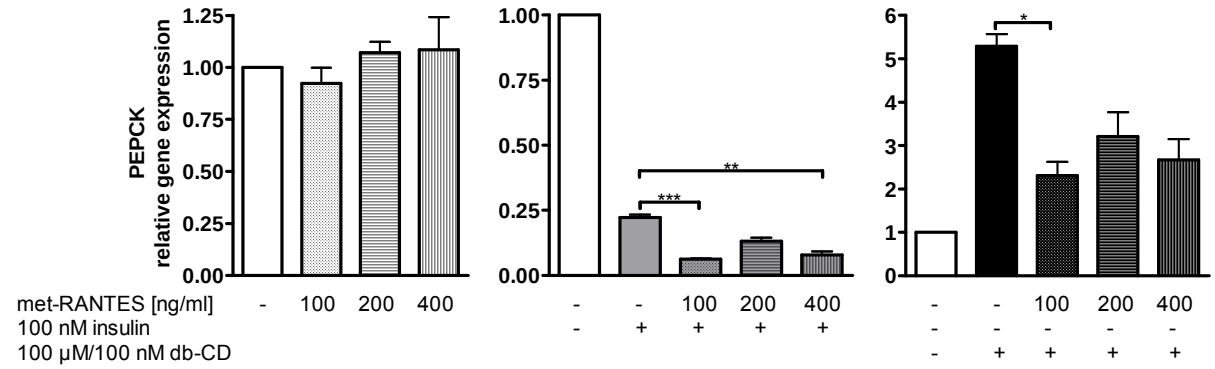

B)

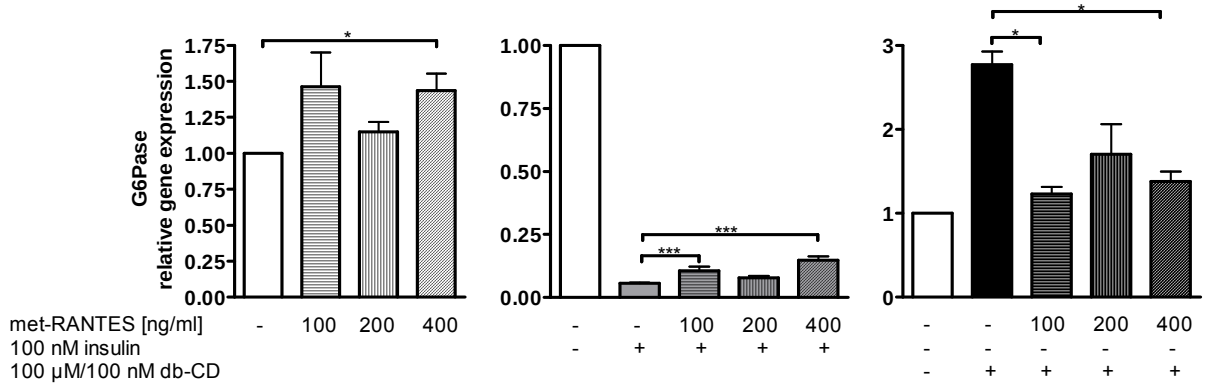

C)

Figure 37: Impact of met-RANTES on hepatic glucose output (A) as well as gene expression of PEPCK (B) and G6Pase (C). Fao cells were treated with different met-RANTES concentrations for 31 hours in order to analyse their impact on hepatic glucose output or for 7 hours to investigate their effect on *PEPCK* and *G6Pase* gene expression. Both glucose release and *PEPCK* and *G6Pase* gene expression were measured as described in Methods. Results are means ± SE of at least 3 independent experiments (one-sample t-test to the untreated control and one-way ANOVA to the insulin- or db-CD-stimulated control *p<0.05; **p<0.01; ***p<0.001).

References

[1] *Klaus S*. Adipose tissue. Georgetown, TX, Austin, TX: Landes Bioscience; Eurekah.com, 2001

[2] *Casteilla L, Penicaud L, Cousin B* et al. Choosing an adipose tissue depot for sampling: factors in selection and depot specificity. Methods Mol Biol 2008; 456: 23–38. doi: 10.1007/978-1-59745-245-8_2

[3] *Cook A, Cowan C*. Adipose. BStemBook. In: 2008

[4] *Kuk JL, Lee S, Heymsfield SB* et al. Waist circumference and abdominal adipose tissue distribution: influence of age and sex. Am J Clin Nutr 2005; 81: 1330–1334

[5] *Albright AL, Stern J. S.* Adipose Tissue. http://www.sportsci.org/encyc/adipose/adipose.html. Accessed 17 Feb 2012

[6] *Schling P, Löffler G*. Cross Talk Between Adipose Tissue Cells: Impact on Pathophysiology. Physiology 2002; 17: 99–104

[7] *Poissonnet CM, Burdi AR, Bookstein FL*. Growth and development of human adipose tissue during early gestation. Early Hum Dev 1983; 8: 1–11

[8] *Spalding KL, Arner E, Westermark PO* et al. Dynamics of fat cell turnover in humans. Nature 2008; 453: 783–787

[9] *Cristancho AG, Lazar MA*. Forming functional fat: a growing understanding of adipocyte differentiation. Nat Rev Mol Cell Biol 2011; 12: 722–734. doi: 10.1038/nrm3198

[10] *Pantoja C, Huff JT, Yamamoto KR*. Glucocorticoid Signaling Defines a Novel Commitment State during Adipogenesis In Vitro. Molecular Biology of the Cell 2008; 19: 4032–4041. doi: 10.1091/mbc.E08-04-0420

[11] *Rosen ED, Walkey CJ, Puigserver P* et al. Transcriptional regulation of adipogenesis. Genes & Development 2000; 14: 1293–1307

[12] *Gregoire FM, Smas CM, Sul HS*. Understanding adipocyte differentiation. Physiol Rev 1998; 78: 783–809

[13] *Smith U*. Impaired ('diabetic') insulin signaling and action occur in fat cells long before glucose intolerance--is insulin resistance initiated in the adipose tissue? Int J Obes Relat Metab Disord 2002; 26: 897-904

[14] *Kasuga M, Hedo JA, Yamada KM* et al. The structure of insulin receptor and its subunits. Evidence for multiple nonreduced forms and a 210,000 possible proreceptor. Journal of Biological Chemistry 1982; 257: 10392–10399

[15] *Kido Y*. The Insulin Receptor and Its Cellular Targets. Journal of Clinical Endocrinology & Metabolism 2001; 86: 972–979. doi: 10.1210/jc.86.3.972

[16] *Massagué J, Czech MP*. Role of disulfides in the subunit structure of the insulin receptor. Reduction of class I disulfides does not impair transmembrane signalling. Journal of Biological Chemistry 1982; 257: 6729–6738

[17] *Pessin JE, Saltiel AR*. Signaling pathways in insulin action: molecular targets of insulin resistance. J Clin Invest 2000; 106: 165–169. doi: 10.1172/JCI10582

[18] *Saltiel AR, Kahn CR*. Insulin signalling and the regulation of glucose and lipid metabolism. Nature 2001; 414: 799–806

[19] *Schmitz-Peiffer C, Whitehead J*. IRS-1 regulation in health and disease. IUBMB Life 2003; 55: 367–374. doi: 10.1080/1521654031000138569

[20] *McCubrey JA, Steelman LS, Chappell WH* et al. Roles of the Raf/MEK/ERK pathway in cell growth, malignant transformation and drug resistance. Mitogen-Activated Protein Kinases: New Insights on Regulation, Function and Role in Human Disease 2007; 1773: 1263–1284. doi: 10.1016/j.bbamcr.2006.10.001

[21] *WHO*. Obesity and overweight.

http://www.who.int/mediacentre/factsheets/fs311/en/. Accessed 17 Feb 2012

[22] *Salans LB, Knittle JL, Hirsch J*. The role of adipose cell size and adipose tissue insulin sensitivity in the carbohydrate intolerance of human obesity. J. Clin. Invest 1968; 47: 153–165. doi: 10.1172/JCI105705

[23] *Weyer C, Foley JE, Bogardus C* et al. Enlarged subcutaneous abdominal adipocyte size, but not obesity itself, predicts Type II diabetes independent of insulin resistance. Diabetologia 2000; 43: 1498–1506. doi: 10.1007/s001250051560

[24] *Pasarica M, Tchoukalova YD, Heilbronn LK* et al. Differential effect of weight loss on adipocyte size subfractions in patients with type 2 diabetes. Obesity (Silver Spring) 2009; 17: 1976–1978. doi: 10.1038/oby.2009.219

[25] *Roberts R, Hodson L, Dennis AL* et al. Markers of de novo lipogenesis in adipose tissue: associations with small adipocytes and insulin sensitivity in humans. Diabetologia 2009; 52: 882–890. doi: 10.1007/s00125-009-1300-4

[26] *Franck N, Stenkula KG, Öst A* et al. Insulin-induced GLUT4 translocation to the plasma membrane is blunted in large compared with small primary fat cells isolated from the same individual. Diabetologia 2007; 50: 1716–1722. doi: 10.1007/s00125-007-0713-1

[27] *Kotani K, Peroni OD, Minokoshi Y* et al. GLUT4 glucose transporter deficiency increases hepatic lipid production and peripheral lipid utilization. J. Clin. Invest. 2004; 114: 1666–1675. doi: 10.1172/JCI21341

[28] *Laurencikiene J, Skurk T, Kulyte A* et al. Regulation of Lipolysis in Small and Large Fat Cells of the Same Subject. Journal of Clinical Endocrinology & Metabolism 2011; 96: E2045. doi: 10.1210/jc.2011-1702

[29] *Pasarica M, Sereda OR, Redman LM* et al. Reduced adipose tissue oxygenation in human obesity: evidence for rarefaction, macrophage chemotaxis, and inflammation without an angiogenic response. Diabetes 2009; 58: 718–725. doi: 10.2337/db08-1098

[30] *Ye J*. Adipose Tissue Vascularization: Its Role in Chronic Inflammation. Curr Diab Rep 2011; 11: 203–210. doi: 10.1007/s11892-011-0183-1

[31] *Helmlinger G, Yuan F, Dellian M* et al. Interstitial pH and pO2 gradients in solid tumors in vivo: High-resolution measurements reveal a lack of correlation. Nat Med 1997; 3: 177–182. doi: 10.1038/nm0297-177

[32] *Carmeliet P, Jain RK*. Angiogenesis in cancer and other diseases. Nature 2000; 407: 249–257. doi: 10.1038/35025220

[33] *Trayhurn P, Wang B, Wood IS*. Hypoxia in adipose tissue: a basis for the dysregulation of tissue function in obesity? Br. J. Nutr 2008; 100: 227–235. doi: 10.1017/S0007114508971282

[34] *Regazzetti C, Peraldi P, Grémeaux T* et al. Hypoxia decreases insulin signaling pathways in adipocytes. Diabetes 2009; 58: 95–103. doi: 10.2337/db08-0457

[35] *Yin J, Gao Z, He Q* et al. Role of hypoxia in obesity-induced disorders of glucose and lipid metabolism in adipose tissue. Am. J. Physiol. Endocrinol. Metab 2009; 296: E333-42. doi: 10.1152/ajpendo.90760.2008

[36] *Yun Z, Maecker HL, Johnson RS* et al. Inhibition of PPAR³2 Gene Expression by the HIF-1-Regulated Gene DEC1/Stra13: A Mechanism for Regulation of Adipogenesis by Hypoxia. Dev Cell 2002; 2: 331–341

[37] *Ye J, Gao Z, Yin J* et al. Hypoxia is a potential risk factor for chronic inflammation and adiponectin reduction in adipose tissue of ob/ob and dietary obese mice. AJP: Endocrinology and Metabolism 2007; 293: E1118. doi: 10.1152/ajpendo.00435.2007

[38] *Wang B, Wood IS, Trayhurn P*. Dysregulation of the expression and secretion of inflammation-related adipokines by hypoxia in human adipocytes. Pflugers Arch - Eur J Physiol 2007; 455: 479–492. doi: 10.1007/s00424-007-0301-8
[39] *Ambrosini G*. Transcriptional Activation of the Human Leptin Gene in Response to Hypoxia. INVOLVEMENT OF HYPOXIA-INDUCIBLE FACTOR 1. Journal of Biological Chemistry 2002; 277: 34601–34609. doi: 10.1074/jbc.M205172200
[40] *Grosfeld A, Zilberfarb V, Turban S* et al. Hypoxia increases leptin expression in human PAZ6 adipose cells. Diabetologia 2002; 45: 527–530. doi: 10.1007/s00125-002-0804-y
[41] *Skurk T, Alberti-Huber C, Herder C* et al. Relationship between adipocyte size and adipokine expression and secretion. J. Clin. Endocrinol. Metab. 2007; 92: 1023–1033. doi: 10.1210/jc.2006-1055
[42] *Hotamisligil GS, Shargill NS, Spiegelman BM*. Adipose expression of tumor necrosis factor-alpha: direct role in obesity-linked insulin resistance. Science 1993; 259: 87–91
[43] *Hotamisligil GS, Arner P, Caro JF* et al. Increased adipose tissue expression of tumor necrosis factor-alpha in human obesity and insulin resistance. J. Clin. Invest 1995; 95: 2409–2415. doi: 10.1172/JCI117936
[44] *Liu Z, Hsu H, Goeddel DV* et al. Dissection of TNF Receptor 1 Effector Functions: JNK Activation Is Not Linked to Apoptosis While NF-κB Activation Prevents Cell Death. Cell 1996; 87: 565–576. doi: 10.1016/S0092-8674(00)81375-6
[45] *Aggarwal BB*. Tumour necrosis factors receptor associated signalling molecules and their role in activation of apoptosis, JNK and NF-kappa B. Annals of the Rheumatic Diseases 2000; 59: 6i. doi: 10.1136/ard.59.suppl_1.i6
[46] *Solinas G, Karin M*. JNK1 and IKKbeta: molecular links between obesity and metabolic dysfunction. FASEB J 2010; 24: 2596–2611. doi: 10.1096/fj.09-151340
[47] *Hotamisligil GS, Peraldi P, Budavari A* et al. IRS-1-mediated inhibition of insulin receptor tyrosine kinase activity in TNF-alpha- and obesity-induced insulin resistance. Science 1996; 271: 665–668
[48] *Stephens JM, Lee J, Pilch PF*. Tumor Necrosis Factor-alpha -induced Insulin Resistance in 3T3-L1 Adipocytes Is Accompanied by a Loss of Insulin Receptor Substrate-1 and GLUT4 Expression without a Loss of Insulin Receptor-mediated Signal Transduction. Journal of Biological Chemistry 1997; 272: 971–976. doi: 10.1074/jbc.272.2.971
[49] *Kawakami M, Murase T, Ogawa H* et al. Human recombinant TNF suppresses lipoprotein lipase activity and stimulates lipolysis in 3T3-L1 cells. J Biochem 1987; 101: 331–338
[50] *Hotamisligil G*. Mechanisms of TNF-α-induced insulin resistance. Exp Clin Endocrinol Diabetes 1999; 107: 119–125. doi: 10.1055/s-0029-1212086
[51] *Maffeis C, Silvagni D, Bonadonna R* et al. Fat Cell Size, Insulin Sensitivity, and Inflammation in Obese Children. The Journal of Pediatrics 2007; 151: 647–652. doi: 10.1016/j.jpeds.2007.04.053
[52] *Houseknecht KL, Baile CA, Matteri RL* et al. The biology of leptin: a review. J Anim Sci 1998; 76: 1405–1420
[53] *Sahu A*. Resistance to the satiety action of leptin following chronic central leptin infusion is associated with the development of leptin resistance in neuropeptide Y neurones. J Neuroendocrinol 2002; 14: 796–804
[54] *Vidal H, Auboeuf D, Vos P de* et al. The expression of ob gene is not acutely regulated by insulin and fasting in human abdominal subcutaneous adipose tissue. J. Clin. Invest. 1996; 98: 251–255. doi: 10.1172/JCI118786

[55] *Considine RV, Sinha MK, Heiman ML* et al. Serum immunoreactive-leptin concentrations in normal-weight and obese humans. N Engl J Med 1996; 334: 292–295. doi: 10.1056/NEJM199602013340503
[56] *Loffreda S, Yang SQ, Lin HZ* et al. Leptin regulates proinflammatory immune responses. The FASEB Journal 1998; 12: 57–65
[57] *Fried SK, Bunkin DA, Greenberg AS*. Omental and subcutaneous adipose tissues of obese subjects release interleukin-6: depot difference and regulation by glucocorticoid. J. Clin. Endocrinol. Metab 1998; 83: 847–850
[58] *Fain JN, Madan AK, Hiler ML* et al. Comparison of the release of adipokines by adipose tissue, adipose tissue matrix, and adipocytes from visceral and subcutaneous abdominal adipose tissues of obese humans. Endocrinology 2004; 145: 2273–2282. doi: 10.1210/en.2003-1336
[59] *Maury E, Ehala-Aleksejev K, Guiot Y* et al. Adipokines oversecreted by omental adipose tissue in human obesity. AJP: Endocrinology and Metabolism 2007; 293: E656. doi: 10.1152/ajpendo.00127.2007
[60] *Gabay C*. Interleukin-6 and chronic inflammation. Arthritis Res Ther 2006; 8 Suppl 2: S3. doi: 10.1186/ar1917
[61] *Xing Z, Gauldie J, Cox G* et al. IL-6 is an antiinflammatory cytokine required for controlling local or systemic acute inflammatory responses. J. Clin. Invest. 1998; 101: 311–320. doi: 10.1172/JCI1368
[62] *Pedersen BK, Steensberg A, Keller P* et al. Muscle-derived interleukin-6: lipolytic, anti-inflammatory and immune regulatory effects. Pflügers Archiv European Journal of Physiology 2003; 446: 9–16. doi: 10.1007/s00424-002-0981-z
[63] *Carey AL*. Interleukin-6 Increases Insulin-Stimulated Glucose Disposal in Humans and Glucose Uptake and Fatty Acid Oxidation In Vitro via AMP-Activated Protein Kinase. Diabetes 2006; 55: 2688–2697. doi: 10.2337/db05-1404
[64] *Klover PJ, Zimmers TA, Koniaris LG* et al. Chronic Exposure to Interleukin-6 Causes Hepatic Insulin Resistance in Mice. Diabetes 2003; 52: 2784–2789. doi: 10.2337/diabetes.52.11.2784
[65] *Franckhauser S, Elias I, Rotter Sopasakis V* et al. Overexpression of Il6 leads to hyperinsulinaemia, liver inflammation and reduced body weight in mice. Diabetologia 2008; 51: 1306–1316. doi: 10.1007/s00125-008-0998-8
[66] *Shi H, Tzameli I, Bjørbaek C* et al. Suppressor of cytokine signaling 3 is a physiological regulator of adipocyte insulin signaling. J. Biol. Chem 2004; 279: 34733–34740. doi: 10.1074/jbc.M403886200
[67] *Rotter V, Nagaev I, Smith U*. Interleukin-6 (IL-6) induces insulin resistance in 3T3-L1 adipocytes and is, like IL-8 and tumor necrosis factor-alpha, overexpressed in human fat cells from insulin-resistant subjects. J Biol Chem 2003; 278: 45777–45784. doi: 10.1074/jbc.M301977200
[68] *Ji C, Chen X, Gao C* et al. IL-6 induces lipolysis and mitochondrial dysfunction, but does not affect insulin-mediated glucose transport in 3T3-L1 adipocytes. J Bioenerg Biomembr 2011; 43: 367–375. doi: 10.1007/s10863-011-9361-8
[69] *Maachi M, Pieroni L, Bruckert E* et al. Systemic low-grade inflammation is related to both circulating and adipose tissue TNFalpha, leptin and IL-6 levels in obese women. Int J Obes Relat Metab Disord 2004; 28: 993–997. doi: 10.1038/sj.ijo.0802718
[70] *Karlsson C, Lindell K, Ottosson M* et al. Human adipose tissue expresses angiotensinogen and enzymes required for its conversion to angiotensin II. J Clin Endocrinol Metab 1998; 83: 3925–3929

[71] *Hajer GR, van Haeften TW, Visseren FLJ*. Adipose tissue dysfunction in obesity, diabetes, and vascular diseases. Eur Heart J 2008; 29: 2959–2971. doi: 10.1093/eurheartj/ehn387
[72] *He FJ, MacGregor GA*. Review: Salt, blood pressure and the renin-angiotensin system. Journal of Renin-Angiotensin-Aldosterone System 2003; 4: 11–16
[73] *Massiera F, Bloch-Faure M, Ceiler D* et al. Adipose angiotensinogen is involved in adipose tissue growth and blood pressure regulation. FASEB J 2001; 15: 2727–2729. doi: 10.1096/fj.01-0457fje
[74] *van Harmelen V, Ariapart P, Hoffstedt J* et al. Increased adipose angiotensinogen gene expression in human obesity. Obes Res 2000; 8: 337–341. doi: 10.1038/oby.2000.40
[75] *Skurk T, Lee YM, Hauner H*. Angiotensin II and its metabolites stimulate PAI-1 protein release from human adipocytes in primary culture. Hypertension 2001; 37: 1336–1340
[76] *Skurk T*. Angiotensin II Stimulates the Release of Interleukin-6 and Interleukin-8 From Cultured Human Adipocytes by Activation of NF- B. Arteriosclerosis, Thrombosis, and Vascular Biology 2004; 24: 1199–1203. doi: 10.1161/01.ATV.0000131266.38312.2e
[77] *Skurk T, van Harmelen V, Blum WF* et al. Angiotensin II promotes leptin production in cultured human fat cells by an ERK1/2-dependent pathway. Obes Res 2005; 13: 969–973. doi: 10.1038/oby.2005.113
[78] *Kalupahana NS, Massiera F, Quignard-Boulange A* et al. Overproduction of angiotensinogen from adipose tissue induces adipose inflammation, glucose intolerance, and insulin resistance. Obesity (Silver Spring) 2012; 20: 48–56. doi: 10.1038/oby.2011.299
[79] *Alessi MC, Peiretti F, Morange P* et al. Production of plasminogen activator inhibitor 1 by human adipose tissue: possible link between visceral fat accumulation and vascular disease. Diabetes 1997; 46: 860–867
[80] *Binder BR, Christ G, Gruber F* et al. Plasminogen activator inhibitor 1: physiological and pathophysiological roles. News Physiol Sci 2002; 17: 56–61
[81] *Juhan-Vague I, Alessi MC, Vague P*. Increased plasma plasminogen activator inhibitor 1 levels. A possible link between insulin resistance and atherothrombosis. Diabetologia 1991; 34: 457–462. doi: 10.1007/BF00403280
[82] *Juhan-Vague I, Alessi MC*. PAI-1, obesity, insulin resistance and risk of cardiovascular events. Thromb Haemost 1997; 78: 656-60
[83] *LANDIN K, TENGBORN L, Smith U*. Elevated fibrinogen and plasminogen activator inhibitor (PAI-1) in hypertension are related to metabolic risk factors for cardiovascular disease. Journal of Internal Medicine 1990; 227: 273–278. doi: 10.1111/j.1365-2796.1990.tb00157.x
[84] *Ma L, Mao S, Taylor KL* et al. Prevention of obesity and insulin resistance in mice lacking plasminogen activator inhibitor 1. Diabetes 2004; 53: 336–346
[85] *Baggiolini M*. Chemokines in pathology and medicine. Journal of Internal Medicine 2001; 250: 91–104. doi: 10.1046/j.1365-2796.2001.00867.x
[86] *Huber J, Kiefer FW, Zeyda M* et al. CC Chemokine and CC Chemokine Receptor Profiles in Visceral and Subcutaneous Adipose Tissue Are Altered in Human Obesity. Journal of Clinical Endocrinology & Metabolism 2008; 93: 3215–3221. doi: 10.1210/jc.2007-2630
[87] *Weisberg SP, McCann D, Desai M* et al. Obesity is associated with macrophage accumulation in adipose tissue. J Clin Invest 2003; 112: 1796–1808. doi: 10.1172/JCI19246

[88] *Xu H*. Chronic inflammation in fat plays a crucial role in the development of obesity-related insulin resistance. Journal of Clinical Investigation 2003; 112: 1821–1830. doi: 10.1172/JCI200319451
[89] *Gutierrez D, Puglisi M, Hasty A*. Impact of increased adipose tissue mass on inflammation, insulin resistance, and dyslipidemia. Current Diabetes Reports 2009; 9: 26–32. doi: 10.1007/s11892-009-0006-9
[90] *Kintscher U, Hartge M, Hess K* et al. T-lymphocyte Infiltration in Visceral Adipose Tissue: A Primary Event in Adipose Tissue Inflammation and the Development of Obesity-Mediated Insulin Resistance. Arteriosclerosis, Thrombosis, and Vascular Biology 2008; 28: 1304–1310. doi: 10.1161/ATVBAHA.108.165100
[91] *Yano T, Liu Z, Donovan J* et al. Stromal cell derived factor-1 (SDF-1)/CXCL12 attenuates diabetes in mice and promotes pancreatic beta-cell survival by activation of the prosurvival kinase Akt. Diabetes 2007; 56: 2946–2957. doi: 10.2337/db07-0291
[92] *Matin K, Salam MA, Akhter J* et al. Role of stromal-cell derived factor-1 in the development of autoimmune diseases in non-obese diabetic mice. Immunology 2002; 107: 222–232
[93] *Nagasawa T, Hirota S, Tachibana K* et al. Defects of B-cell lymphopoiesis and bone-marrow myelopoiesis in mice lacking the CXC chemokine PBSF/SDF-1. Nature 1996; 382: 635–638. doi: 10.1038/382635a0
[94] *McGrath KE, Koniski AD, Maltby KM* et al. Embryonic expression and function of the chemokine SDF-1 and its receptor, CXCR4. Dev Biol 1999; 213: 442–456. doi: 10.1006/dbio.1999.9405
[95] *Fain JN*. Release of interleukins and other inflammatory cytokines by human adipose tissue is enhanced in obesity and primarily due to the nonfat cells. Vitam Horm 2006; 74: 443–477. doi: 10.1016/S0083-6729(06)74018-3
[96] *Bruun JM*. Monocyte Chemoattractant Protein-1 Release Is Higher in Visceral than Subcutaneous Human Adipose Tissue (AT): Implication of Macrophages Resident in the AT. Journal of Clinical Endocrinology & Metabolism 2005; 90: 2282–2289. doi: 10.1210/jc.2004-1696
[97] *Sartipy P*. Monocyte chemoattractant protein 1 in obesity and insulin resistance. Proceedings of the National Academy of Sciences 2003; 100: 7265–7270. doi: 10.1073/pnas.1133870100
[98] *Ohman MK, Wright AP, Wickenheiser KJ* et al. Monocyte chemoattractant protein-1 deficiency protects against visceral fat-induced atherosclerosis. Arterioscler. Thromb. Vasc. Biol 2010; 30: 1151–1158. doi: 10.1161/ATVBAHA.110.205914
[99] *Schall TJ, Jongstra J, Dyer BJ* et al. A human T cell-specific molecule is a member of a new gene family. The Journal of Immunology 1988; 141: 1018–1025
[100] *Schall TJ, Bacon K, Toy KJ* et al. Selective attraction of monocytes and T lymphocytes of the memory phenotype by cytokine RANTES. Nature 1990; 347: 669–671. doi: 10.1038/347669a0
[101] *Maury E, Noel L, Detry R* et al. In Vitro Hyperresponsiveness to Tumor Necrosis Factor- Contributes to Adipokine Dysregulation in Omental Adipocytes of Obese Subjects. Journal of Clinical Endocrinology & Metabolism 2009; 94: 1393–1400. doi: 10.1210/jc.2008-2196
[102] *Skurk T, Mack I, Kempf K* et al. Expression and Secretion of RANTES (CCL5) in Human Adipocytes in Response to Immunological Stimuli and Hypoxia. Horm Metab Res 2009; 41: 183–189. doi: 10.1055/s-0028-1093345
[103] *Wu H, Ghosh S, Perrard XD* et al. T-Cell Accumulation and Regulated on Activation, Normal T Cell Expressed and Secreted Upregulation in Adipose Tissue

in Obesity. Circulation 2007; 115: 1029–1038. doi: 10.1161/CIRCULATIONAHA.106.638379

[104] *Herder C, Haastert B, Muller-Scholze S* et al. Association of Systemic Chemokine Concentrations With Impaired Glucose Tolerance and Type 2 Diabetes: Results from the Cooperative Health Research in the Region of Augsburg Survey S4 (KORA S4). Diabetes 2005; 54: S11. doi: 10.2337/diabetes.54.suppl_2.S11

[105] *Luo Y, Berman MA, Zhai Q* et al. RANTES stimulates inflammatory cascades and receptor modulation in murine astrocytes. Glia 2002; 39: 19–30. doi: 10.1002/glia.10079

[106] *Veillard NR*. Antagonism of RANTES Receptors Reduces Atherosclerotic Plaque Formation in Mice. Circulation Research 2004; 94: 253–261. doi: 10.1161/01.RES.0000109793.17591.4E

[107] *Zhang Y, Yao F, Yao X* et al. Role of CCL5 in invasion, proliferation and proportion of CD44+/CD24- phenotype of MCF-7 cells and correlation of CCL5 and CCR5 expression with breast cancer progression. Oncol Rep 2009; 21: 1113–1121

[108] *Seki E, Minicis S de, Gwak G* et al. CCR1 and CCR5 promote hepatic fibrosis in mice. J. Clin. Invest. 2009. doi: 10.1172/JCI37444

[109] *Coffey MJ, Woffendin C, Phare SM* et al. RANTES inhibits HIV-1 replication in human peripheral blood monocytes and alveolar macrophages. Am J Physiol 1997; 272: L1025-9

[110] *Choe H, Farzan M, Sun Y* et al. The beta-chemokine receptors CCR3 and CCR5 facilitate infection by primary HIV-1 isolates. Cell 1996; 85: 1135–1148

[111] *Nardese V, Longhi R, Polo S* et al. Structural determinants of CCR5 recognition and HIV-1 blockade in RANTES. Nat. Struct Biol. 2001; 8: 611–615. doi: 10.1038/89653

[112] *Langin D, Dicker A, Tavernier G* et al. Adipocyte Lipases and Defect of Lipolysis in Human Obesity. Diabetes 2005; 54: 3190–3197. doi: 10.2337/diabetes.54.11.3190

[113] *Holm C, Olivecrona G, Ottosson M*. Assays of lipolytic enzymes. Methods Mol Biol 2001; 155: 97–119. doi: 10.1385/1-59259-231-7:097

[114] *Wahrenberg H, Engfeldt P, Bolinder J* et al. Acute adaptation in adrenergic control of lipolysis during physical exercise in humans. Am J Physiol 1987; 253: E383-90

[115] *Green A, Dobias SB, Walters DJ* et al. Tumor necrosis factor increases the rate of lipolysis in primary cultures of adipocytes without altering levels of hormone-sensitive lipase. Endocrinology 1994; 134: 2581–2588

[116] *Gasic S, Tian B, Green A*. Tumor necrosis factor alpha stimulates lipolysis in adipocytes by decreasing Gi protein concentrations. J Biol Chem 1999; 274: 6770–6775

[117] *Xu C, He J, Jiang H* et al. Direct Effect of Glucocorticoids on Lipolysis in Adipocytes. Molecular Endocrinology 2009; 23: 1161–1170. doi: 10.1210/me.2008-0464

[118] *Coppack SW, Evans RD, Fisher RM* et al. Adipose tissue metabolism in obesity: lipase action in vivo before and after a mixed meal. Metabolism 1992; 41: 264–272

[119] *Kiens B, Lithell H, Mikines KJ* et al. Effects of insulin and exercise on muscle lipoprotein lipase activity in man and its relation to insulin action. J. Clin. Invest. 1989; 84: 1124–1129. doi: 10.1172/JCI114275

[120] *Farese RV, JR, Yost TJ, Eckel RH*. Tissue-specific regulation of lipoprotein lipase activity by insulin/glucose in normal-weight humans. Metabolism 1991; 40: 214–216

[121] *Reynisdottir S*. Comparison of Hormone-Sensitive Lipase Activity in Visceral and Subcutaneous Human Adipose Tissue. Journal of Clinical Endocrinology & Metabolism 1997; 82: 4162–4166. doi: 10.1210/jc.82.12.4162

[122] *Neuschwander-Tetri B*. Nonalcoholic steatohepatitis: Summary of an AASLD Single Topic Conference. Hepatology 2003; 37: 1202–1219. doi: 10.1053/jhep.2003.50193
[123] *Bellentani S, Saccoccio G, Masutti F* et al. Prevalence of and risk factors for hepatic steatosis in Northern Italy. Ann Intern Med 2000; 132: 112–117
[124] *Jimba S, Nakagami T, Takahashi M* et al. Prevalence of non-alcoholic fatty liver disease and its association with impaired glucose metabolism in Japanese adults. Diabet Med 2005; 22: 1141–1145. doi: 10.1111/j.1464-5491.2005.01582.x
[125] *Chen C, Huang M, Yang J* et al. Prevalence and Risk Factors of Nonalcoholic Fatty Liver Disease in an Adult Population of Taiwan: Metabolic Significance of Nonalcoholic Fatty Liver Disease in Nonobese Adults. Journal of Clinical Gastroenterology 2006; 40
[126] *Adams LA, Feldstein AE*. Non-invasive diagnosis of nonalcoholic fatty liver and nonalcoholic steatohepatitis. Journal of Digestive Diseases 2011; 12: 10–16. doi: 10.1111/j.1751-2980.2010.00471.x
[127] *Vernon G, Baranova A, Younossi ZM*. Systematic review: the epidemiology and natural history of non-alcoholic fatty liver disease and non-alcoholic steatohepatitis in adults. Alimentary Pharmacology & Therapeutics 2011; 34: 274–285. doi: 10.1111/j.1365-2036.2011.04724.x
[128] *Fabbrini E, Sullivan S, Klein S*. Obesity and nonalcoholic fatty liver disease: Biochemical, metabolic, and clinical implications. Hepatology 2010; 51: 679–689. doi: 10.1002/hep.23280
[129] *Hashimoto E, Tokushige K*. Prevalence, gender, ethnic variations, and prognosis of NASH. J Gastroenterol 2011; 46: 63–69. doi: 10.1007/s00535-010-0311-8
[130] *Gutierrez-Grobe Y, Ponciano-Rodriguez G, Ramos M* et al. Prevalence of non alcoholic fatty liver disease in premenopausal, posmenopausal and polycystic ovary syndrome women. The role of estrogens. Ann Hepatol 2010; 9: 402–409
[131] *Ayonrinde OT, Olynyk JK, Beilin LJ* et al. Gender-specific differences in adipose distribution and adipocytokines influence adolescent nonalcoholic fatty liver disease. Hepatology 2011; 53: 800–809. doi: 10.1002/hep.24097
[132] *Lovejoy JC, Champagne CM, Jonge L de* et al. Increased visceral fat and decreased energy expenditure during the menopausal transition. Int J Obes (Lond) 2008; 32: 949–958. doi: 10.1038/ijo.2008.25
[133] *Petersen KF, Dufour S, Hariri A* et al. Apolipoprotein C3 Gene Variants in Nonalcoholic Fatty Liver Disease. New England Journal of Medicine. N Engl J Med 2010; 362: 1082–1089. doi: 10.1056/NEJMoa0907295
[134] *Day CP, James OFW*. Steatohepatitis: A tale of two “hits”? Gastroenterology 1998; 114: 842–845. doi: 10.1016/S0016-5085(98)70599-2
[135] *Day C*. Pathogenesis of steatohepatitis. Best Practice & Research Clinical Gastroenterology 2002; 16: 663–678. doi: 10.1053/bega.2002.0333
[136] *Zhou J, Stubhaug I, Torstensen BE*. Trans-membrane uptake and intracellular metabolism of fatty acids in Atlantic salmon (Salmo salar L.) hepatocytes. Lipids 2010; 45: 301–311. doi: 10.1007/s11745-010-3396-1
[137] *Donnelly KL*. Sources of fatty acids stored in liver and secreted via lipoproteins in patients with nonalcoholic fatty liver disease. Journal of Clinical Investigation 2005; 115: 1343–1351. doi: 10.1172/JCI200523621
[138] *Gan L, Chitturi S, Farrell GC*. Mechanisms and Implications of Age-Related Changes in the Liver: Nonalcoholic Fatty Liver Disease in the Elderly. Current Gerontology and Geriatrics Research 2011; 2011: 1–12. doi: 10.1155/2011/831536

[139] *Pérez-Carreras M, Del Hoyo P, Martín MA* et al. Defective hepatic mitochondrial respiratory chain in patients with nonalcoholic steatohepatitis. Hepatology 2003; 38: 999–1007. doi: 10.1002/hep.1840380426
[140] *Charlton M, Sreekumar R, Rasmussen D* et al. Apolipoprotein synthesis in nonalcoholic steatohepatitis. Hepatology 2002; 35: 898–904. doi: 10.1053/jhep.2002.32527
[141] *Alkhouri N, Carter-Kent C, Feldstein AE*. Apoptosis in nonalcoholic fatty liver disease: diagnostic and therapeutic implications. Expert Rev Gastroenterol Hepatol 2011; 5: 201–212. doi: 10.1586/egh.11.6
[142] *Berres M, Koenen RR, Rueland A* et al. Antagonism of the chemokine Ccl5 ameliorates experimental liver fibrosis in mice. J. Clin. Invest 2010; 120: 4129–4140. doi: 10.1172/JCI41732
[143] *Tilg H, Moschen A*. Evolution of inflammation in nonalcoholic fatty liver disease: the multiple parallel hits hypothesis. Hepatology 2010; 52: 1836–1846. doi: 10.1002/hep.24001
[144] *Valenzuela A, Morgado N*. Trans fatty acid isomers in human health and in the food industry. Biol. Res. 1999; 32: 273–287
[145] *Lopez-Garcia E, Schulze MB, Meigs JB* et al. Consumption of Trans Fatty Acids Is Related to Plasma Biomarkers of Inflammation and Endothelial Dysfunction. The Journal of Nutrition 2005; 135: 562–566
[146] *Collison KS, Maqbool Z, Saleh SM* et al. Effect of dietary monosodium glutamate on trans fat-induced nonalcoholic fatty liver disease. The Journal of Lipid Research 2009; 50: 1521–1537. doi: 10.1194/jlr.M800418-JLR200
[147] *Spruss A, Bergheim I*. Dietary fructose and intestinal barrier: potential risk factor in the pathogenesis of nonalcoholic fatty liver disease. J Nutr Biochem 2009; 20: 657–662. doi: 10.1016/j.jnutbio.2009.05.006
[148] *Pahl HL*. Signal Transduction From the Endoplasmic Reticulum to the Cell Nucleus. Physiological Reviews 1999; 79: 683–701
[149] *Puri P, Mirshahi F, Cheung O* et al. Activation and dysregulation of the unfolded protein response in nonalcoholic fatty liver disease. Gastroenterology 2008; 134: 568–576. doi: 10.1053/j.gastro.2007.10.039
[150] *Pahl HL, Baeuerle PA*. The ER-overload response: activation of NF-κB. Trends in Biochemical Sciences 1997; 22: 63–67. doi: 10.1016/S0968-0004(96)10073-6
[151] *Tomita K, Tamiya G, Ando S* et al. Tumour necrosis factor α signalling through activation of Kupffer cells plays an essential role in liver fibrosis of non-alcoholic steatohepatitis in mice. Gut 2006; 55: 415–424. doi: 10.1136/gut.2005.071118
[152] *Dara L, Ji C, Kaplowitz N*. The contribution of endoplasmic reticulum stress to liver diseases. Hepatology 2011; 53: 1752–1763. doi: 10.1002/hep.24279
[153] *Ferre P, Foufelle F*. Hepatic steatosis: a role for de novo lipogenesis and the transcription factor SREBP-1c. Diabetes Obes Metab 2010; 12 Suppl 2: 83–92. doi: 10.1111/j.1463-1326.2010.01275.x
[154] *Harte AL, da Silva NF, Creely SJ* et al. Elevated endotoxin levels in non-alcoholic fatty liver disease. J Inflamm 2010; 7: 15. doi: 10.1186/1476-9255-7-15
[155] *Farhadi A, Gundlapalli S, Shaikh M* et al. Susceptibility to gut leakiness: a possible mechanism for endotoxaemia in non-alcoholic steatohepatitis. Liver Int 2008; 28: 1026–1033. doi: 10.1111/j.1478-3231.2008.01723.x
[156] *Su GL*. Lipopolysaccharides in liver injury: molecular mechanisms of Kupffer cell activation. American Journal of Physiology - Gastrointestinal and Liver Physiology 2002; 283: G256. doi: 10.1152/ajpgi.00550.2001
[157] *Shen Z, Liang X, Rogers CQ* et al. Involvement of adiponectin-SIRT1-AMPK signaling in the protective action of rosiglitazone against alcoholic fatty liver in

mice. AJP: Gastrointestinal and Liver Physiology 2010; 298: G364. doi: 10.1152/ajpgi.00456.2009
[158] *Pagano C*. Plasma adiponectin is decreased in nonalcoholic fatty liver disease. European Journal of Endocrinology 2005; 152: 113–118. doi: 10.1530/eje.1.01821
[159] *Deng X, Chen L, Li N*. The expression of SIRT1 in nonalcoholic fatty liver disease induced by high-fat diet in rats. Liver Int 2007; 27: 708–715. doi: 10.1111/j.1478-3231.2007.01497.x
[160] *Buechler C, Wanninger J, Neumeier M*. Adiponectin, a key adipokine in obesity related liver diseases. World J Gastroenterol 2011; 17: 2801–2811. doi: 10.3748/wjg.v17.i23.2801
[161] *Pandey AK, Bhardwaj V, Datta M*. Tumour necrosis factor-α attenuates insulin action on phosphoenolpyruvate carboxykinase gene expression and gluconeogenesis by altering the cellular localization of Foxa2 in HepG2 cells. FEBS Journal 2009; 276: 3757–3769
[162] *Pankaja N*. Essentials of biochemistry. New Delhi, Londres: Jaypee Brothers Medical Pub, op. 2012
[163] *Magnusson I, Rothman DL, Katz LD* et al. Increased rate of gluconeogenesis in type II diabetes mellitus. A 13C nuclear magnetic resonance study. J. Clin. Invest. 1992; 90: 1323–1327. doi: 10.1172/JCI115997
[164] *Shams MEE, Al-Gayyar MMH, Barakat EAME*. Type 2 Diabetes Mellitus-Induced Hyperglycemia in Patients with NAFLD and Normal LFTs: Relationship to Lipid Profile, Oxidative Stress and Pro-Inflammatory Cytokines. Sci Pharm 2011; 79: 623–634. doi: 10.3797/scipharm.1104-21
[165] *Skurk T, Hauner H*. Primary culture of human adipocyte precursor cells: expansion and differentiation. Methods Mol Biol 2012; 806: 215–226. doi: 10.1007/978-1-61779-367-7_15
[166] *Pairault J, Green H*. A study of the adipose conversion of suspended 3T3 cells by using glycerophosphate dehydrogenase as differentiation marker. Proc Natl Acad Sci U S A 1979; 76: 5138–5142
[167] *Wilson K, Walker J*. Principles and Techniques of Biochemistry and Molecular Biology: Cambridge University Press, 2010
[168] *Pais R*. Role of adipokines in the regulation of intestinal GLP-1 secretion, 2012
[169] *Aebersold R, Mann M*. Mass spectrometry-based proteomics. Nature 2003; 422: 198–207. doi: 10.1038/nature01511
[170] *Huang DW, Sherman BT, Lempicki RA*. Systematic and integrative analysis of large gene lists using DAVID bioinformatics resources. Nat Protoc 2009; 4: 44–57. doi: 10.1038/nprot.2008.211
[171] *Huang DW, Sherman BT, Lempicki RA*. Bioinformatics enrichment tools: paths toward the comprehensive functional analysis of large gene lists. Nucleic Acids Res 2009; 37: 1–13. doi: 10.1093/nar/gkn923
[172] *The UniProt Consortium*. Update on activities at the Universal Protein Resource (UniProt) in 2013. Nucleic Acids Research 2013; 41: D43. doi: 10.1093/nar/gks1068
[173] *van Iersel MP, Kelder T, Pico AR* et al. Presenting and exploring biological pathways with PathVisio. BMC Bioinformatics 2008; 9: 399. doi: 10.1186/1471-2105-9-399
[174] *Kelder T, van Iersel MP, Hanspers K* et al. WikiPathways: building research communities on biological pathways. Nucleic Acids Research 2011; 40: D1301. doi: 10.1093/nar/gkr1074
[175] *Fodor SP, Read JL, Pirrung MC* et al. Light-directed, spatially addressable parallel chemical synthesis. Science 1991; 251: 767–773

[176] *Gautier L, Cope L, Bolstad BM* et al. affy--analysis of Affymetrix GeneChip data at the probe level. Bioinformatics 2004; 20: 307–315. doi: 10.1093/bioinformatics/btg405
[177] *Schinke-Braun M, Couget JA*. Expression profiling using affymetrix genechip probe arrays. Methods Mol Biol 2007; 366: 13–40. doi: 10.1007/978-1-59745-030-0_2
[178] *R Development Core Team*. R: A language and environment for statistical computing. Vienna, Austria: R Foundation for Statistical Computing, 2005
[179] *Rainer J, Sanchez-Cabo F, Stocker G* et al. CARMAweb: comprehensive R- and bioconductor-based web service for microarray data analysis. Nucleic Acids Res 2006; 34: W498-503. doi: 10.1093/nar/gkl038
[180] *Reen D*. Enzyme-Linked Immunosorbent Assay (ELISA). In: Walker J (ed). Basic Protein and Peptide Protocols: Humana Press, 1994: 461-466
[181] *Walker J, Rapley R, Royal Society of Chemistry*. Molecular Biology And Biotechnology: Royal Society Of Chemistry, 2009
[182] *Livak KJ, Schmittgen TD*. Analysis of relative gene expression data using real-time quantitative PCR and the 2(-Delta Delta C(T)) Method. Methods 2001; 25: 402–408. doi: 10.1006/meth.2001.1262
[183] *Renart J, Reiser J, Stark GR*. Transfer of proteins from gels to diazobenzyloxymethyl-paper and detection with antisera: a method for studying antibody specificity and antigen structure. Proc Natl Acad Sci U S A 1979; 76: 3116–3120
[184] *Goor H, Gerrits PO, Grond J*. The application of lipid-soluble stains in plastic-embedded sections. Histochemistry 1986; 85: 251-253. doi: 10.1007/BF00494811
[185] *Tarnowski BI, Spinale FG, Nicholson JH*. DAPI as a useful stain for nuclear quantitation. Biotech Histochem 1991; 66: 297–302
[186] *Berridge MV, Tan AS*. Characterization of the cellular reduction of 3-(4,5-dimethylthiazol-2-yl)-2,5-diphenyltetrazolium bromide (MTT): subcellular localization, substrate dependence, and involvement of mitochondrial electron transport in MTT reduction. Arch Biochem Biophys 1993; 303: 474–482. doi: 10.1006/abbi.1993.1311
[187] *Matthae S, May S, Hubersberger M* et al. Protein Normalization in Different Adipocyte Models and Dependence on Cell Size. Horm Metab Res 2013. doi: 10.1055/s-0033-1341429
[188] *Oliveros JC*. VENNY. An interactive tool for comparing lists with Venn Diagrams. http://bioinfogp.cnb.csic.es/tools/venny/index.html
[189] *Ricchi M, Odoardi MR, Carulli L* et al. Differential effect of oleic and palmitic acid on lipid accumulation and apoptosis in cultured hepatocytes. J. Gastroenterol. Hepatol. 2009; 24: 830–840. doi: 10.1111/j.1440-1746.2008.05733.x
[190] *Kusminski CM, Holland WL, Sun K* et al. MitoNEET-driven alterations in adipocyte mitochondrial activity reveal a crucial adaptive process that preserves insulin sensitivity in obesity. Nat Med 2012; 18: 1539–1549. doi: 10.1038/nm.2899
[191] *Kovacs P, Hanson RL, Lee Y* et al. The Role of Insulin Receptor Substrate-1 Gene (IRS1) in Type 2 Diabetes in Pima Indians. Diabetes 2003; 52: 3005–3009. doi: 10.2337/diabetes.52.12.3005
[192] *Carvalho E, Jansson PA, Nagaev I* et al. Insulin resistance with low cellular IRS-1 expression is also associated with low GLUT4 expression and impaired insulin-stimulated glucose transport. FASEB J 2001; 15: 1101–1103
[193] *Kimura A, Baumann CA, Chiang SH* et al. The sorbin homology domain: a motif for the targeting of proteins to lipid rafts. Proc Natl Acad Sci U S A 2001; 98: 9098–9103. doi: 10.1073/pnas.151252898

[194] *Mitra P, Zheng X, Czech MP*. RNAi-based Analysis of CAP, Cbl, and CrkII Function in the Regulation of GLUT4 by Insulin. Journal of Biological Chemistry 2004; 279: 37431–37435
[195] *Liu J, Kimura A, Baumann CA* et al. APS Facilitates c-Cbl Tyrosine Phosphorylation and GLUT4 Translocation in Response to Insulin in 3T3-L1 Adipocytes. Molecular and Cellular Biology 2002; 22: 3599–3609. doi: 10.1128/MCB.22.11.3599-3609.2002
[196] *Wadley GD, Bruce CR, Konstantopoulos N* et al. The effect of insulin and exercise on c-Cbl protein abundance and phosphorylation in insulin-resistant skeletal muscle in lean and obese Zucker rats. Diabetologia 2004; 47: 412–419. doi: 10.1007/s00125-003-1322-2
[197] *Ribon V, Saltiel AR*. Insulin stimulates tyrosine phosphorylation of the proto-oncogene product of c-Cbl in 3T3-L1 adipocytes. Biochem. J 1997; 324: 839–846
[198] *Andoniou CE, Thien CB, Langdon WY*. The two major sites of cbl tyrosine phosphorylation in abl-transformed cells select the crkL SH2 domain. Oncogene 1996; 12: 1981–1989
[199] *Feshchenko EA, Langdon WY, Tsygankov AY*. Fyn, Yes, and Syk Phosphorylation Sites in c-Cbl Map to the Same Tyrosine Residues That Become Phosphorylated in Activated T Cells. Journal of Biological Chemistry 1998; 273: 8323–8331
[200] *JeBailey L*. Skeletal Muscle Cells and Adipocytes Differ in Their Reliance on TC10 and Rac for Insulin-Induced Actin Remodeling. Molecular Endocrinology 2003; 18: 359–372. doi: 10.1210/me.2003-0294
[201] *Lee JO, Lee SK, Kim JH* et al. Metformin regulates glucose transporter 4 (GLUT4) translocation through AMP-activated protein kinase (AMPK)-mediated Cbl/CAP signaling in 3T3-L1 preadipocyte cells. J Biol Chem 2012; 287: 44121–44129. doi: 10.1074/jbc.M112.361386
[202] *Villena JA, Viollet B, Andreelli F* et al. Induced adiposity and adipocyte hypertrophy in mice lacking the AMP-activated protein kinase-alpha2 subunit. Diabetes 2004; 53: 2242–2249
[203] *Bost F, Aouadi M, Caron L* et al. The Extracellular Signal-Regulated Kinase Isoform ERK1 Is Specifically Required for In Vitro and In Vivo Adipogenesis. Diabetes 2004; 54: 402–411. doi: 10.2337/diabetes.54.2.402
[204] *Fujishiro M*. Three Mitogen-Activated Protein Kinases Inhibit Insulin Signaling by Different Mechanisms in 3T3-L1 Adipocytes. Molecular Endocrinology 2002; 17: 487–497. doi: 10.1210/me.2002-0131
[205] *Farnier C, Krief S, Blache M* et al. Adipocyte functions are modulated by cell size change: potential involvement of an integrin/ERK signalling pathway. Int J Obes Relat Metab Disord 2003; 27: 1178–1186. doi: 10.1038/sj.ijo.0802399
[206] *Carlson CJ, Koterski S, Sciotti RJ* et al. Enhanced basal activation of mitogen-activated protein kinases in adipocytes from type 2 diabetes: potential role of p38 in the downregulation of GLUT4 expression. Diabetes 2003; 52: 634–641
[207] *Scacco S, Petruzzella V, Budde S* et al. Pathological mutations of the human NDUFS4 gene of the 18-kDa (AQDQ) subunit of complex I affect the expression of the protein and the assembly and function of the complex. J Biol Chem 2003; 278: 44161–44167. doi: 10.1074/jbc.M307615200
[208] *Kirkinezos IG, Moraes CT*. Reactive oxygen species and mitochondrial diseases. Semin Cell Dev Biol 2001; 12: 449–457. doi: 10.1006/scdb.2001.0282
[209] *Ozcan U, Cao Q, Yilmaz E* et al. Endoplasmic reticulum stress links obesity, insulin action, and type 2 diabetes. Science 2004; 306: 457–461. doi: 10.1126/science.1103160

[210] *Lee G, Proenca R, Montez JM* et al. Abnormal splicing of the leptin receptor in diabetic mice. Nature 1996; 379: 632–635. doi: 10.1038/379632a0
[211] *Pihlajamäki J, Lerin C, Itkonen P* et al. Expression of the Splicing Factor Gene SFRS10 Is Reduced in Human Obesity and Contributes to Enhanced Lipogenesis. Cell Metabolism 2011; 14: 208–218. doi: 10.1016/j.cmet.2011.06.007
[212] *Sjoholm K, Palming J, Olofsson LE* et al. A microarray search for genes predominantly expressed in human omental adipocytes: adipose tissue as a major production site of serum amyloid A. J Clin Endocrinol Metab 2005; 90: 2233–2239. doi: 10.1210/jc.2004-1830
[213] *Uhlar CM, Whitehead AS*. Serum amyloid A, the major vertebrate acute-phase reactant. Eur J Biochem 1999; 265: 501–523
[214] *Ye XY, Xue YM, Sha JP* et al. Serum amyloid A attenuates cellular insulin sensitivity by increasing JNK activity in 3T3-L1 adipocytes. J Endocrinol Invest 2009; 32: 568–575. doi: 10.3275/6111
[215] *Jernas M, Palming J, Sjoholm K* et al. Separation of human adipocytes by size: hypertrophic fat cells display distinct gene expression. FASEB J 2006; 20: 1540–1542. doi: 10.1096/fj.05-5678fje
[216] *Hirosumi J, Tuncman G, Chang L* et al. A central role for JNK in obesity and insulin resistance. Nature 2002; 420: 333–336. doi: 10.1038/nature01137
[217] *David J, Boelens WC, Grongnet J*. Up-regulation of heat shock protein HSP 20 in the hippocampus as an early response to hypoxia of the newborn. J Neurochem 2006; 99: 570–581. doi: 10.1111/j.1471-4159.2006.04071.x
[218] *Rhee J, Kim R, Choi H* et al. Molecular and biochemical modulation of heat shock protein 20 (Hsp20) gene by temperature stress and hydrogen peroxide (H2O2) in the monogonont rotifer, Brachionus sp. Comparative Biochemistry and Physiology Part C: Toxicology & Pharmacology 2011; 154: 19–27. doi: 10.1016/j.cbpc.2011.02.009
[219] *Zhong J, Krawczyk SA, Chaerkady R* et al. Temporal profiling of the secretome during adipogenesis in humans. J. Proteome Res. 2010; 9: 5228–5238. doi: 10.1021/pr100521c
[220] *Pham CT, Ley TJ*. Dipeptidyl peptidase I is required for the processing and activation of granzymes A and B in vivo. Proc. Natl. Acad. Sci. U.S.A. 1999; 96: 8627–8632
[221] *Toomes C, James J, Wood AJ* et al. Loss-of-function mutations in the cathepsin C gene result in periodontal disease and palmoplantar keratosis. Nat Genet 1999; 23: 421–424. doi: 10.1038/70525
[222] *Shea J, French CR, Bishop J* et al. Changes in the transcriptome of abdominal subcutaneous adipose tissue in response to short-term overfeeding in lean and obese men. The American Journal of Clinical Nutrition 2009; 89: 407–415
[223] *Michael Fähling APDT*. Regulation of collagen prolyl 4-hydroxylase and matrix metalloproteinases in fibrosarcoma cells by hypoxia. Comparative biochemistry and physiology. Toxicology & pharmacology : CBP 2004; 139: 119–126. doi: 10.1016/j.cca.2004.09.013
[224] *Mariman ECM, Wang P*. Adipocyte extracellular matrix composition, dynamics and role in obesity. Cell. Mol. Life Sci. 2010; 67: 1277–1292. doi: 10.1007/s00018-010-0263-4
[225] *Lolmede K, Durand Saint Front V de, Galitzky J* et al. Effects of hypoxia on the expression of proangiogenic factors in differentiated 3T3-F442A adipocytes. Int J Obes Relat Metab Disord 2003; 27: 1187–1195. doi: 10.1038/sj.ijo.0802407
[226] *Nagase H, Woessner JF*. Matrix Metalloproteinases. Journal of Biological Chemistry 1999; 274: 21491–21494

[227] *Sternlicht MD, Werb Z*. How matrix metalloproteinases regulate cell behavior. Annu Rev Cell Dev Biol 2001; 17: 463–516. doi: 10.1146/annurev.cellbio.17.1.463
[228] *van Lint P, Libert C*. Chemokine and cytokine processing by matrix metalloproteinases and its effect on leukocyte migration and inflammation. Journal of Leukocyte Biology 2007; 82: 1375–1381. doi: 10.1189/jlb.0607338
[229] *Khan T, Muise ES, Iyengar P* et al. Metabolic Dysregulation and Adipose Tissue Fibrosis: Role of Collagen VI. Molecular and Cellular Biology 2009; 29: 1575–1591. doi: 10.1128/MCB.01300-08
[230] *Muller C, Assimacopoulos-Jeannet F, Mosimann F* et al. Endogenous glucose production, gluconeogenesis and liver glycogen concentration in obese non-diabetic patients. Diabetologia 1997; 40: 463–468. doi: 10.1007/s001250050701
[231] *Gastaldelli A, Baldi S, Pettiti M* et al. Influence of obesity and type 2 diabetes on gluconeogenesis and glucose output in humans: a quantitative study. Diabetes 2000; 49: 1367–1373
[232] *Christ B, Nath A*. Impairment by interleukin 1 beta and tumour necrosis factor alpha of the glucagon-induced increase in phosphoenolpyruvate carboxykinase gene expression and gluconeogenesis in cultured rat hepatocytes. Biochem J 1996; 320 (Pt 1): 161–166
[233] *Liu H, Wen G, Han J* et al. Inhibition of Gluconeogenesis in Primary Hepatocytes by Stromal Cell-derived Factor-1 (SDF-1) through a c-Src/Akt-dependent Signaling Pathway. Journal of Biological Chemistry 2008; 283: 30642–30649. doi: 10.1074/jbc.M803698200
[234] *Whitton PD, Rodrigues LM, Hems DA*. Stimulation by vasopressin, angiotensin and oxytocin of gluconeogenesis in hepatocyte suspensions. Biochem J 1978; 176: 893–898
[235] *Coimbra CC, Garofalo MA, Foscolo DR* et al. Gluconeogenesis activation after intravenous angiotensin II in freely moving rats. Peptides 1999; 20: 823–827
[236] *GREMPLER R, KIENITZ A, WERNER T* et al. Tumour necrosis factor α decreases glucose-6-phosphatase gene expression by activation of nuclear factor κB. Biochem. J. 2004; 382: 471. doi: 10.1042/BJ20040160
[237] *Metzger S, Begleibter N, Barash V* et al. Tumor necrosis factor inhibits the transcriptional rate of glucose-6-phosphatase in vivo and in vitro. Metabolism 1997; 46: 579–583. doi: 10.1016/S0026-0495(97)90197-9
[238] *Ritchie DG*. Interleukin 6 stimulates hepatic glucose release from prelabeled glycogen pools. American Journal of Physiology - Endocrinology And Metabolism 1990; 258: E57
[239] *DeWitt LM, Putney Jr JW*. Stimulation of glycogenolysis in hepatocytes by angiotensin II may involve both calcium release and calcium influx. FEBS Letters 1983; 160: 259–263. doi: 10.1016/0014-5793(83)80978-8
[240] *Machado LJ, Mihessen-Neto I, Marubayashi U* et al. Hyperglycemic action of angiotensin II in freely moving rats. Peptides 1995; 16: 479–483
[241] *Bertran E, Caja L, Navarro E* et al. Role of CXCR4/SDF-1 alpha in the migratory phenotype of hepatoma cells that have undergone epithelial-mesenchymal transition in response to the transforming growth factor-beta. Cell Signal 2009; 21: 1595–1606. doi: 10.1016/j.cellsig.2009.06.006
[242] *Arellano-Plancarte A, Hernandez-Aranda J, Catt KJ* et al. Angiotensin-induced EGF receptor transactivation inhibits insulin signaling in C9 hepatic cells. Biochem. Pharmacol. 2010; 79: 733–745. doi: 10.1016/j.bcp.2009.10.014
[243] *Kanda H*. MCP-1 contributes to macrophage infiltration into adipose tissue, insulin resistance, and hepatic steatosis in obesity. Journal of Clinical Investigation 2006; 116: 1494–1505. doi: 10.1172/JCI26498

[244] *Clément S, Juge-Aubry C, Sgroi A* et al. Monocyte chemoattractant protein-1 secreted by adipose tissue induces direct lipid accumulation in hepatocytes. Hepatology 2008; 48: 799–807. doi: 10.1002/hep.22404
[245] *Inoue H, Ogawa W, Asakawa A* et al. Role of hepatic STAT3 in brain-insulin action on hepatic glucose production. Cell Metab 2006; 3: 267–275. doi: 10.1016/j.cmet.2006.02.009
[246] *Kim H, Higashimori T, Park S* et al. Differential Effects of Interleukin-6 and -10 on Skeletal Muscle and Liver Insulin Action In Vivo. Diabetes 2004; 53: 1060–1067. doi: 10.2337/diabetes.53.4.1060
[247] *Kirovski G, Gäbele E, Dorn C* et al. Hepatic steatosis causes induction of the chemokine RANTES in the absence of significant hepatic inflammation. Int J Clin Exp Pathol 2010; 3: 675–680
[248] *Gaudy AM, Clementi AH, Campbell JS* et al. Suppressor of Cytokine Signaling-3 Is a Glucagon-inducible Inhibitor of PKA Activity and Gluconeogenic Gene Expression in Hepatocytes. Journal of Biological Chemistry 2010; 285: 41356–41365. doi: 10.1074/jbc.M110.159111
[249] *Zhang Y, Luo Y, Zhai Q* et al. Negative role of cAMP-dependent protein kinase A in RANTES-mediated transcription of proinflammatory mediators through Raf. FASEB J. 2003; 17: 734–736. doi: 10.1096/fj.02-0962fje
[250] *Hirano F, Komura K, Fukawa E* et al. Tumor necrosis factor α (TNF-α)-induced RANTES chemokine expression via activation of NF-κB and p38 MAP kinase: roles of TNF-α in alcoholic liver diseases. Journal of Hepatology 2003; 38: 483–489. doi: 10.1016/S0168-8278(02)00456-7
[251] *Wieckowska A, Papouchado BG, Li Z* et al. Increased Hepatic and Circulating Interleukin-6 Levels in Human Nonalcoholic Steatohepatitis. Am J Gastroenterology 2008; 103: 1372–1379. doi: 10.1111/j.1572-0241.2007.01774.x
[252] *Hashizume M, Mihara M*. IL-6 and lipid metabolism. Inflammation and Regeneration 2011; 31: 325–333. doi: 10.2492/inflammregen.31.325
[253] *Eberle D, Hegarty B, Bossard P* et al. SREBP transcription factors: master regulators of lipid homeostasis. Biochimie 2004; 86: 839–848. doi: 10.1016/j.biochi.2004.09.018
[254] *Shimomura I, Bashmakov Y, Horton JD*. Increased levels of nuclear SREBP-1c associated with fatty livers in two mouse models of diabetes mellitus. J Biol Chem 1999; 274: 30028–30032
[255] *Nagaya T, Tanaka N, Suzuki T* et al. Down-regulation of SREBP-1c is associated with the development of burned-out NASH. J. Hepatol. 2010; 53: 724–731. doi: 10.1016/j.jhep.2010.04.033
[256] *Qiao L, MacLean PS, You H* et al. knocking down liver ccaat/enhancer-binding protein alpha by adenovirus-transduced silent interfering ribonucleic acid improves hepatic gluconeogenesis and lipid homeostasis in db/db mice. Endocrinology 2006; 147: 3060–3069. doi: 10.1210/en.2005-1507
[257] *Huang G, Zhang J, Tang Q*. Involvement of C/EBP-alpha gene in in vitro activation of rat hepatic stellate cells. Biochem. Biophys. Res. Commun. 2004; 324: 1309–1318. doi: 10.1016/j.bbrc.2004.09.196
[258] *Schwabe RF, Bataller R, Brenner DA*. Human hepatic stellate cells express CCR5 and RANTES to induce proliferation and migration. American Journal of Physiology - Gastrointestinal and Liver Physiology 2003; 285: G949-G958
[259] *Friedman SL*. Seminars in medicine of the Beth Israel Hospital, Boston. The cellular basis of hepatic fibrosis. Mechanisms and treatment strategies. N Engl J Med 1993; 328: 1828–1835. doi: 10.1056/NEJM199306243282508

[260] *Lee YH, Sauer B, Johnson PF* et al. Disruption of the c/ebp alpha gene in adult mouse liver. Mol Cell Biol 1997; 17: 6014–6022
[261] *Yang J*. Metabolic Response of Mice to a Postnatal Ablation of CCAAT/Enhancer-binding Protein. Journal of Biological Chemistry 2005; 280: 38689–38699. doi: 10.1074/jbc.M503486200